AN ABSTRACT OF THE DISSERTATION OF

Nicholas Bira for the degree of Doctor of Philosophy in Robotics presented on September 12, 2022.

Title: Robotic Actuation and Control with Programmable, Field-Activated Material Systems

Abstract approved: ____

Joseph Davidson

This dissertation presents novel, field-activated smart material systems for the actuation and control of autonomous robots. Smart materials, a type of material whose properties can be changed with an external stimuli, represent a promising direction to expand upon existing robotic control and actuation methods, particularly in the sub-fields of soft robotics and robotic grasping. Specifically, this work makes the following contributions: i) a literature review that synthesizes recent work on field-activated smart materials and their use in soft robotics; ii) an electrorheological fluid (ERF) valve to control soft actuators; iii) magnetic elastomers (MEs) to increase the grip strength of soft grippers; and iv) a low-power method for torque transmission enabled by magnetorheological fluid (MRF) and electropermanent magnet arrays. After the introduction, this dissertation presents a comprehensive literature review paper (Chapter 2) regarding the use of field-activated materials in soft robotics, with an emphasis on magnetic elastomers. The second paper (Chapter 3) describes the development of a 3D-printed pressure valve intended to leverage the pressuring-holding properties of ERF when under the influence of a high voltage field to actuate soft actuators. The third paper (Chapter 4) demonstrates how magnetic elastomers and magnetic fields can

enhance soft robotic grip strength and versatility. The fourth paper (Chapter 5) models, fabricates, and characterizes a MRF-containing clutch device able to rapidly and reversibly module the amount of torque transmitted from an input shaft to an output by leveraging low-power electropermanent magnet arrays. Each work focuses on a field-activated smart material to perform a specific robotic function, with particular emphasis given to compliant mechanisms and soft robotics, as well as to reducing cost and improving ease of fabrication with the use of modern fabrication techniques. In these described papers, field-activated materials are first modeled and then deployed in functional prototypes, and their robotic utility is described in detail after extensive experimental characterization.

Robotic Actuation and Control with Programmable, Field-Activated Material Systems

by

Nicholas Bira

A DISSERTATION

submitted to

Oregon State University

in partial fulfillment of
the requirements for the
degree of

Doctor of Philosophy

Presented September 12, 2022
Commencement June 2023

Doctor of Philosophy dissertation of Nicholas Bira presented on September 12, 2022.

APPROVED:

Major Professor, representing Robotics

Associate Dean of Graduate Studies for the College of Engineering

---

Dean of the Graduate School

Nicholas Bira, Author

ACKNOWLEDGEMENTS

To my research mentors: Joe, thank you for your ceaseless support and encouragement over the past four years. Your guidance was invaluable, and I will always be grateful for being kept on track and grounded. Pallavi, thank you for your dependable and detailed feedback. Your course and positive feedback led me towards new ideas and ways of thinking about research. Yiğit, thank you for being the inspiration to pursue robotics and materials in the first place. Your passion and excitement for the field left a lasting impression, and your insights continue to shape how I think about research as a whole. Kevin, thank you for being the original motivation to pursue research and higher education. Your infectious enthusiasm for learning and problem solving will stick with me forever. Steph, thank you for your guidance over the years as a role model and peer. Watching your journey through academia has been hugely valuable for my understanding of how to make it through this process.

To all my peers at both OSU and elsewhere, thank you for your patience and support. To Gina, Dogan, Callie and Callen, thank you for helping me get through my first year in graduate school. Your collaboration and assistance in my courses was instrumental in allowing me to finish this degree. To Scott, Anna, Connor, and Kevin, thank you for going through this journey as a student alongside me, and for working through the hardships along the way. To Miranda, Hannah, Farhan, Nidhi, Nathan, Aiden, Darin and other friends both in the robotics department and beyond, thank you for keeping me sane with countless games of D&D, cooking, sharing culture, and painting miniatures. Your companionship has been irreplaceable. I hope I have been able to provide a similar amount of encouragement and support to you all during your own journeys, and I will always be grateful for our time together in graduate school.

To my family and long-time friends, thank you for your support through these past few years. They have been the most challenging years of my life thus far, and I cannot thank you enough for your support.

Thank you Mom, for countless supportive conversations on long walks to escape my apartment. Thank you Dad, for cookies in the mail and many other gestures to prop me up along my struggles. Thank you to my siblings Ben, Claire, and Emily and their spouses Kim, Chris, and Franco, for visiting me in Oregon, talking and sharing your lives with me, and always being available to talk as your also go through your own trails and tribulations. Thank you to my family, for being there and being true with integrity, generosity, and kindness. My parents, you raised an incredible family, and you should be eternally proud.

Thank you to my close friends Josh and Christine for playing all the D&D with me, supporting me, exercising with me, and surviving together through the past few incredibly difficult years. Your friendship means the world to me.

Thank you to my girlfriend Grace. Your presence with me the past four years has made the graduate experience all the more bearable, and I am so grateful for all the video games, the shows, the hikes, the camping and cooking and adventures together. Thank you for surviving through the pandemic and years of hard work. I look forward to seeing your own dissertation soon, and to whatever the future holds.

Thank you everyone, more than I can possibly express.

CONTRIBUTION OF AUTHORS

Chapter 1:	Nicholas Bira - writing and editing Joseph Davidson - editing
Chapter 2:	Nicholas Bira - writing and editing Joseph Davidson - editing, adviser for the project Pallavi Dhagat - editing, adviser for experimental design
Chapter 3:	Nicholas Bira - wrote paper, edited paper, designed experiments, analyzed experimental data, created figures Joseph Davidson - edited the paper, co-adviser for the project Yiğit Mengüç - edited the paper, co-adviser for the project
Chapter 4:	Nicholas Bira - wrote paper, edited paper, designed experiments, analyzed experimental data, created figures Joseph Davidson - edited the paper, adviser for the project Pallavi Dhagat - editing, helped design experiments
Chapter 5:	Nicholas Bira - wrote paper, edited paper, designed experiments, analyzed experimental data, created figures Joseph Davidson - edited the paper, contributed to modeling, helped design experiments, adviser for the project Pallavi Dhagat - editing, advising
Chapter 6:	Nicholas Bira - writing and editing Joseph Davidson - editing

TABLE OF CONTENTS

TABLE OF CONTENTS (Continued)

Page

Page

LIST OF FIGURES

LIST OF TABLES

Chapter 1: Introduction

1.1 Soft Robotics and Smart Materials

Within the field of robotics, traditional rigid robotic systems are well studied and developed for a multitude of applications, including factory automation, medical procedures, exploration, transportation, and much more. Despite this, many seemingly simple tasks continue to be best performed by humans, or require intensive fine-tuning to approach comparable levels to tasks living organisms perform with ease. For some of these challenging tasks, soft robotics stand out as a promising space for innovation. The field of soft robotics contains ongoing investigations concerning the design, modeling, manufacturing, and control of soft bodies. Despite over a decade of research within this field, there are no commonly agreed upon solutions to such soft robotic design challenges as autonomy, robustness, and portability. There is a continuous demand for higher actuation strengths, more freedom of movement, less power consumption, and greater durability in the design of these soft robots [164]. Research into these subjects continues to expand, and alternative mechanisms, materials, and strategies are actively developing to enable fully soft and functional robots.

Certain organisms, such as the octopus, snake, or earthworm, are often looked to as both inspiration and the standard to reach for with soft robotics. They function autonomously, independently utilizing effective actuation strategies to move themselves through complex environments, or other techniques to interact with food or others of their own species. Modern robots demonstrate sophisticated techniques for locomotion and interaction, but still struggle to replicate the specific actuation strategies so effectively utilized by soft creatures. The approaches often used by soft roboticists require pressurised chambers, or necessitate hard elements to achieve the desired effects, falling short of the goal to replicate fully soft robots.

As a result, many elements present in traditional rigid robotics are left out of the broader soft robotics toolset, to adhere to this goal. Certain commonplace robotic tools, such as electromagnets, are entirely composed of rigid elements. Developing new materials to bring these tools into the soft space will create new avenues for soft robotic behavior, currently overlooked in the pursuit of soft design. Living creatures utilize electromagnetic fields and electrochemical gradients to sense, think, and act on their environments. Some species of birds demonstrate the ability to navigate by detecting the earth's magnetic field through small deposits of magnetite present in receptors in their beaks [166], while sharks demonstrate the ability to sense and react to changing magnetic fields [107]. These creatures are composed of complex hybrid materials (bone, cartilage, and blood), and leverage each material with incredible robustness to live our their lives.

In the natural world, hydraulic control is present in living systems. Some plants transmit water and nutrients through thin tubes that facilitate movement throughout the plant against gravity using chemical gradients. In most multicellular animals, nutrients and oxygen are transported throughout the body by blood or a carrier fluid which is pressurized and moved through similarly small channels. In humans, the heart pumps blood through arteries, capillaries, and veins with both passive and active elements. Local control of the flow of blood through tissues is regulated by chemical gradients, pressure, and muscular control. Comparably, soft robotic mechanisms frequently utilize pressure gradients to perform actuation and control their position. The current state-of-the-art for soft robotic actuation and control is typically pneumatic or hydraulic, with the necessary valve systems for pressure regulation consisting of traditional solenoids, hoses, pumps, and pressure transducers [125]. Although researchers have proposed and demonstrated various methods for actuation, such as soft snakes [21], soft tentacles [116], rolling soft robots [98], and more, there continues to be a demand for more robust systems. One way to innovate in this space is to focus on the material mechanisms behind robotic actuation, and on the control methods of these mechanisms. Smart materials are well-suited for this approach, demonstrating a wide array of different control and actuation strategies based around the unique properties of soft and flexible materials [65]. By utilizing intelligent materials while designing the key mechanisms of a robot, the strengths of both hard and soft robots can be brought together for maximum effect.

1.2 The Spectrum of Material Stiffness and Robotics

Soft robotics are frequently designed with the key principle that they must be soft in some capacity through their actuation, sensing, or control methodologies. This could be obvious, such as having a tentacle-like actuator comprised entirely of elastomers, or it could be the less obvious case of a deforming structure composed of individually rigid links, but with flexible interconnects that creates a flexible gross morphology. When referring to a *soft robot* in this document, the term refers to a robot comprised of a majority of flexible or deformable material. In nature, most multicellular organisms are a combination of both hard and soft systems. This hybrid structure is best realized within the human hand, one of the most precise and compliant grippers known to the entire field of robotics. The human hand is a composite structure, comprised of different tissues of varying elasticity, rigidity, and compliance. Traditional rigid robots thrive in highly constrained environments, but quickly lose robustness when external factors occur outside of the expected scenarios. Robots made from highly elastic materials such as silicone tend to demonstrate lower forces and slower deformations than actuators made from stiffer materials, relying on rapid changes in pressure to achieve quick actuation or larger forces [111]. When choosing a material for a soft robot, this trade-off limits the design options for roboticists. Utilizing additional multi-functional materials presents opportunities to overcome some of these issues. Realistically, there is no clear delineation between a hard or a soft robot, but merely a spectrum of hardness between the two extremes. As such, the material choices made when designing a robot should enable variable stiffness and material strength to respond to a number of tasks or demands, and present a balance between robustness and accuracy, compliance and strength, speed and safety.

1.3 Hybrid Materials and Agriculture

One specific example of the way in which a hybrid materials approach benefits a given task is evident within fruit harvesting in the field of agriculture. Every year, skilled laborers are hired to walk through countless rows of plants and manually pick fruits and vegetables in specific ways so as to maximize their freshness and prevent damage to the product. The nuance of a gentle yet firm, encompassing grasp stems from the innate compliance of the human hand and fingertips, the strength of the fingers for twisting and pulling, and the rigidity of the underlying skeletal structure to prevent large deformation of the overall grip. A rigid robotic gripper could easily grasp an apple and pull it from a branch, but it risks damaging the fruit if it applies slightly too much pressure. A fully soft gripper may easily conform to an apple, preventing local pressure points and preventing bruising, but it may lack sufficient strength to maintain a grasp through the whole picking motion and instead drop the apple or let go before separating it from the stem. Both aspects of hard and soft materials should be considered when designing for a given robotic task in order to arrive at an optimal solution.

1.4 Dissertation Structure and Contributions

The focus of this dissertation is to examine multiple approaches to creating and controlling compliant robotic mechanisms through the application of electromagnetic fields. Field-activated materials are able to demonstrate variable characteristics well-suited for the demands of hybrid hard and soft robots. This dissertation proposes numerous ways through which to control robotic mechanisms that incorporate hard and soft materials reacting to applied fields, which create new strategies for robot design. Both electric and magnetic fields are commonly utilized in modern technology and traditional robotic design with hard components. The research presented here aims to enable greater compatibility between these well-studied technologies and the research space of soft robotics, bridging the gap between hard and soft robotic disciplines with intelligent material and mechanism design.

This dissertation proposal is structured as follows. Chapter 2 presents an extensive study of the underlying principles of electromagnetically reactive materials, their current uses in the field of soft robotics, and identifies delineations between similar but distinct smart materials. Chapter 3 details the methodology for controlling a soft robot with electrorheological fluid (ERF) and high voltage electric fields. Chapter 4 examines the differences between similar magnetic elastomers (MEs) and characterizes some of their magnetic characteristics, before creating and discussing the significance of a magnetically-enhanced soft actuator with a ME fingertip capable of improved grip strength and trajectory control. Chapter 5 focuses on the proposed remaining work, describes this dissertation's primary contributions, and establishes a schedule for delivering on this work in a timely fashion. The first proposed research path concerns magnetic control of rigid, underactuated robotic fingers, while the second path seeks to create an elastic electromagnet for soft robotic actuation and sensing techniques. The contributions of this dissertation are as follows:

- A 3D printed electrorheological fluid valve for use in soft robotic systems, involving a characterization and flow-forward demonstration of independent soft actuator control using a custom high voltage control board.

- A novel soft robotic gripper design and demonstration of grip strength improvement through development of a magnetic elastomer coupled with permanent magnets in the palm.

- A low-power torque transmission clutch which utilizes electropermanent magnet arrays to control the yield stress of MRF within it. This demonstrates a novel method for low-power magnetic field generation within a MRF clutch, and models and characterizes the torque output of the device.

Chapter 2: Background

Soft robotic actuators, which are mechanisms designed to move or interact with their environment, demonstrate high amounts of flexibility, elasticity, and conformability when compared with their rigid counterparts. Frequently, soft actuators utilize different strategies to act, and these strategies are incorporated into soft robots to enable functionalities which hard robots struggle or fail to do. These strategies tend to fall into a few of the following categories: field-activated, pressure-driven, or thermally/chemically active. Pressure-driven actuators are the most widespread within the field of soft robotics and see active use on modern factory assembly lines and pick-and-place systems due to their safe, inert, and conformational attributes.

2.1 Pressure-Driven Actuator Designs

Many pervasive soft robotic actuator principles were established in the 1990s, with a basic, three-chamber pneumatic actuator design being published in 1992 [148]. The principle behind this device is that as an elastic chamber is pressurized, it will expand to compensate for the pressure differential between the inner and outer chambers. This expansion causes a shape change, and when this is coupled with antagonistic elements, the result is expansion and curvature. Selectively inflating one or multiples of each chamber can allow for tunable rigidity as well as various degrees of curvature about the central axis.

2.1.1 PneuNet Actuators

A common design is the PneuNet (pneumatic network) actuator [111]. In this design, multiple small chambers are arrayed in series and inflated simultaneously. When a fluid is pumped into the actuator, these chambers will expand in the direction of least resistance, bulging outwards. The local expansions forces the actuator to bend, allowing for large curvatures. Adding inextensible and flexible layers of fabric, or alternating layers of elastomer with varying degrees of stiffness, enables the designer to create a curving actuator that performs for a variety of different applications and loading conditions.

2.1.2 Fiber-reinforced Actuators

Fiber-reinforced soft actuators act with a similar mechanism, except the expansion of the elastomer substrate is constrained by wrapping or embedding inextensible and flexible materials to force expansion in the desired way [46]. A cylindrical elastic tube would normally expand in all directions like a balloon, but included fibers reinforce it and restrict this expansion, instead focusing the action of expansion to exclusively lengthening or curvature, depending on the application.

2.1.3 Pneumatic Artificial Muscles

Pneumatic Artificial Muscles, also known as McKibbin actuators [132], consist of a cylinder of elastic material surrounding by an interwoven mesh. This mesh, coupled with the elastic chamber, has the property of shortening in length while expanding in diameter. When pressurized, it creates a muscle fiber-like mechanism which shortens under increasing pressure [32]. All three of these actuator types utilize a pressurized chamber and various methods of strain-limitation to create curvature and actuation. One commonality for these pressure driven designs is that they all rely upon programmed anisotropy of elastomers or deformable materials coupled to elastomers [52, 119]. As the elastomer deforms, it adheres to the intended shape change embedded during its fabrication. These predetermined motions are present in almost all soft robotic actuators, but other methods expand beyond pure elastomers by utilizing using smart materials. Further reading about these actuators, as well as the previously mentioned mechanisms, are detailed within the Soft Robotics Toolkit [66].

2.2 Electrically Activated Materials

2.2.1 Ionic Polymer Metal Composites

One example of smart materials utilized for soft robotics are ionic polymer metal composites (IPMCs). An applied voltage results in the migration of ions towards a different region of the material, resulting in swelling of the material. IPMCs are synthetic materials composed of an ionic polymer with coated surfaces constituting a conductor [138]. This material can be 3D printed into the shape of an actuator and plated with electrodes to achieve deformation and actuation under voltage activation [73]. In a following publication, [26] utilized the same principle to 3D print shapes which enabled a variety of different actuation methods, and with multiple degrees of freedom. Combining multiple printed units created an actuation device, similar in operating principle to the motion of a caterpillar. This application took a smart material, in this case an IPMC, and shaped it through 3D printing to allow an input signal (an applied voltage) to actuate it. This is a typical methodology for using smart materials in robotic actuators; a characteristic of a smart material is exploited by inputting a signal into the system to actuate though shape change.

2.2.2 Hydrogels

Under the same principle, a soft robot actuator was constructed from hydrogels filled with electrolytes [110]. These walking actuators were submerged into an ionic solution, and electric fields applied to the gel created an osmotic pressure difference, causing the desired shape change for actuation The actuation motion is similar to the previously described IPMCs, but with entirely different materials, input signals, and environments. A more recent publication created a more sophisticated hydrogel walker with 3D printed hydrogels, allowing for more complex 3D structures for actuation [59]. This actuation method is limited, in that the signals and environments needed to actuate doped hydrogels are far more situation specific than the general-purpose scenario with the IPMCs. This highlights a major drawback of smart materials as a whole; namely, that most of the methods which use them are limited to specific scenarios due to the design constraints necessary to achieve the desired actuation. In this case, it was a controlled environment where an electric field could be generated, and the media through which the actuator moves was a concentrated ionic solution. While it is possible that these conditions may be replicable in certain regions outside a lab, precisely controlling the solution composition and electric field around the actuator is unlikely to occur easily. Under the criteria of applicability, the IPMC is more widely useful, and more easily controlled with voltage instead of an applied electric field. Both of these smart materials have the advantage of being 3D printable, enabling complex shapes and 3D motion.

IPMCs and hydrogel-based actuators operate under specific conditions to achieve shape change and actuation. In the case of the hydrogels, the actuators were monolithic structures, comprised entirely of the single substance which underwent shape change based on electrical and chemical gradients and programmed anisotropy. The IPMCs incorporated multiple materials (ionic polymers and metal electrodes) to achieve actuation, and other methods similarly utilize smart materials in conjunction with elastomers. Thermal actuators are designed to cause the evaporation and expansion of ethanol mixed and cured inside porous silicone. As an electrically powered, resistive heating element within the actuator is activated and the internal temperature rises above room temperature, the liquid ethanol contained within the surrounding silicone transitions to a gaseous phase, rapidly expanding, and causing the uniform expansion of the silicone outwards [108]. While able to produce large strains (up to 900%) at low density and low cost, this approach has some disadvantages compared to the previous methods. The ability to retain the ethanol over many cycles is poor, as the gas escapes each time it is heated, eventually rendering the actuator inert. It also relies on a central heating element, in this case a coiled Nichrome 80 resistance wire, which provides a non-uniform distribution of heat during the activation process. It is slow to expand, and often does so non-uniformly, violating many necessary assumptions for accurate modeling. This highlights a few more drawbacks of utilizing smart materials in soft actuators; sometimes, the actuation speeds and predictability of smart material actuators are inferior or dependant on fabrication. Additionally, when the system experiences substantial degradation with time, every actuation cycle is different or lesser than the first, as the elastomers expand less and less as the smart materials degrade or are lost to the environment. These thermally driven actuators achieve much larger expansion and resulting force output than hydrogels and IPMCs, are able to operate in any environment, and are resilient to damage, but their degradation over time lessens their practical use.

2.2.3 Actuation Control Strategies

Established control strategies are frequently iterated upon to improve the reliability and performance over the initial design methods. Often that takes the form of replacing a single element of an actuator's design, to focus on decreasing response time, or making the response more predictable and uniform. One paper focused on the previously mentioned thermal actuator and replaced the coiled resistive wire with a cylindrical bulk mass of graphite and silicone composite [10]. This approach allows for an all-soft compressible design, and side-steps the potential drawback of plastic deformation of the resistive heater during large deformations. This central portion resulted in a resistive heater of various resistances (25 to 65 Ω), which outperformed the resistive wire methods on uniformity of heating and maximal actuation forces (200 to 300 N). Later research approached the issue from a different angle, attempting to replace the coiled wire core with a folding, conductive fabric heater [27]. The folded fabric also has much greater surface area, providing more even heating, more predictable expansion, and faster response times. These iterations on the same base mechanism provided improvements on actuator performance and reliability, while providing alternative methods to produce actuators on the same working principle.

2.2.4 Embedding Smart Materials

Other approaches incorporate smart materials into the actuator itself or the working-fluid of a pressure-driven actuator to enable different control mechanisms. Dielectric elastomer actuators (DEAs) create elastic deformations by placing an elastomer between two compliant electrodes and energizing a high voltage field to create contraction [127, 91]. Layering this mechanism in a thick stack can result in a device similar in action to an pneumatic artificial muscle, creating contraction in length once activated. This method generates large forces without a pressure source. This concept of utilizing the material composition of the actuator to achieve actuation with an added control signal is significantly different than pressure-driven methods, as it acts without the need for bulky pressure sources, valving, and pressure regulation hardware. However, it replaces these tools with high voltage power supplies and waveform generators. More recent developments with DEAs see the use of ionic hydrogels, taking advantage of the same principles previously discussed to create a functional DEA [126]. Balancing the needs for softness, actuation force, durability and size dictate the choice of smart material for this approach.

2.2.5 Field-Activated Smart Fluids

Using smart materials as the working fluid within an actuator presents unique opportunities. Two examples of smart materials used in this manner are electrorheological fluids (ERFs) and magnetorheological fluids (MRFs). ERFs respond to the presence of a high voltage field, forming particle-like chains and changing their shear behavior, flowing more slowly. If the applied high voltage field is large enough, the fluid behaves like a solid, until it has enough stress applied to begin flow again. ERFs have been utilized in automotive braking systems [136], fast-acting valves [142], and rehabilitation devices [115, 37]. ERFs use in soft robotics research has been less frequent that of MRFs, likely due to the need for high voltage (the order of kilovolts) and few manufacturers capable of producing it.

2.3 Magnetically Activated Materials

Transitioning from electric fields to magnetic fields introduces new complexities. Traditionally, electrical fields are created from the potential different between two parallel plates, creating a relatively uniform intensity between them. Magnetic fields are more complex in shape, and are highly dependant on factors such as the shape of the magnetic field generating coil, its orientation, and the magnetic circuit and how it contains the divergence of the magnetic field. As such, many approaches utilizing magnetic fields in soft robotics attempt to control the research environment. Another method utilizing hydrogels created a six-fingered actuating grasper [22] in a liquid environment. The hydrogels were photo-patterned (etched by light) to create folding micro-structures, which actuate in response to varying thermal or pH environments. The actuator consisted of two layers, a hydrogel and a stiff polymer backbone. The authors also demonstrated the viability of embedded magnetic particles (Fe_2O_3) within the hydrogel to allow for remote guidance of the grasper by manipulating magnetic fields. The shortcomings of the previous hydrogel approach still apply, but this approach included a rigid backbone to improve stability and potential actuation strength compared to previous examples. Furthermore, positioning and orientation is partially controlled by magnetic fields, leading to more precise manipulation and location control. This control method is as much of a drawback as it is an improvement, as it adds to the ever-present issue of a well-controlled environment incorporating pH, temperature, and magnetic fields. In certain situations, such as robotic surgery or experimental setups, these parameters may align, but these constraints severely reduce the possible practical applications.

2.3.1 Magnetorheological Fluid

In the same way as ERFs, MRFs were also developed in the 1990s, but present different challenges and advantages [75, 24]. These fluids rapidly respond to a magnetic field instead of an electric one, but otherwise create a similar result, in which the yield stress increases to the point of nearing viscoelastic solid behavior. One potential application of MRFs in soft actuators include artificial muscles, where the contraction is locally and reversible controlled by electromagnets embedded nearby [135]. Both MRFs and ERFs demonstrate rapid response times, but rely on expensive and bulky equipment such as high voltage power supplies or electromagnets as the input signal source for actuation. The constant obstacle of bringing these mechanisms out of the laboratory setting remains, as the accessory equipment to enable these approaches must be brought along. MRFs were considered for automotive systems involving shock absorption and differential clutches [51, 83], and were suggested to be suitable in areas such as earthquake mitigation in structures and car seat vibration mitigation [75]. Other recent work developed an impact damper that demonstrates low-velocity sensitivity compared to conventional methods [41]. MRFs have demonstrated uses in soft robotic systems, such as in a recent publication involving encapsulated MRF and applied magnetic fields to generate a crawling gait in an inchworm robot [69].

2.3.2 Magnetorheological Elastomers

Magnetorheological elastomers (MREs) as a class of materials have the ability to change both their shape and material properties when exposed to a magnetic field [99]. MREs have been researched mainly within the areas of vibration damping and control, with few applications within soft robotic mechanisms. These particles can be other magnetic materials instead of iron, but the majority of published literature on MREs uses iron for its soft magnetic properties [5]. MREs are different from MRFs, in that they are elastic solids, instead of fluids. In addition to the desirable properties of silicone (e.g. high elastic modulus, durability, flexibility, etc). MREs resist environmental contamination, retain the magnetic particles well when sealed, and respond well to magnetic fields. These advantages are promising, and overcome several of the issues of using ERFs or MRFs, but once again highlight a major shortcoming; namely, that magnetic flux is required for the smart material to be of use. Delivering the magnetic flux to the material, resulting in actuation, is an ongoing investigation.

For the purpose of clarity, this dissertation will be referring more broadly to magnetic elastomers (MEs): elastic, magnetic smart materials designed to respond to magnetic fields which affect their geometry, as well as their rheology and electromagnetic properties. In the following section, we discuss the historical use of MEs in research, including previous applications and directions, before focusing on contemporary uses of MEs in soft robotic systems. We sort different types of MEs, differentiating by both application as well as materials used, and discuss future directions and opportunities for MEs in soft robotics. Overall, this review seeks to summarize and discuss the current state of work regarding MEs and their role in soft robotics, as well as identify promising research directions using MEs.

A Review of Magnetic Elastomers and their Role in Soft Robotics

Notes on Chapter 2:

This following section of Chapter 2 contains a literature review regarding the role of magnetic elastomers within the field of soft robotics. This work investigates the state of the art for these materials, describes and compares them. It identifies gaps within existing literature and highlights potential applications of MEs in soft robotics.

Authors: Nicholas Bira [1*], Pallavi Dhagat [2], Joseph R. Davidson [1]

1. Collaborative Robotics and Intelligent Systems Institute, Oregon State University, Corvallis, OR 97331, USA
2. School of Electrical Engineering and Computer Science, Oregon State University, Corvallis, OR 97331, USA

Published in Frontiers in Robotics and AI on October 23, 2020.

2.4 Abstract

Soft robotics as a field of study incorporates different mechanisms, control schemes, as well as multifunctional materials to realize robots able to perform tasks inaccessible to traditional rigid robots. Conventional methods for controlling soft robots include pneumatic or hydraulic pressure sources, and some more recent methods involve temperature and voltage control to enact shape change. Magnetism was more recently introduced as a building block for soft robotic design and control, with recent publications incorporating magnetorheological fluids and magnetic particles in elastomers, to realize some of the same objectives present in more traditional soft robotics research. This review attempts to organize and emphasize the existing work with magnetism and soft robotics, specifically studies on magnetic elastomers, while highlighting potential avenues for further research enabled by these advances.

2.5 Review of Magnetic Elastomers (MEs) in Soft Robotics

This section reviews past and current research on magnetic elastomers and their applications in soft robotics. It is structured into subsections based on material properties and characterization of MEs, elastomers made from hard magnetic particles (hMEs), as well as elastomers made from soft magnetic particles (sMEs) and their applications in soft robotics. The terms soft and hard magnetism relate to the intrinsic coercivity (H_{ci}) of these particles, i.e. the external applied field necessary to demagnetize the material (see Figure 2.1A). Hard magnets require a larger applied field to demagnetize and retain their magnetization in the absence of a field. Soft magnetic materials, in contrast, are easier to demagnetize and have a low remanence magnetization.

MEs in the literature are referred to by a variety of terms, usually depending on the application. Some of these terms include MREs, magnetically responsive elastomers, shape-programmable magnetic matter [101], or magnetoactive elastomers (MAEs) [19]. In some cases, it may be appropriate to refer to the material as an

MRE when the focus or study explicitly concerns the material properties of the ME and how to control them. In other cases, the term magneto-morphological elastomers (MMEs) may be more appropriate, as many studies concerning soft robotics typically focus on shape deformation, over material property variation. For simplicity, we refer to all of these materials as magnetic elastomers (MEs) with differentiation given for whether they utilize magnetically soft or magnetically hard particles (sMEs or hMEs, respectively).

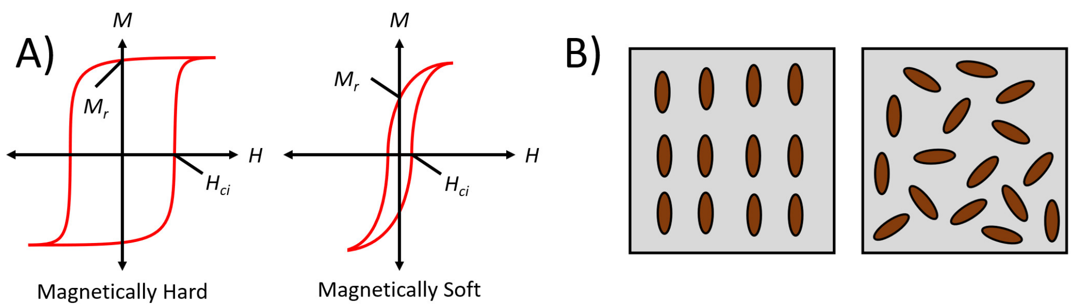

Figure 2.1: A) The magnetization, M, versus the applied field, H, for a hard (left) and soft (right) magnetic material. On these plots, M_r represents the remanence magnetization (i.e., magnetization in the absence of a field). H_{ci} represents coercivity. B) A representation of elastomers cured with (left) and without (right) an applied field during curing. Application of a field yields an anisotropic ME with particles aligned in the direction of the applied field. In the absence of a field, an isotropic ME, with randomly oriented particles, is obtained.

2.5.1 ME Material Characterization

MEs typically consist of an elastomer with embedded hard or soft magnetic particles, occasionally with other additives to achieve different performance goals [28, 50, 81, 100, 181, 39]. The elastomer, usually silicone or polyurethane rubber, is mixed with a certain volume percentage of the additives and magnetic particles. The resulting mixture is then cured, usually in a heat chamber, to prevent the particles from settling out of the mixture. Other methods for producing MEs from flexible materials involve ultraviolet curing and 3D printing, such as in masked stereolithography (MSLA) 3D printing [63]. MEs can be cured under the influence of an external magnetic field, which aligns the magnetic particles within into chains [76, 77, 25, 9]. These types of MEs are referred to as anisotropic, while isotropic MEs are cured without an external field, and have random orientation of the particles within [39] (see Figure 2.1B). In anisotropic samples, the MEs demonstrate enhanced properties, improving their responsiveness to external applied fields in the form of greater shear stresses and larger magnetic attraction forces [16, 17, 56]. Alignment of the particles under an applied field is also dependent on the viscosity of the elastomer during curing, and some research models this interaction to better predict alignment success and the resulting magnetic properties [33]. Some researchers attempted to model and predict the magnetic and physical properties of isotropic MEs [42], having some success with modeling the shear stiffness of a cylindrical ME. When subjected to a sufficiently strong external field, it is possible for an isotropic ME to become anisotropic, as the particles break their orientation and rotate within the elastomer matrix to become aligned [34]. Isotropic MEs are still being studied and characterized in various loading conditions [185], as removing the magnetization step for anisotropy in ME fabrication can improve the general utility of the material.

These properties of MEs, specifically their microstructure, have been confirmed through various methods such as scanning electron microscopy, which can show the isotropic or anisotropic arrangement [114, 50, 80, 36]. Energy-dispersive x-ray spectroscopy [114, 80] and three-dimensional nano-computed tomography imaging have also been used to validate the alignment of the magnetic particles within the matrix [36].

2.5.2 MEs in Damping Systems and Material Property Control

Research regarding specifically MREs exists primarily within the areas of vibration damping and control. The magnetostrictive (change in shape during the application of a magnetic field) properties of MREs are of interest for application in damping systems and for precision control of vibration mitigation [192]. Other research in the area of MREs and damping control include: inserting carbon nanotubes and investigating their effect on the MRE's shear modulus [190, 189], adding carbon black to enhance desirable damping properties [114], studying the impact of magnetic anisotropy on storage modulus [80], studying the impact of acetone on particle alignment and storage modulus [36], investigating the contributions of different additives such as ammonium bicarbonate on material properties [79], inspecting the impact of heat and radiation on MRE performance [188, 157], exploring the role of particle volume percentage on vibration isolation [95], testing a variable stiffness MRE spring for use in a prosthetic device [54], and creating variable stiffness and damping isolators with MREs [7].

2.5.3 hMEs and Soft Robotic Applications

The fields of bio-medicine, bio-mimicry, and robotic grasping are all targets for soft robotic research using soft actuators [52]. Within this space, there are several promising applications for MEs, specifically hMEs, to achieve manipulation and guidance of soft actuators. There has been an increase in the number of publications concerning the use of hMEs during the past few years. All of the publications involving hard magnetic particles found by the authors utilize a specific hard magnetic powder embedded in various elastomers to achieve shape deformation, namely, NdFeB. This magnetic particle demonstrates high coercivity and remanence, and MEs with NdFeB can be fabricated with domains or regions of different magnetic alignment, allowing them to change shape and orientation when subjected to a varying (both in time or space) applied magnetic field [101] (See Fig. 2.2A). These traits are utilized by research involving 3D printing of hMEs with embedded electromagnets around the printing nozzle to create anisotropic hMEs with variable magnetic domains within the soft robot [88]. The control of magnetic alignment is achieved by curing the elastomer in the presence of a magnetic field (of appropriate strength) and switching its orientation throughout the printing process to program varying domains within a single print. Specific deformations of this fabricated hME can then be achieved upon application of a magnetic field to realize complex remote manipulation and repeatable movements such as rolling, twisting and folding (see Fig. 2.2B).

Other research using similar approaches created a soft robotic swimmer composed of hMEs with varying magnetic domains. Two research groups produced millimeter-scale soft robots able to rotate, swim and roll by varying the intensity and direction of the applied magnetic field [68, 184](see Fig 2.2C). Similar research expanded upon this approach, adding a triangular tail and undulating gait behavior [103](See Fig. 2.2D). In biomedical applications, a long, thin soft microbot containing hME was guided remotely within a 3D phantom vascular network [74]. A comparable work created a steerable soft robotic wire, enabling remote guidance of this wire through tortuous and narrow paths, potentially delivering optical fibers or micro-surgical tools to locations deep within a complex network of small passages [87](see Fig. 2.2F). This opens the possibility of varied medical uses, where magnetic fields, such as those generated by magnetic resonance imaging machines, may be used to remotely manipulate a soft robot. Another approach created a wearable, magnetic skin composed of hME for multiple applications, including eye-tracking and remote gesture control when used in coordination with other sensors [3]. Remote inputs, or on-board control methods, could build on the existing control methodologies frequently utilizing standard electromagnetic motors to actuate origami soft robots [129]. Some folded, origami-based soft robots were able to achieve swimming locomotion by embedding a solid NdFeB magnet into a folded origami shape made from paper, resembling a fish [147](see Fig. 2.2E). While not elastic, the remote control aspect of a hard magnetic element embedded within a soft robot is a consistent approach. Remote manipulation of a folding origami structure was achieved by adhering permanent bar magnets to a pre-bent polypropylene sheet and applying a magnetic field [19], which the authors suggest could be applied to hMEs embedded in flexible silicone origami shapes. Recent research utilized a shape-memory polymer with magnetic materials to design a soft actuator capable of functioning as a wireless reversible bi-stable stent in medical applications [152].

Soft robotic control techniques often rely on traditional mechanisms and techniques, utilizing bulky off-board solenoids, direct connections, tethers and more. Robotic motion control utilizing magnetic materials is an area of emerging interest for applications where such bulk is impractical, for example, in guided robotic surgery or robotic exploration in confined spaces. Research is ongoing to model and analytically predict elastic deformation resulting from hME materials under applied magnetic fields [190, 189]. By developing robust models for these kinds of situations, further hME-based soft actuators and remote actuation methods can be developed for different needs and applications.

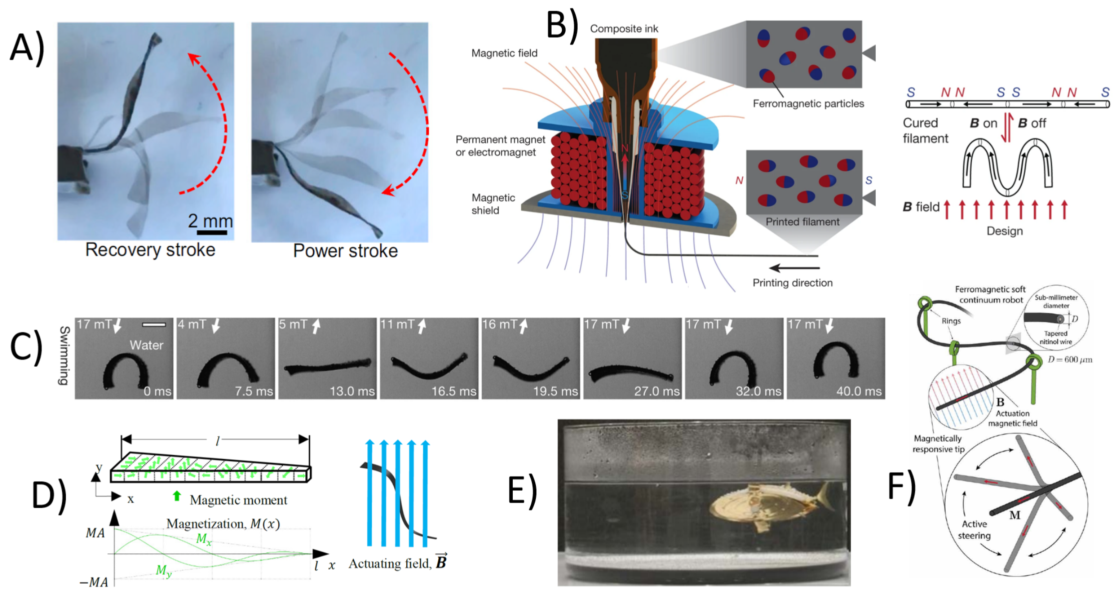

Figure 2.2: A compilation of hMEs and their soft robotic applications: A) a bending hME actuator, controlled by the application of a magnetic field [101], B) 3D printer head with electromagnet around the nozzle to program magnetic domains of the extruded hME throughout the print [88], C) soft swimmer with varying applied fields to enable shape change and a swimming gait [68], D) a triangular tail soft swimmer with varying magnetic domains to enable an undulating swimming motion [103], E) origami-inspired folded fish robot swimming utilizing remote magnetic guidance [147], and F) steerable hME-based wire, guided remotely [87].

2.5.4 sMEs and Soft Robotic Applications

While some soft robotic researchers utilize the high magnetic remanence of hard magnetic materials, other work is focused on soft magnetic powders. A common material is Fe_3O_4 (iron oxide, also known as magnetite), which is relatively inexpensive and well-characterized for its soft magnetic properties. Some initial work developed an sME created from Fe_3O_4 and sought to control its elastic modulus and shear properties with an applied magnetic field [192]. These material traits are of significant interest to soft robotics, as selectively controlling the elastic modulus of a soft material can be crucial to the overall performance and function of a soft robot. A recent publication reported on a multi-jointed laparoscopic manipulator, utilizing an sME and electromagnets to control individual joint material properties and flexion angles [90](See Fig. 2.3G).

Other researchers sought to create an actuator utilizing magnetostriction and the elastic properties of an sME, i.e., contraction of the sME when it is magnetized by an electromagnet at the center of the device [82] (See Fig. 2.3A). Beyond demonstrating that magnetostriction is possible with sMEs, this work demonstrates that sMEs are suitable for facilitating magnetic flux to flow through them when coupled with a source, and have the potential for inclusion in magnetic circuits. Other work created micro-actuators, making use of particle alignment to reversibly deform small bending actuators in the presence of an externally applied field [86](See Figure 2.3B).

Small, swimming soft robots were made with sME heads and helical flagella, which responded to externally applied magnetic fields to enable rotation of the flagella and linear swimming [186]. Other work created remotely movable micro-grippers made from sME and a thermally responsive material [117]. These grippers were positioned using external fields, and then actuated to grasp by changing the local temperature. Similarly, [151] used the heating effect of an alternating magnetic field on Fe_3O_4 to curl and grasp with a hydrogel-based sME. For terrestrial locomotion, researchers developed soft inchworm-inspired robots, capable of demonstrating an inchworm-like gait. These robots were 3D printed using MSLA

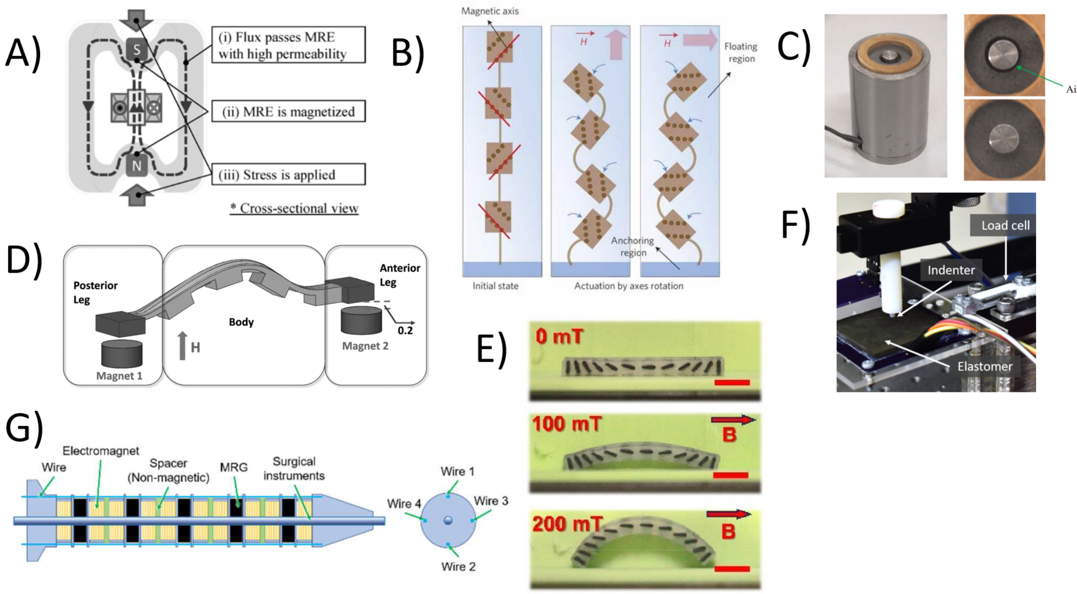

Figure 2.3: A compilation of sMEs and their soft robotic applications: A) a magnetostriction-based actuator utilizing an electromagnet core to contract the sME shell [82], B) a linkage of sMEs with aligned particles at 90 degree offsets, enabling linkage rotation depending on the direction of the applied H field [86], C) a pneumatic valve composed of an sME around a solid core [18], D) an inchworm soft robot with sME anchor points for an inchworm-like gait [78], E) an applied field causing shape deformation of embedded 3D-printed magnetic elements in silicone [123], F) a sME-based sensing skin coupled with Hall effect sensors and a neural network to localize deformations [63], and G) a variable stiffness manipulator utilizing electromagnets and sMEs to control flexion joint angles [90].

techniques, and an sME was embedded within the end effectors of the soft robot to enable remote manipulation and flexion of the inchworm robot [78](See Fig. 2.3D). Another inchworm-inspired soft robot utilized a carbonyl iron-based 3D printing filament printed into small segments of rigid, magnetically aligned regions, which were then cast in silicone to create a type of sME with distinct separation between the magnetic elements and the elastic elements [123](See Fig. 2.3E).

Researchers attempted to characterize the responsiveness of an sME to an applied magnetic field, producing an sME-based valve for controlling the flow of air

[18](See Fig. 2.3C). The resulting valve was mostly rigid, with both isotropic and anisotropic sMEs providing varying valve performances. This work demonstrated that sMEs could be used in valving systems for air, as well as for liquid valving. A comparable publication developed a ME-based pneumatic valve to control the inflation of pneumatic soft actuators, demonstrating the viability of this method for soft robotics [159]. More recently, others sought to produce a peristaltic pump, utilizing the action of multiple electromagnets compressing a tube of MRE to squeeze fluid forward [170]. The same researchers also provided a numerical analysis and framework of the performance of their designed device, attempting to model and optimize its performance [169]. Control of fluid flow was previously only realized in micro-fluidic systems, but with a similar concept of deforming an ME locally to displace fluid [64].

In a recent publication, researchers developed a soft skin comprised of sME to sense touch and local deformations [63](See Fig. 2.3F). This skin utilized an array of Hall effect sensors below the skin to detect changes in the sME as it was prodded and deformed across the surface. Based on those changes, they used a neural network to interpret the output data and reproduce the state of the contacts on the sME-based skin. Another publication developed a hME skin with permanent magnets and sensors embedded, able to sense the deformation and contact forces on the soft skin. The entire design is on flexible PCB, and represents an improvement over previous attempts [71]. [2] attempted to create a cilia-inspired sensing composite material using silicone and magnetized iron nanowires for sensing applications.

2.5.5 Analytical and Empirical ME Modeling

MEs are a complex material to study, as the behavior of the material is governed by elastic deformations, magnetic fields, and other nonlinear characteristics. Models concerning MEs primarily exist in studies about the material as a vibration or damping control device [99], with limited literature on the magnetic properties of an ME in an actuation mechanism. In general, there are several types of modeling approaches for MEs: empirical, analytical, numerical or finite element analysis

(FEA) [52]. In the following studies, MEs are modeled in different ways which involve one or several of these approaches.

One publication aimed to obtain the dependence of the natural frequency and the damping ratio of a isotropic ME structure on an applied magnetic field. To do so, they determined the shear properties (shear storage modulus and the damping factor) for damped free vibration of a system composed of a ME and a mass. MEs are expected to act within the pre-yield dynamic stress region, as the chains do not separate during deactivation of the magnetic field, unlike a MRF.

This method utilized a ME composed of silicone rubber and carbonyl iron particles with a volume fraction of about 27%. The ME was placed within a coil with the assumption that the average induction outside of the ME is proportional to the induction within. The authors explain their calculations to evaluate the properties of their ME and the magnetic flux within it as follows:

1. Magnetic resistance is defined as $R_{mi} = \frac{l_{mi}}{\mu_i * \mu_0 * S_{mi}}$, where l_{mi} and S_{mi} are the equivalent length and the equivalent cross-sectional area respectively of the magnetic circuit, and μ_i is the relative permeability of the corresponding magnetic resistance

2. The ratio of the magnetic flux of Rm1 and Rm2: $\frac{\Phi_{m1}}{\Phi_{m2}} = \frac{R_{m2}+R_{m3}}{R_{m1}}$

3. Flux: $\Phi = B * S$ (where B is the magnetic induction associated with the magnetic resistance)

4. Combining these equations together and substituting known values to solve for B_{m2}, the average magnetic induction in the MRE sample. The value for B_{m1} is measured using a Hall Sensor.

They model the vibration of the mass and MRE as a spring-mass damper system, with single degree of freedom and general solution of the form $X(t) = A * exp(-\xi * \omega * t) * sin(\sqrt{1 - \xi^2 * \omega * t + \varphi})$. The authors continue, relating the strength of the field to the relative change in strength of the modulus. Their findings indicate that the field-dependant modulus of the MRE is proportional to the applied magnetic field. Additionally, they found the damping factor to be independent of the the magnetic field, and attributable to the elastic silicone rubber alone. This approach introduces a large number of important variables and equations to consider during the design of mechanisms based on MREs, including magnetic flux, magnetic resistance, the permeability of magnetic resistance, and magnetic induction. Also of note was that the magnetic saturation of the MRE occurs eventually, around an induction value of around 800 mT in this case. The choice of magnetic particles, and the ratios of particles to elastomer, will dictate this maximum saturation.

Another publication sought to define the modulus of an isotropic MRE under different loading and orientation conditions [154]. In these scenarios, a cube of the same material was compressed and the isotropically aligned particles were oriented differently to examine the impact the relative directions can have. The greatest effect was observed when the applied field was found to be parallel to the particle alignment. The authors approximated the elastic modulus as the following equation, where the 1/3 value comes from an approximation of the experimental data by Hooke's Law with Young's Modulus $E = 3G$, δW_{el} = the change in strain energy density function for an ideal network, and $\delta\lambda_x$ = the change in the principal deformation ratio along the x-axis:

$$G_0 = \frac{1}{3} * \lim_{x \to 1}\left(\frac{\delta^2 W_{el}}{\delta\lambda_x^2}\right)$$

The amount of excess modulus that is induced by the magnetic field was defined as G_M^E, and depends on the concentration of the particles and the strength of the applied fields. The authors expressed the elastic modulus measured under uniform external field as the sum of two contributions: $G = G_0 + G_M^E$. When the applied stress, columns of aligned particles, and the magnetic field are all aligned, this value was on the order of 32 kPa. with 30 wt%. Overall, this approach demonstrated an analytical method of characterizing the effects that particle orientation and magnetic field orientation have on the change in the modulus of the MRE material.

Approximating the modulus is significant for future work seeking to model the deformation of an MRE with a known composition and magnetic field orientation.

A computational analysis approach accounted for the geometric micro-scale properties of MREs to predict behavior [106]. They highlight how modeling approaches to MREs are generally either from a microscopic scale on particle-interactions or from extrapolating macro-scale properties from energetic terms [35, 60, 72, 76, 120]. They claim this approach to be inadequate, since it approximates each magnetic particle to be a point dipole, which only applies if the MRE is dilute. The authors point to other publications [49, 76] as using a homogenization scheme which allows for the consideration of each component of the MRE separately. This opens up study of the influences of these on deformations independently. The authors modeled anisotropic as well as isotropic behavior for structured and unstructured MRE particle arrangements. This computational approach was informative in its commentary on other modeling methods, as well as its consideration of the micro-scale and different particle arrangements.

2.5.6 Finite Element Analysis and Numerical ME Modeling

One publication argues that the effective magnetic permeability of MREs can be approximated with Maxwell-Garnet equations [183], and that these properties behavior linearly. These equations have the advantage of reducing a physically varied MRE to a homogeneous medium, making it far easier to approximate properties for modeling [104]. The authors also claim that this only applies when the applied magnetic field is held stationary, and that if it is alternating or rotating, nonlinearities accumulate that cannot be ignored. The authors explore the magnetic and material properties of an MRE using 1D alternating and 2D rotating magnetic flux density excitations with a single sheet tester [191]. This method used a numerical averaging method to eliminate angular error, as well as correct for the effects of the internal field during rotation. Incorporating the orientation of the magnetic field and its interaction with the MRE into models of MRE deformation is valuable for scenarios where an MRE may be in motion through a changing magnetic field.

In a different approach, a master's thesis from Penn State created MREs, which the author designates as magneto-active elastomers (MAEs), and used finite element analysis (FEA) to predict and model the potential deformations of the custom MAEs [140]. His fabrication method for MAEs uses hard-magnetic particles of Barium-Ferrite instead of the more traditional soft-magnetic particles of carbonyl iron used in MRFs or MREs. The author created folding actuators, where each isotropic sample of MAE was adhered to a continuous piece of silicone in antagonistic positions corresponding to their particle alignment. The magnetic field was oriented from the side, causing the entire apparatus to shrink in length as the MAEs attempt to rotate to align with the magnetic field and pull on the length of silicone, folding it slightly. FEA was performed using Comsol, and used the Maxwell stress tensor applied as a traction boundary condition for the regions where the MAEs and the non-magnetic silicone were adhered. The differences between observed and modeled deformations were attributable to assumptions made in the FEA about the perfect alignment and dispersion of magnetic particles within the MAE. Additionally, the parametric curve fitting used during the FEA was approximated point to point, and does not solve and overarching equations which dictate the true behavior.

Another paper noted that while many other publications formulate theoretical models for their specific test scenarios, those models are generally specific to the type of MRE they use, which include the material composition, the general macro-scale shape of the MRE sample, and the test arrangement. [84] attempts to reconcile some of these differences by using FEA on both macro- and micro- scales to create better models which include the micro-scale structure in the macro-scale simulation. They found that the magnetic fields within and without the specimen have differing effects on the shape change, which should incorporated into future computational models of MREs. The authors demonstrated it is possible to reconstruct the stress state of an MRE sample using Maxwell tractions at the boundary [23], but is limited by assumptions of homogeneity and shape. This is valuable for possible FEA of MREs, as it provides a useful approach which redeems many of experiment-specific approaches used previously. It also demonstrates that simpler models of homogeneous MRE behavior is still useful, if extra care is taken in the fabrication to produce close to ideal materials.

Other researchers created a hybrid MRE, with magnetorheological fluid (MRF) embedded within an elastomer in different positions using 3D printing [6]. To evaluate the viscous damping coefficient C_{eq} for this material, the authors used its relationship with the energy dissipated per cycle $E = 2\pi^2 f a^2 C_{eq}$. In this equation, $f = \omega/2\pi$ is the sinusoidal frequency in Hz, ω is the angular frequency in radians and a is the strain amplitude in m. The energy loss under a stress-strain loop was found using numerical integration with a trapezoidal rule [53]. The dynamic stiffness was calculated from the slope of the stress-strain loop. Overall, the researchers found that their approach for a 3D printed hybrid MRE yielded higher damping capacity than standard MREs. This methodology is significant as it provides another approach toward understanding the material properties of an MRE by examining energy dissipation. Models of MRE-based mechanisms could monitor energy loss in their system to predict material parameters such as viscous damping.

MEs have many material properties that are specific to the different compositions of magnetic particles and elastomers they are comprised of. Analytical models for how magnetic fields are felt by the ME and provide insightful relationships between the particle sizes, particle densities, and magnetic intensities. Modeling these materials is generally experiment specific, but a decent body of work exists which indicates that FEA is possible for MEs when the ME is prepared with care and the geometric properties are well-defined.

The prior work discussed in this paper highlight a variety of significant research into the nature of MEs and their applications. More recently, MEs have begun to make their way into soft robotics publications, demonstrating unique solutions to broader soft robotic issues. Utilizing hyperelastic materials as the basis for soft magnetic hybrid materials enables unique applications within soft robotics and related fields. Molding MEs into deformable shapes through casting or 3D printing enables novel deformation and actuation driven by magnetic fields. Embedding MEs into soft robotic systems draws closer to realizing fully soft, flexible, and tetherless robotic systems with diverse applications. A summary of the various works described in this paper can be found below in Table 1.

2.5.7 Research Directions, Paths Forward

Given the research discussed in this paper, there exist multiple paths forward for further developments. The development of MEs containing both hard and soft powders with different properties will enable more unique electromagnetic applications. One direction would be to create deformable electromagnets, with sMEs providing the core, and flexible windings made of wire or liquid metal providing current to generate a magnetic flux. Such a mechanism would enable the generation of magnetic fields within a soft robot, as opposed to relying upon the application of a distant external magnetic field. This reliance upon an external field is currently one of the largest drawbacks for soft robotics, as while it does succeed in wireless control and actuation, it only does so within highly constrained systems (see Fig. 2.4A). Generating magnetic fields from the soft robot itself opens the path many important robotic actions, such as self-sensing, magnetic coupling with other systems, controlled local deformations, and more.

Electropermanent magnets could also be developed, utilizing both a sME and hME to create the on-off properties of an electromagnet and the persistent properties of a permanent magnet with remanent magnetization. Controllable magnetic fields arising within a soft robot could be used for soft robotic valve control, gating the flow of pressure through a system. This could be accomplished through a physical valve, collapsing or pinching shut, or possibly with the use of MRFs, stopping their flow through a system when exposed to a magnetic field. This was demonstrated recently with hard electropermanent valves and MRFs to create a jamming MRF valve, and could feasibly be expanded upon to allow for fully soft electropermanent magnets made from sMEs and hMEs performing the same action ([96]) (see Fig. 2.4B).

Table 2.1: MEs in Soft Robotic Applications

Application	Magnetic Material	Authors
sME Actuator	Carbonyl Iron	[82]
Rheology Control	Carbonyl Iron	[80]
Micro-wire Steering	NdFeB	[74]
Micro-wire Steering	NdFeB	[87]
Rotation of Flagella	Cr/Ni/Au Trilayer	[186]
Controllable VSDI	Carbonyl Iron	[7]
Actuator Positioning	Fe_2O_3	[117]
Origami Folding	Bar Magnet, NdFeB	[19]
Origami Fish Steering	Bar Magnet, NdFeB	[147]
Inchworm Control	Black Iron Oxide	[78]
Inchworm Control	Carbonyl Iron	[123]
Inchworm Soft Robot	MRF (Iron)	[69]
sME Air Valve	Carbonyl Iron	[18]
sME Flexing Joint	Carbonyl Iron	[90]
3D Deformable Structures	NdFeB	[89]
Elastic Beam Deformation	NdFeB	[102]
Millimeter Unthethered Swimmers	NdFeB	[184]
Millimeter Unthethered Swimmers	NdFeB	[68]
Millimeter Unthethered Swimmers	NdFeB	[103]
Variable Length Linkages	Superparamagnetic Fe_3O_4	[86]
Magnetothermal Shape Change	Fe_3O_4	[151]
Sensing Tactile Skin	Nd-Pr-Fe-B	[63]
Sensing Tactile Skin	Iron Nanowires	[2]
Sensing Tactile Skin	Iron Nanowires	[2]
Wearable hME Skin	NdFeB	[3]
Peristaltic Pump	Carbonyl Iron	[170]

A soft robotic gripper could be made from an elastic electromagnet and a hME, which pinches shut when turned on, grasping objects. Solenoids could be created from flexible wire or liquid metal embedded within elastomers, as this has been shown to be effective for creating flexible circuit elements within elastic substrates

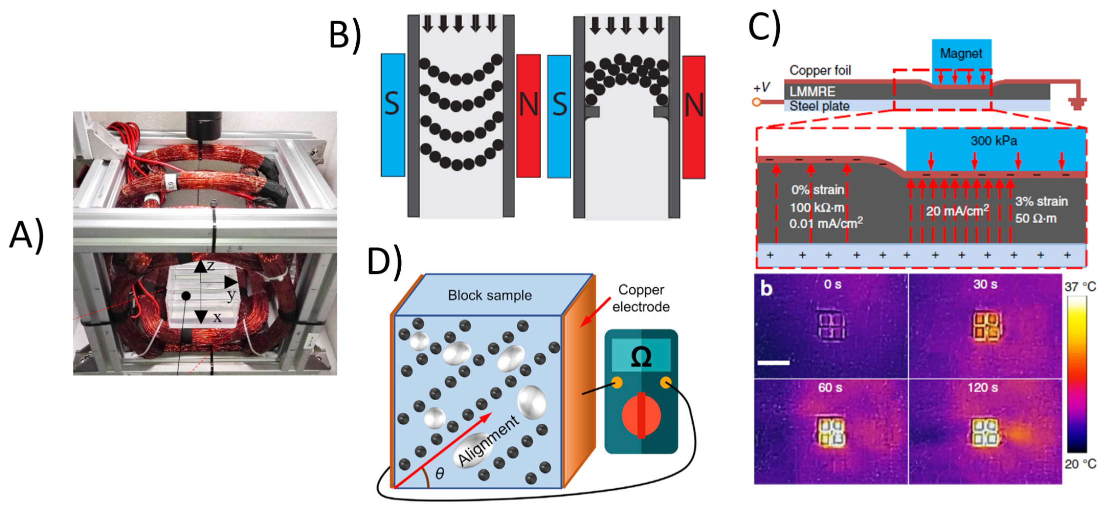

Figure 2.4: A) Large, bulky magnetic field generators necessary for the control of small soft robots comprised of MEs ([103]), B) a rigid MRF valve, showing both traditional and jamming designs ([96]), C) a magnetically-selected sME-based joule heater ([179]), and D) an anisotropic hybrid sME with varying resistivity and piezoelectric properties based on the anisotropy angle of the magnetic particles ([180]).

([14]). These embedded solenoids could measure the state of a deforming soft robotic tentacle as it moves in space, measuring the changing remanent magnetism. These values could be fed into neural nets to better interpret the physical state of the robot ([63]).

The elastic properties of MEs could also be utilized to generate varying magnetic fields arising from the expansion or compression of the source material. An anisotropic hME with a remanent magnetization could be modulated by its changing shape, allowing for a device where the expansion of the hME directly impacts its magnetic attractive force to other magnetic elements. Most of the research discussed in this review focuses on flexibility or rheological control using external fields, but few attempt to control the electromagnetic properties of the ME through its deformation. Research has shown that the relative positioning and angle of the magnetic particles greatly impacts the resulting magnetic properties of the ME ([57]). Some research asserts that the electrical properties of an ME are dependent on both applied mechanical and magnetic changes ([160]), and it can be assumed that the magnetic properties will similarly vary. More recently, researchers created hybrid sMEs containing both carbonyl iron or nickel particles and liquid metal (eutectic Gallium–Indium) ([179]). They demonstrated that the sME displays resistivity changes both from physical deformation as well as an applied magnetic field. Their application allowed for the creation of a selective Joule heater, where positioned magnets locally reduced the resistivity of the sME, enabling selective heating based on the positioning of the magnets (see Fig. 2.4C). In a following publication, they introduced anisotropy to their sMEs through magnetic alignment, and characterized its resistivity and piezoelectric properties in response to changes in strain for different angles of anisotropy ([180])(see Fig. 2.4D).

2.6 Conclusions

The fundamental properties of MEs are not well-documented, as many disparate areas of research utilize MEs for differing reasons. This review attempts to collect and summarize the state of known properties of MEs, as well as their applications in soft robotics. MEs are currently being used for remote actuation and positioning, damping and vibration control, soft structure deformation, and sensing modalities. Each of these functions has applications within the field of soft robotics, as well as beyond it, and advances in manufacturing techniques such as 3D printing and programmable magnetic domains during curing of the MEs continues to expand the possibilities of working with these materials. Many studies examine the rheological response of MEs to applied magnetic fields but rely on bulky and highly constrained environments to do so. Little, if any, research exists that attempts to study the magnetic response of MEs in response to dynamic physical changes. While work that analyzes the effects of particle size and concentration on the storage modulus ([17]) exists, the authors are unaware of a comprehensive comparison of the magnetic properties of various MEs, with the exception of the magnetic properties of a single hME analyzed by [190]. Characterization of various MEs, on both their physical and magnetic properties, will be a valuable starting point for future work on specific applications in soft robotics. This could inform intentional ME composition choices, instead of the occasionally arbitrary choices of a magnetic powder to develop an ME.

The authors anticipate that hMEs will continue to be chosen for remote manipulation applications such as crawling and swimming soft robots. The use of sMEs in soft robotics will also increase, as their magnetic properties are characterized and differentiated from hMEs to enable alternative sensing and electromagnetic control methods within soft robots. Until better local control mechanisms are developed, the utility of MEs in soft robotics will be limited to scenarios where highly constrained, external magnetic fields can be produced, limiting the potential real-world applications to medical and research settings. Once this significant obstacle is overcome, MEs may become much more common within untethered soft robotic systems, or in more traditional hard robotic systems where sensing and soft interfaces are needed.

In summary, while there exist many smart materials with applications within soft robotics, each demonstrate different strengths and drawbacks to being widely applicable. Highly constrained lab environments, material degradation, and extensive equipment or tools restrict the adaptation of these materials within more traditional robotic work spaces. Field activated materials, such as ERFs, MRFs or MEs, have the advantage of prior applications within rigid systems, and may more easily bridge the gap to traditional robotics. Modeling and control of these materials is possible with FEA and some analytical approaches.

Acknowledgments

The authors would like to thank the members of the OSU robotics and electrical engineering departments for their assistance in investigating current research in this field and relating to this topic. This material is based upon work supported by the National Science Foundation Graduate Research Fellowship under Grant No. 1840998.

3D-Printed Electroactive Hydraulic Valves for Use in Soft Robotic Applications

Notes on Chapter 3:

This following chapter contains a study which develops a 3D printed electrorheological fluid valve for use in soft robotic systems. It contains a characterization and flow-forward demonstration of independent soft actuator control using a custom high voltage control board. The ERF and valve flow control design can be incorporated into future soft robotic systems as an alternative hydraulic control strategy.

Authors: Nicholas Bira [1*], Yiğit Mengüç [2], Joseph R. Davidson [1]

1. Collaborative Robotics and Intelligent Systems Institute, Oregon State University, Corvallis, OR 97331, USA
2. Courtesy faculty, Collaborative Robotics and Intelligent Systems Institute, Oregon State University; Facebook Reality Labs, Redmond, WA 98052, USA

Published and Presented in the IEEE International Conference on Robotics and Automation in Paris, France (Remote) May 31 2020

Chapter 3: Smart Fluid Control Strategies for Soft Robotic Systems

3.1 Abstract

Soft robotics promises developments in the research areas of safety, bio-mimicry, manipulation, human-robot interaction, and alternative locomotion techniques. The research presented here is directed towards developing an improved, low-cost, and open-source method for soft robotic control using electrorheological fluids in compact, 3D-printed electroactive hydraulic valves. We construct high-pressure electrorheological valves and deformable actuators using only commercially available materials and accessible fabrication methods. The printed valves were characterized with industrial-grade electrorheological fluid (RheOil 3.0), but the design is generalizable to other electrorheological fluids. Valve performance was shown to be an improvement over comparable work with demonstrated higher yield pressures at lower voltages (up to 230 kPa), larger flow rates (up to 15 ml/min) and lower response times (1 to 3 seconds, depending on design). The resulting valve and actuator systems enable future novel applications of electrorheological fluid-based control and hydraulics in soft robotics and other disciplines.

3.2 Introduction

Soft robotics is a maturing field requiring improved control mechanisms to facilitate development of new actuation methods and integrated systems. The current state-of-the-art for soft robotic actuation and control is typically pneumatic or hydraulic, with the necessary valve systems for pressure regulation consisting of traditional solenoids, hoses, pumps, and pressure transducers [125]. The research described in this paper aims to expand upon these options. Here we explore and characterize the behavior of 3D printed, electrorheological (ER) fluid valves with the goal of establishing an alternative mechanism for hydraulic control for use by the soft

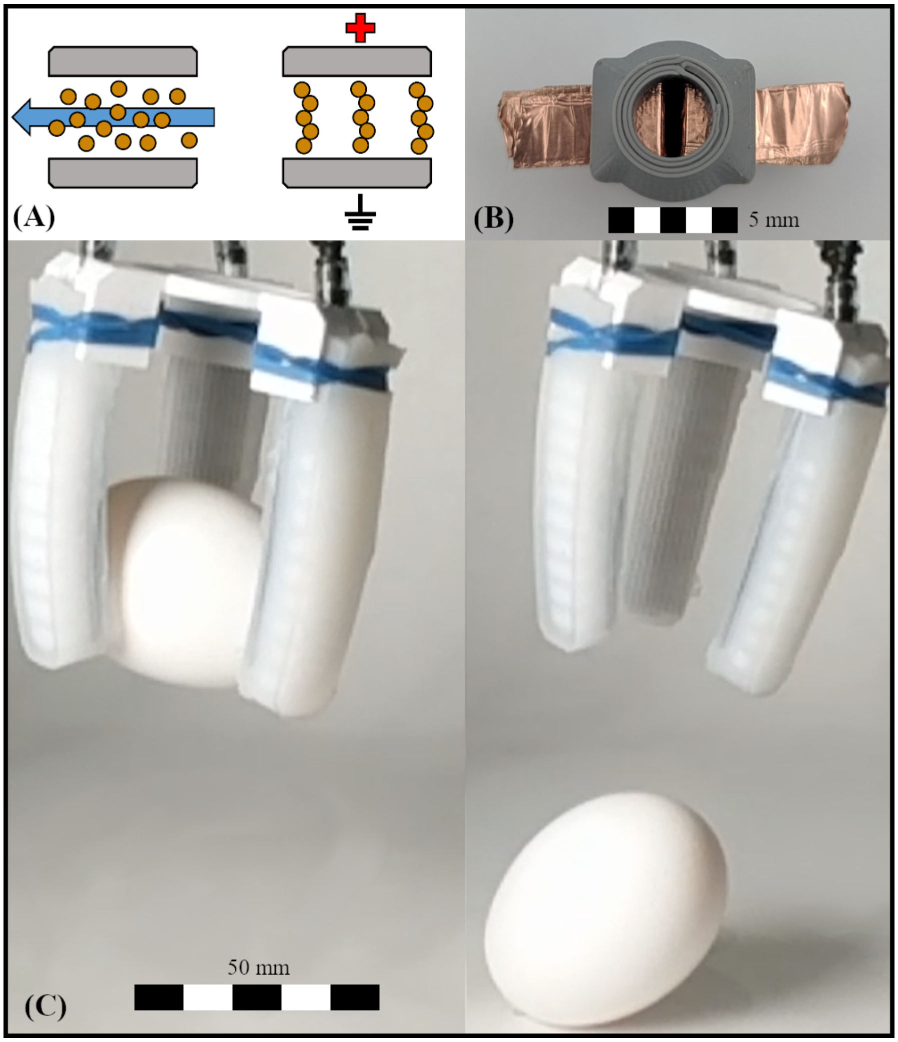

Figure 3.1: Visual Abstract: (A) The operating principle of an ER valve, where an applied DC voltage creates an electric field across the direction of fluid flow, increasing the yield stress of the ER fluid by formation of polymer-like chains and ceasing flow (B) a 3D-printed (Prusa Mk3, PLA filament) ER valve with a 1.0 mm channel gap (C) Demonstration of a soft gripper lifting and dropping an egg through controlled actuation using ER valves.

robotics community. The valves demonstrated in this paper selectively control the flow of a fluid through a system by modulating the fluid's yield stress.

During use of an ER fluid, a high voltage electric field imposed across the direction of fluid flow within a channel causes the suspended dielectric particles of the ER fluid to align and form chains across the field lines, rapidly changing the yield stress of the fluid (on the order of milliseconds [167, 165, 43, 67], see Figure 3.1A). In an ER fluid-based hydraulic valve, this change results in a cessation of flow, forming a plug and effectively creating a valve [142, 145, 62, 112]. First introduced in 1947 [167], ER fluids were originally considered for applications such as automotive braking systems [136, 61] and fast-acting valves [142], but saw little commercial implementation due to such issues as particle sedimentation and limited temperature ranges. Prior robotic applications of ER fluids include variable-stiffness fingertips [1], active dampers [149, 44], and torque control in rehabilitative devices [115, 38]. Recent improvements in material composition has produced Giant-ER fluids, which have higher yield strengths for the same voltage ranges [162].

ER fluid research, especially within the field of soft robotics, has been relatively limited in recent years. A significant drawback to using high-performing ER fluids in research is that accessing these materials is difficult due to their relative obscurity and high manufacturing costs. Research publications concerning applications of these materials has slowed in the past decade, which may be partly due to their difficulty to obtain. Despite challenges in accessing ER fluids, recent research has highlighted the advantages of robotic control with the ER fluid-based approach, but this work required sophisticated fabrication methods, materials, and industrial grade equipment (e.g. high voltage bench-top power supplies, industrial 3D printers, liquid metal, proprietary ER Fluids and 3D printing substrate compositions) [62, 182, 130]. Increasingly useful applications for robotics have been demonstrated over the years, as shown in Figure 3.2).

ER fluid valves have the potential to be widely applied in soft robotics, once the materials and fabrication methods are demonstrated to be both functional and accessible without highly specific equipment or expensive facilities. The approach described in this paper has several desirable characteristics: ease of manufacturing,

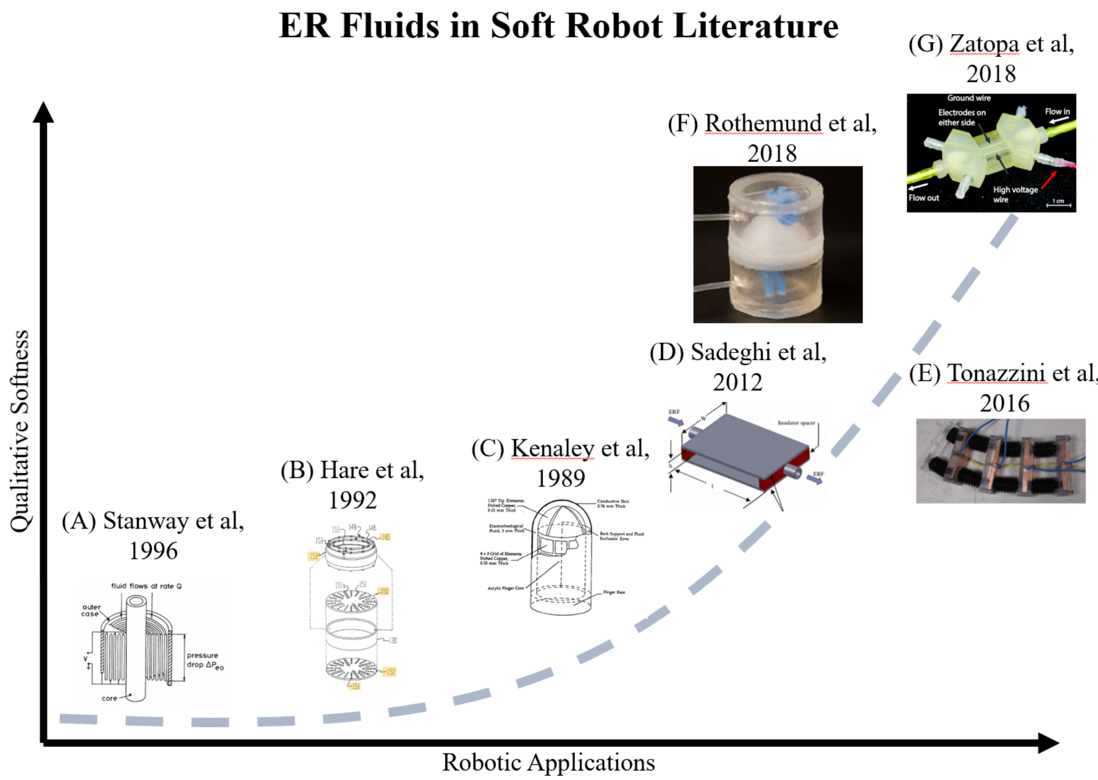

Figure 3.2: Increasing softness and robotic applications of ER fluid technology in research over the years: A) ER Fluid Flow Control: Mechanical Vibration Damping (1996) [146], B) ER Fluid Shock Absorber (1992) [61], C) ER Soft Fingertip for Capacitive Sensing (1989) [85], D) ER Fluid Soft Robotic Applications (2012) [130], E) ER Fluids in Flexible Fluidic Actuators (2016) [153], F) A Soft, Bistable Valve for Autonomous Control of Soft Actuators [128], G) Fully Soft 3D-Printed Electroactive Fluidic Valve for Soft Hydraulic Robots (2018) [182].

simplicity of design, low cost of entry, scalability, and performance. Here, we compare valve performance of different designs using the maximum sustainable yield pressure before the ER effect is overcome, the required voltage ranges, the material costs and equipment needed for fabrication, and the volumetric footprint of the ER valve itself (size). Ideally, a high-performing valve can sustain higher pressures and flow rates, at lower voltages, with a smaller form factor and at a lower cost than other designs. These criteria were adapted and added to from a previous performance evaluation of the role of electrode geometry in rigid ER valves [162].

In prior work [182], a single channel forward-flow valve was created and shown to maintain approximately 264 kPa (38 psi) at 5 kV in unflexed conditions, and maintained high pressures in the 3-5 kV range for various angles of flexion and twist. Here we expand upon that method using inexpensive fabrication methods, such as consumer-grade desktop 3D printers and casting elastomers in printed molds. We compare the performance of 3D printed ER valves with direct contact between the electrodes and the ER fluid and different channel geometries.

As part of the broad range of improving research on soft robots, electrorheological valves have been utilized as a way to provide control. Electrorheological (ER) valves operate on the application of high-voltage, electric fields; the electrorheological fluid within the valve changes viscosity and shear stress at a variety of voltages, using in the kV range [176]. These fluids can be made up of nematic liquid crystals, suspensions of polarizable particles in fluids like silicone oil, or other homogeneous ER fluids [176]. In general, ER valves are a promising method for controlling the flow through a system and enabling smaller components for use in soft robotics. There are some drawbacks regarding expense of materials, as ER fluids are difficult to manufacture reliably and most modern applications lie in braking applications in more traditional mechanical systems.

In order to simulate the flow of fluid through an ER valve properly, this work draws on previous work by [182]. In this work, the author aimed to characterize the pressure-holding capabilities of a novel soft ER valve, given a constant volumetric flow source. The author recorded the pressure data on the upstream side of the valve as a specified voltage was applied across its electrodes using a DAQ from the MATLAB Data Acquisition Toolbox. This was collected over a time interval of around 25 seconds, and the valve was characterized for its pressure holding abilities under strain. By collecting the voltage output of the pressure transducer, the author was able to show the differences in a few different shape profiles for the

ER Valve.

This was similarly done on a novel soft microgripper that utilized flexible ER valves [174, 175]. In Yoshida et al.'s work, the authors looked at the the pressure variation in a soft ER valve to be used on a soft microgripper. In their work, their DE-FERV (Divided Electrode type Flexible ER microValve) was simulated by an equation where they focus on total length, width and gap height of electrodes as inputs as well as flow rate and differential pressure [175]. By utilizing a mathematical characterization of the ER valve, the authors were able to form a basis for performance which they tested [174]. However, they did not compare their pressure to time as we saw in [182]. In this work, we use an off-the-shelf industrial ER fluid for all experiments described in this paper (RheOil 3.0; FLUDICON GmbH). ER fluids, which are essentially a suspension of small, dielectric particles in an electrically insulating carrier fluid, can be produced from cornstarch and mineral oil, but with lower responsiveness to high voltage than an industrial equivalent.

The functional design of the ER valve in this paper is partially inspired by research to produce a flexible ER valve [182]. The main contributions of this research differ from the cited work in several key aspects:

1. Faster ER valve response times, at lower voltages and equivalent pressures (voltages between 0 to 3 kV, and pressures up to 230 kPa instead of 180 kPa at 3 kV [182]).

2. Modified design including plate electrode geometry with copper tape in direct contact with the ER fluid, instead of printed features requiring extensive post processing and expensive liquid metal.

3. Faster actuator response times (on the order of 10 sec, over the prior 70 sec [182]), at lower pressures (0 to 9 kPa over 0 to 150 kPa), due to more actuators per valve, larger hydraulic diameter, higher flow rates, and use of silicone molding.

4. Use of a commercially available desktop 3D printer, instead of industrial 3D

fabrication, to allow for reproducibility in other laboratory settings that lack access to expensive, high-end manufacturing resources.

5. Use of off-the-shelf and commercially available fabrication materials, such as PLA 3D printing filament, cyanoacrylate adhesives, copper tape, and two-part silicones (Smooth-On, Dragon Skin 10), which are commonly used in the soft robotics community.

3.3 Methods

3.4 ERF Valve Design Parameters

Several key factors contribute to the performance of an ER valve:

- Electrode spacing and channel geometry (hydraulic diameter)
- Electric field strength as a function of voltage and electrode spacing
- ER fluid volumetric flow rate ($\dot{Q}$)
- The ER fluid potency/response and its composition [47, 163, 150, 144, 142, 67, 131]

Our design parameters are the following:

- The valves need to be fabricated on a desktop, consumer-grade 3D printer or similarly accessible device.
- The size of the valve should be small enough that its incorporation as a hard element into a soft robot will not impact its soft nature.
- The valve should be able to produce pressures in a hydraulic system of between 0 to 55 kPa, as this is a typical range of pressure required to actuate soft actuators [21].

3.4.1 Modeling

In response to the criteria listed in Section 3.4, design considerations resulted in each 3D printed valve having a length L of 15 mm and a height H (the width of copper tape electrodes) of 6.35 mm (Figure 3.3). To predict the behavior of the 3D printed ER valves, we drew from available literature on estimating the yield pressure of an ER valve according to hydraulic diameter and volumetric flow rate $\dot{Q}$ (m^3/s) [62]. For the valves in this paper, the hydraulic diameter is determined by H and the electrode gap W, and we vary W to change the hydraulic diameter. The values for the yield stress of RheOil 3.0 used to predict behavior were obtained from prior work [55] that experimentally characterized fluid performance in shear mode at 0, 1, 2, and 3 kV/mm.

For RheOil 3.0, τ_y values for the yield stress are assumed to be 200, 290, 400, 660, 950, 1300 and 1800 [55] (for electric field strengths of 0, 0.5, 1.0, 1.5, 2.0, 2.5 and 3.0 kV/mm, respectively). As described by [62], we can estimate the expected yield pressure P_y of a 3D printed ER valve by analyzing the global force balance on the system:

$$P_y = \frac{2 \cdot \tau_y \cdot L \cdot (H + W)}{H \cdot W} \tag{3.1}$$

Given the selected hydraulic diameters, we expected performance in the range of 10 to 80 kPa for a valve with a W-value of 0.5 mm, 5 to 40 kPa for $W = 1.0$ mm, and 2 to 20 kPa for a $W = 2.0$ mm. This predicted performance, based on ER Fluid data reported in the literature and collected in different flow modalities than used in this paper, proved to be inaccurate, and the real world performance is discussed in Section 3.5. The τ_y values reported in [55] were collected in shear mode at high shear rates, which has an impact on the accuracy of prediction when applied to our experimental data collected in flow mode [62].

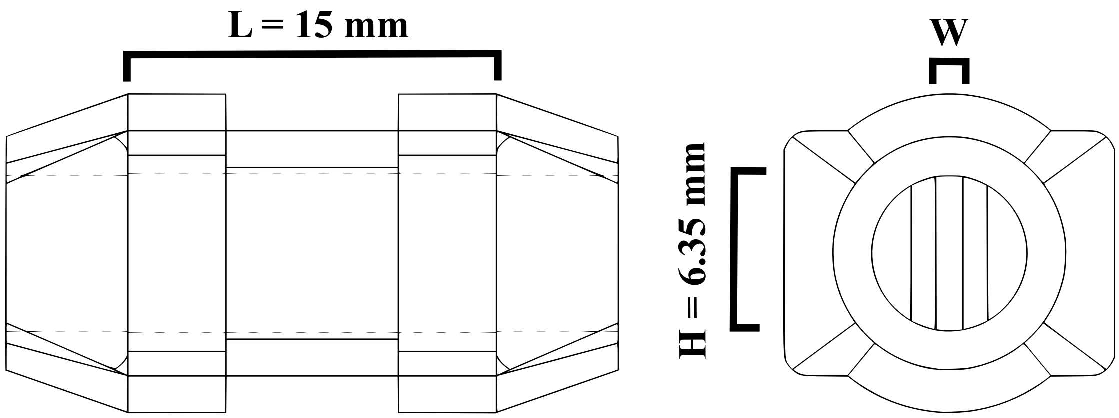

Figure 3.3: Front and side views of a CAD model (available at [15]) of an ER valve, with the electrode gap W varying between designs.

3.4.2 Valve Fabrication

To examine the effects of electrode gap W on valve performance, several rigid valve designs of varying gap were 3D printed in PLA plastic using a consumer-grade desktop 3D printer (Prusa MK3S; Prusa Research, Prague). The three electrode gaps selected for examination were 0.5 mm, 1.0 mm, and 2.0 mm. Copper tape (6.35 mm width) was used for the electrode surfaces. The positive terminal connected to a high voltage power supply, and the negative terminal connected to ground.

Each valve was connected to a syringe pump containing ER fluid. Flexible tubing with 3.175 mm inner diameter (ID) (6.35 mm outer diameter (OD)) was used to deliver the ER fluid to each valve. These tubes were placed centrally, with the copper electrodes positioned on either side of the direction of flow within the valve (Figure 3.4).

The fabrication steps for assembling 3D printed ER valves are shown in Figure 3.4. After assembly, attach one end of the valve tubing to the ER fluid supply line, and the other to an exit reservoir. Attach both positive and ground electrodes from the high voltage power supply to either end of the exposed copper loops, and allow fluid flow to reach steady state before applying voltage. This arrangement

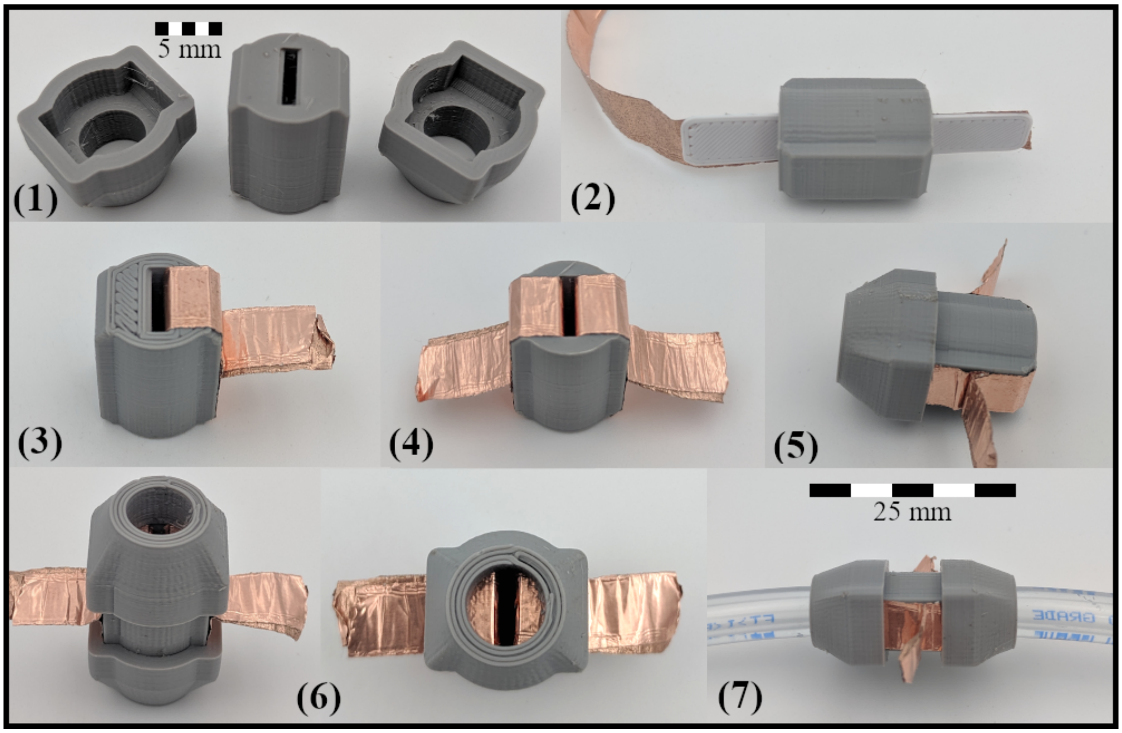

Figure 3.4: Fabrication Steps: (1) 3D print three valve components (two caps and one central piece) on a Prusa Mk3S using PLA plastic. (2) After finishing/cleaning the parts, insert a 6.35 mm strip of copper tape into the central piece, using a 3D printed shim. (3) Adhere it to one of the two flat sides of the internal chamber. (4) Repeat steps 2 and 3, smoothing any bumps in the tape to ensure an even distance between each side. Bring the equal length sides of tape protruding from each end of the central piece and wrap them back and around to make a loop. Press the tape down to the surface, so that both ends meet in the middle on the outside of the tube piece. (5) Apply a small amount of cyanoacrylate adhesive onto the central piece before pushing one of the caps onto one side of the valve, pressing it down as far as it will go. (6) Repeat with the other side, completing the valve. Each electrode tab is accessible for electrical connections, and the inlets to the valve can be seen on each side, with the flow channel running through the center. (7) Take 3.175 mm ID flexible tubing (with 1.5875 mm wall thickness) and firmly insert the desired length into each of the cap pieces (after lightly coating with cyanoacrylate adhesive) until the tubing is flush with the inner surface.

is shown in Figure 3.5.

3.4.3 Valve Testing

For the valve validation tests, a syringe pump was used to supply a constant volumetric flow $\dot{Q}$ (3 mL/min) of ER fluid into the central channel of an ER valve. The pressure within the system was monitored by an Omega PX40-100G5V pressure transducer (capable of reading from 0 to 100 psi) connected to an Arduino Uno in line with the fluid flow at the inlet of the valve. The pressure transducer output was on the scale of 0.5 to 4.5 V, and was converted in software to units of psi. The pressure readings were visually validated with a 0 to 100 psi pressure gauge. A standard bench-top power supply was utilized to output a DC voltage signal, between 0-10 V, which was then amplified by a factor of 1000 with a Trek Model 10/10BHS high-voltage power amplifier to provide the necessary voltage potential to affect the flow of ER fluid through the valve (Figure 3.5). After these tests, the effect of variable flow rate $\dot{Q}$ on valve response time was also measured using the same experimental setup, but with varying flow rates at a set voltage value (Table 3.1).

3.4.4 Actuator Fabrication and Testing

To examine the viability of 3D printed ER valves in soft robotic applications, we chose to create an accordion style actuator design that could rely on an ER fluid valve for control and inflation. This actuator design is commonly used in soft robotics, and is often referred to as a PneuNet actuator [70]. Both components of the mold were 3D printed using the same materials and settings as the ER valves (Figure 3.6A). Both actuator components were cast in the two-part platinum cure silicone material Dragon Skin 10. After curing, the two halves of the actuator and ER valve were demolded and bonded with more Dragon Skin 10 to create the final actuator (Figure 3.6B).

We performed characterization of an actuator and ER fluid valve combination

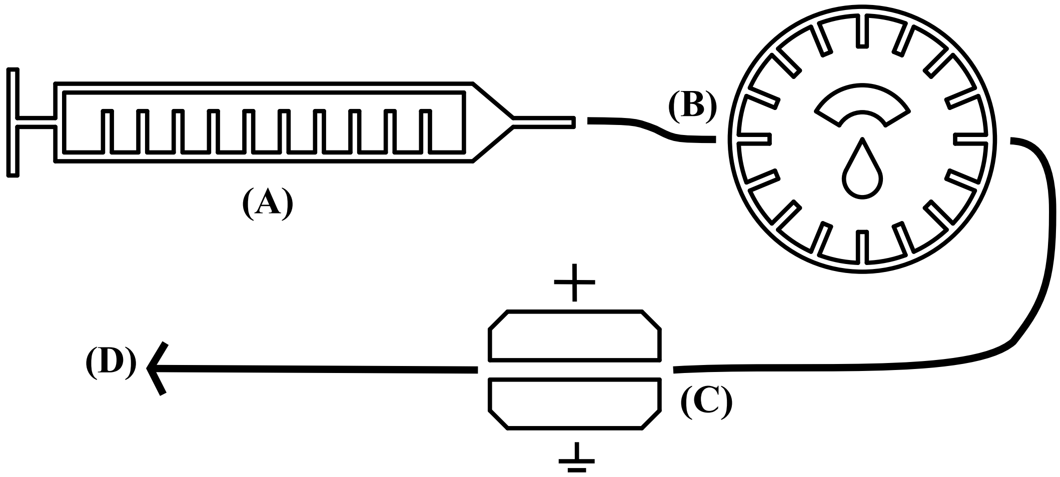

Figure 3.5: Valve validation and data collection experimental arrangement measuring performance of ER valves with different channel geometries at different voltages and flow rates: (A) Syringe pump and ER fluid-filled syringe, (B) Digital and analog pressure readings to record data and validate measurements, (C) ER valve and high voltage supply lines, and (D) Ambient pressure reservoir.

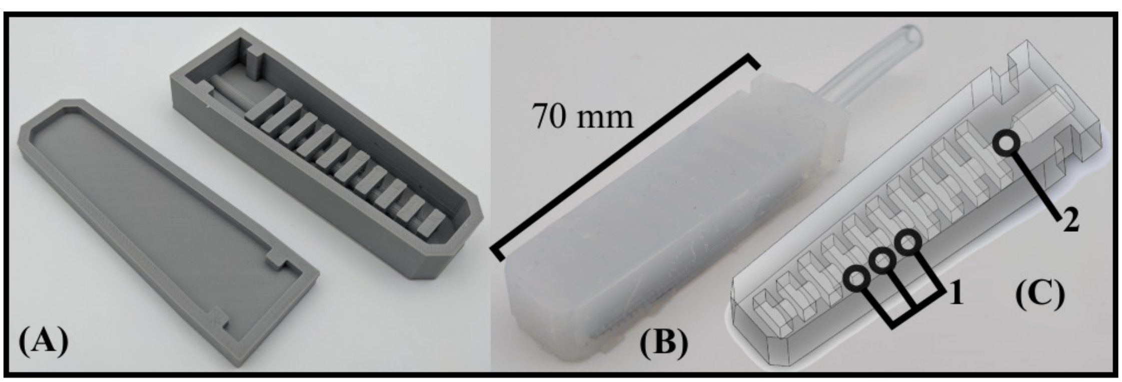

Figure 3.6: (A) The mold design for the bellows actuator, displaying interior geometry to create the designed cavities for expansion, (B) A completed and molded tentacle for use with an ER fluid valve, (C1) Three cavities of the actuator bellows, able to expand under pressure, and (C2) The inlet/outlet port for ER fluid to enter or leave the actuator. Files are available at [15].

with a blocked force test (experimental setup shown in Figure 3.7). The actuator was seated in a solid, 3D printed base and inflated at various voltage values (0 - 2 kV applied to a $W = 1.0$ mm valve), at which point the force in Newtons was recorded upon reaching steady-state. These tests were repeated for three actuators with three trials each, resulting in nine total trials displayed in Figure 3.11.

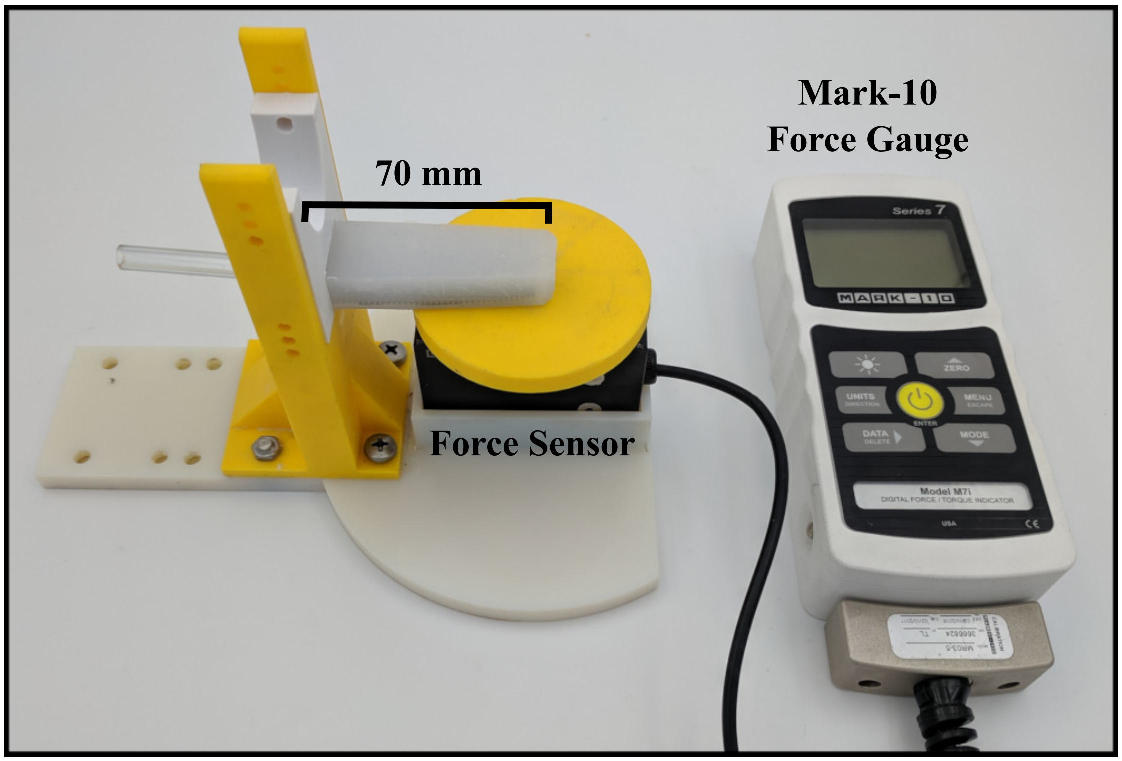

Figure 3.7: Data collection setup of actuator force output using a MARK-10 force sensor connected via USB to a laptop running MESUR Lite software (MARK-10, Copiague, USA).

After characterizing the force output of a single actuator, and choosing the control parameters for our ideal ER valve, we created a gripper apparatus (see Figure 3.8). This gripper was controlled by selectively applying 700 V across individual ER valves ($W = 0.5$ mm) using a custom two-layer PCB designed to allow for the control of multiple ER valves simultaneously with high voltage transistors as low-side switches (Figure 3.8C). When coupled with a check valve on the inlet side to prevent back flow, each ER valve controlled the buildup of pressure within each actuator. The three-actuator gripper, when programmed using an Arduino and controlled using the custom high voltage control board, demonstrated effectiveness with grasping of various objects, as shown in Figure 3.12. It was also able to selectively actuate individual tentacles based on which ER valve was active as demonstrated in Figure 3.13.

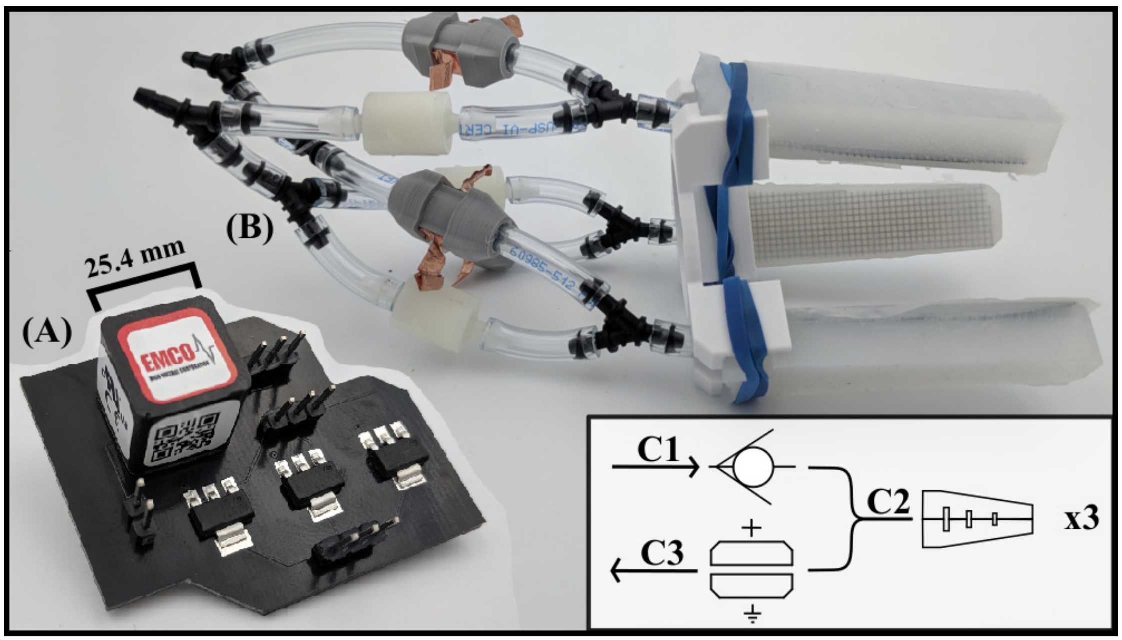

Figure 3.8: A three-actuator gripper, with each actuator controlled by a single ER valve: (A) A custom designed PCB, consisting of high voltage-rated transistors and a DC to DC high voltage converter (GERBER files available at [15]), (B) The inlets and outlets for ER fluid flow, (C1) ER fluid flows into a one-way check valve, (C2) ER fluid accumulates in the actuator, and (C3) a single ER valve controls the pressure within one actuator, allowing for actuation patterns as shown in Figure 3.13.

3.5 Results

We performed tests for several hydraulic diameters at varying field strengths. Each valve was tested three times, and each valve design utilized three fabricated instances, for a total of n = 9 for each design. The maximum holding pressure and standard deviations are plotted in the top of Figure 3.9. In the bottom of Figure 3.9, approximate τ_y values were calculated from the experimental data using Equation 3.1, providing a more accurate numerical basis for future predictive modeling and improving on the initial predictions from Section 3.4.1 of fluid properties. Results exceeded the design goal of high pressures over 55 kPa for use in soft robotics. We observed that the maximum yield pressure has larger values for smaller valve channel diameters, but with higher variability, which informed our choice of the 1.0 mm ER valve for our actuator characterizations.

After characterizing the performance of the ER valves for varying channel diameters and voltages, we examined the response time of a valve at different flow rates for a set volume of fluid. For these tests, we chose the 6.35 mm electrode width and 1.0 mm electrode gap at 2 kV. The flow rate into the valve incrementally increased from 0 to 5 ml/min in steps of 0.2 ml/min. These results can be seen in Figure 3.10. For both the 0.5 mm and 1.0 mm valve designs, strong oscillations began at 1.0 ml/min and 1.2 ml/min, respectively. The 2.0 mm valve did not oscillate at flow rates under 5 ml/min. This would indicate an important balance between the maximum flow rate through the valve and the valve's W value (and pressure holding performance).

To examine the responsiveness of the different designs, we incremented the flow rates at 5, 10 and 15 ml/min for the three valve designs. As expected, with increasing flow rates there were decreases in time needed to respond to the high voltage and reach the maximum yield pressures. Additionally, the relative time to respond went up as W decreased. The average rate of pressure increase was more similar across the valves, indicating that response time is more directly influenced by flow rate $\dot{Q}$ than by the valve design. These results are shown in Table 3.1.

The estimated power consumption of a single ER valve is approximately 14.2875

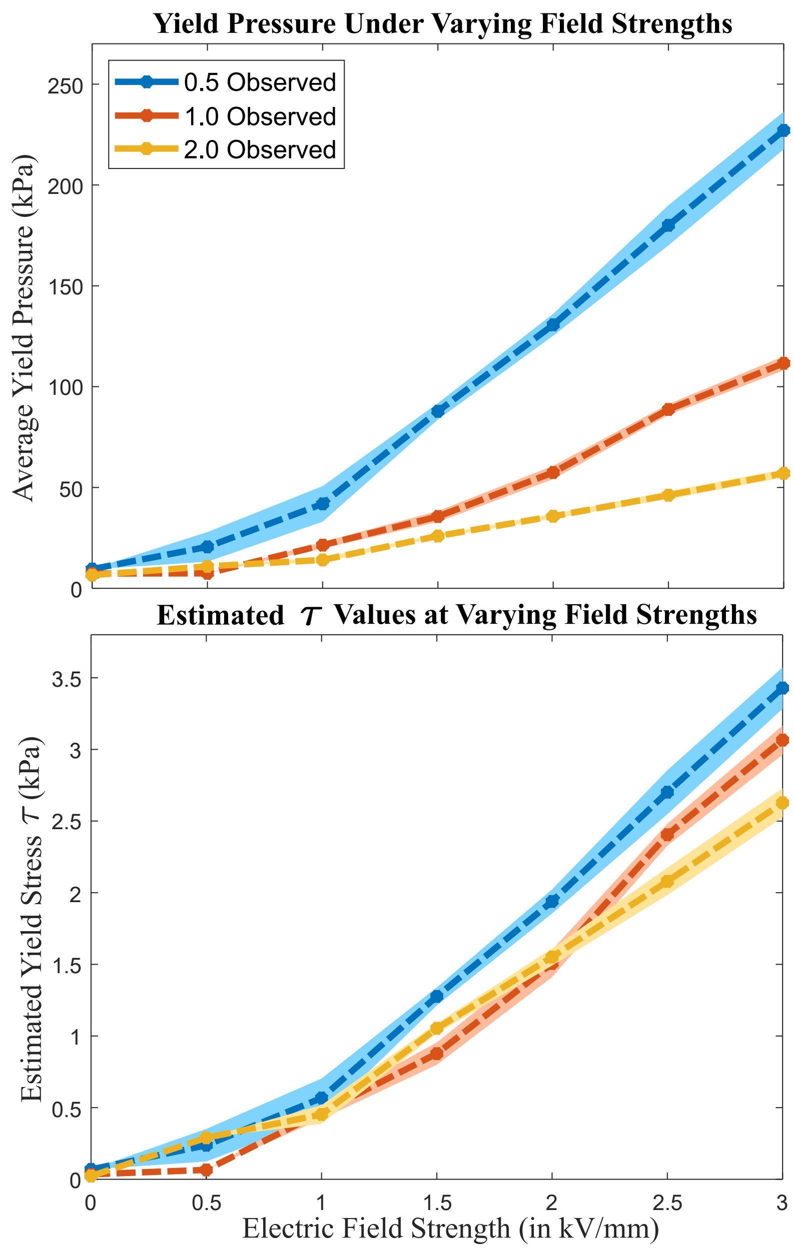

Figure 3.9: (A) Varying DC voltages and maximum yield pressures for different channel gap W. (B) Estimated τ_y values back-calculated from max yield pressures using Equation 3.1.

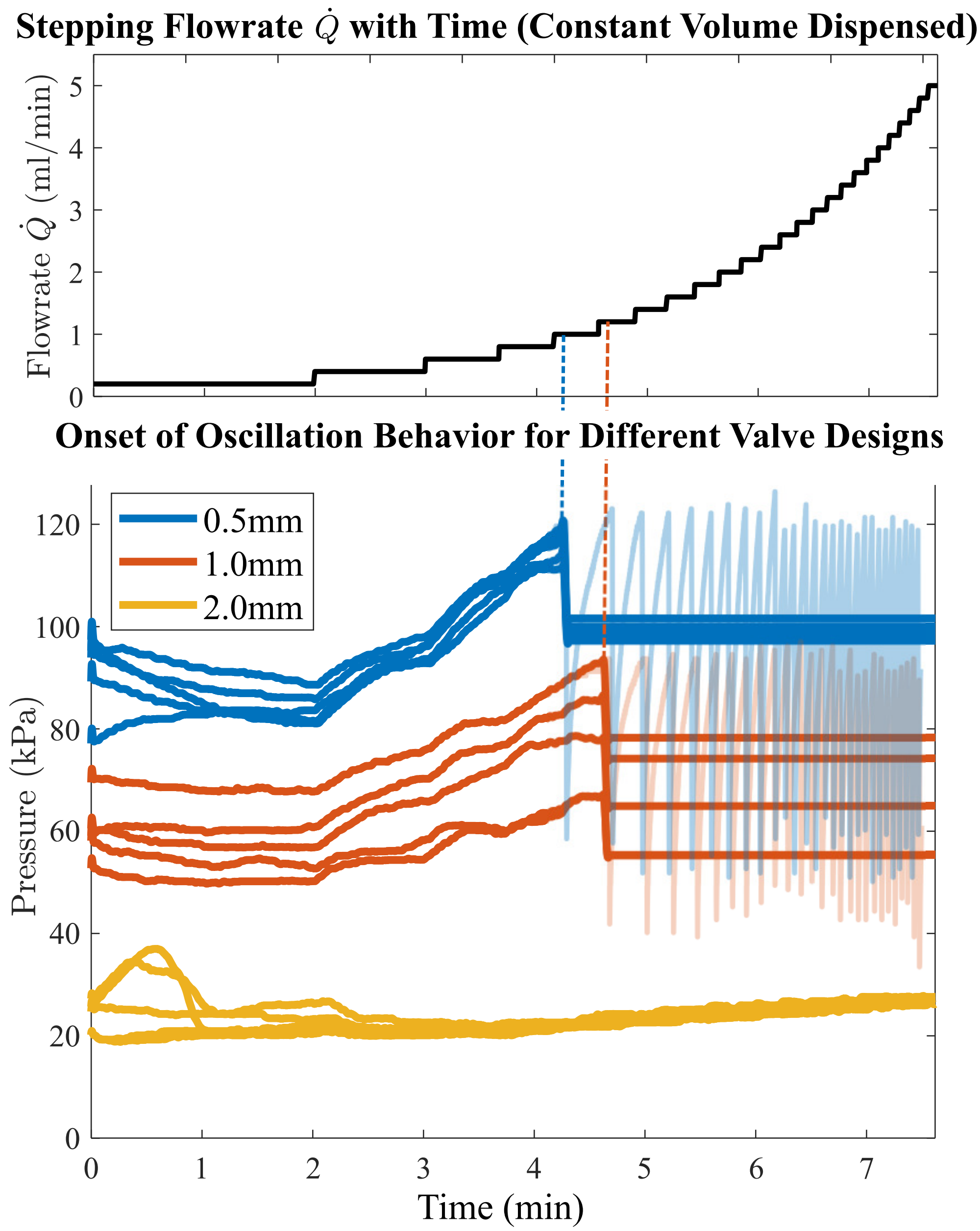

Figure 3.10: Variable flow rate tests, examining the onset of oscillatory behavior for different W values.

Table 3.1: Average 0 to 90 percent of max pressure rise times for each of three designs at variable flow rates and rates of pressure buildup.

	5 ml/min	10 ml/min	15 ml/min
0.5 mm	12.30 s	5.38 s	3.62 s
1.0 mm	9.84 s	3.30 s	2.12 s
2.0 mm	5.26 s	1.48 s	1.02 s
0.5 mm	9.46 kPa/s	20.20 kPa/s	28.69 kPa/s
1.0 mm	7.08 kPa/s	19.12 kPa/s	27.20 kPa/s
2.0 mm	5.30 kPa/s	17.82 kPa/s	25.85 kPa/s

mW, based on the estimated current density for RheOil 3.0 of 10 μA/cm^2 at 3 kV/mm (values gathered from [55]) and a surface area of one electrode at 0.9525 cm^2. While this estimate is likely under the true power consumption of a single valve, given the likely difference in current density for our fluid versus the ideal case demonstrated in [55], this conforms to the design goal of low power.

From these tests we concluded that the 1.0 mm gap valve with 6.35 mm copper tape performed optimally, balancing the necessary possible pressures for actuation, small size, manufacturability, power consumption, and required voltage ranges. Using this design, we moved forward into actuation tests. To determine actuation force, a series of voltages (0 to 1.2 kV) were applied to the outlet ER valve. This test demonstrates the average force each actuator is capable of generating, given its material composition, internal pressures, valve parameters, and design constraints. Figure 3.11 demonstrates the viability of 3D printed ER valves actuating standard soft robotics actuators. The actuator curved under pressure to different amounts based on the steady-state pressure in the system (Figure 3.11). The maximum pressure of approximately 70 kPa was chosen because the likelihood of rupture became high above 70 kPa, even though the actuators could inflate to over 100 kPa. Improvements in the design of the soft actuators or different material choices would yield higher maximum force output.

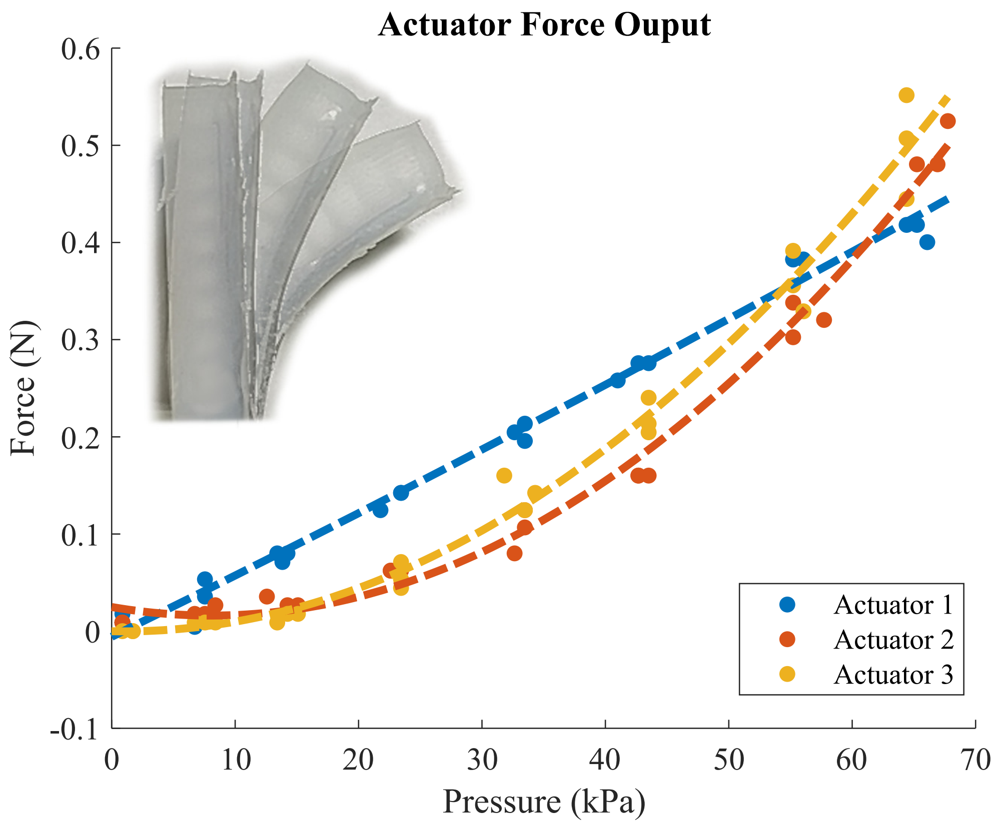

Figure 3.11: Force outputs of molded silicone actuators (n=3) paired with a single ER valve (1.0 mm) at varying pressures. The plotted lines are second-order polynomial fits, one for each actuator. Changing curvatures of an actuator under increasing pressures are shown in the corner.

To demonstrate one potential application of 3D printed ER valves, a three actuator gripper was designed with a single pressure source and addressable ER valves to perform manipulation tasks. Here, we show this gripper able to grasp 3D printed shape primitives as well as an egg (Figure 3.12). We also individually moved each actuator by energizing individual ER valves, allowing for variable grips (Figure 3.13). After all three are activated, each actuator is deactivated individually, without impacting the actuation of the other two. We demonstrate using ER valves to maintain an internal actuator pressure without an active pressure source after the flow has been switched off.

3.6 Conclusions

We considered whether ER fluid valve technology could be constructed using commonly available materials and methods, and if such devices could be implemented in soft robotic designs. Building on prior research that demonstrated the possibility of functional valves from deformable materials, we demonstrated an example of repeatable and accessible fabrication of ER fluid valves and actuators for soft robotic control.

While the work discussed in this paper describes one aspect of soft robotic control, there are still many systems and mechanical elements to improve before fully untethered soft robots can be efficient and reliable. Better comparisons between industrial and lab-made ER fluids (e.g. cornstarch and silicone oil) would be useful for evaluating performance. Lab-made ER fluids represent an appealing alternative to industrial ER fluid, and readily available materials may provide better results, as indicated by literature on the topic [93, 62]. Optimizing the valve design based on volume or baseline fluidic resistance may provide an effective cost metric to obtain the maximum possible performance for a valve printable on a desktop 3D printer. Additionally, preliminary samples of fresh industrial ER fluid resulted in pressures of over 450 kPa in a 1.5 mm test valve, which indicates the design is robust when coupled with an ideal-case fluid. The components of this study lacking accessibility for a standard research lab would be the high voltage power supply and the syringe fluid pump. Both of these devices could be replaced with simpler components (as shown by the custom high voltage PCB used in the demonstrations), especially with higher performing ER fluid which would operate under much lower electric field strengths. While the maximum feature size of the valve is limited at about 0.4 mm in diameter, due to the nozzle size of the 3D printer, smaller nozzles for detail fabrication exist (0.2 mm). This might enable even smaller feature sizes, reducing volume and increasing maximum yield pressures.

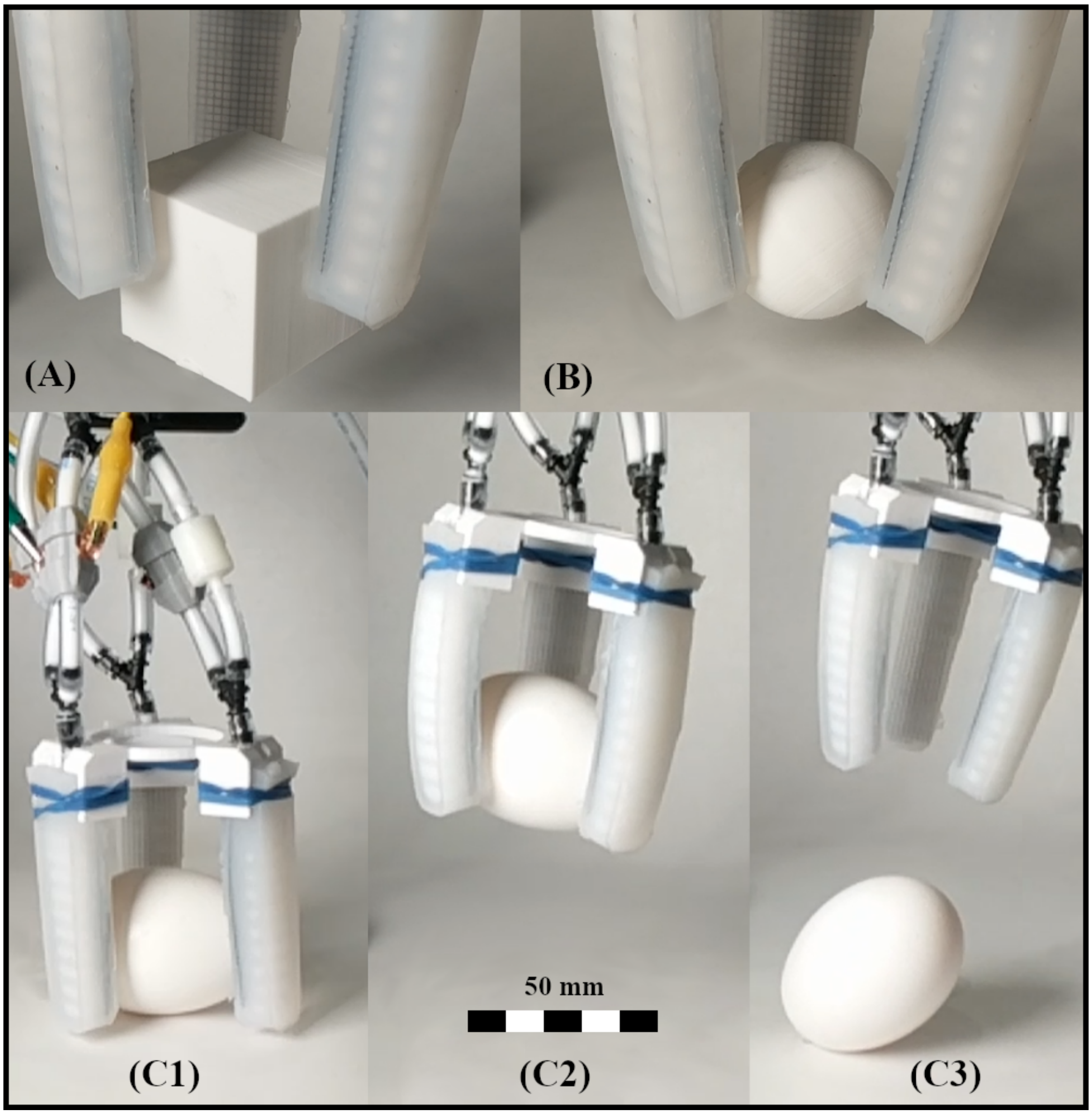

Figure 3.12: A three-actuator gripper demonstrating grasping capability: (A) Picking up a cuboid 3D printed primitive (B) Picking up a spherical 3D printed primitive, (C1), Positioning around an egg (C2) Lifting the egg during ER valve activation, and (C3) Deactivating the ER valves and dropping the egg.

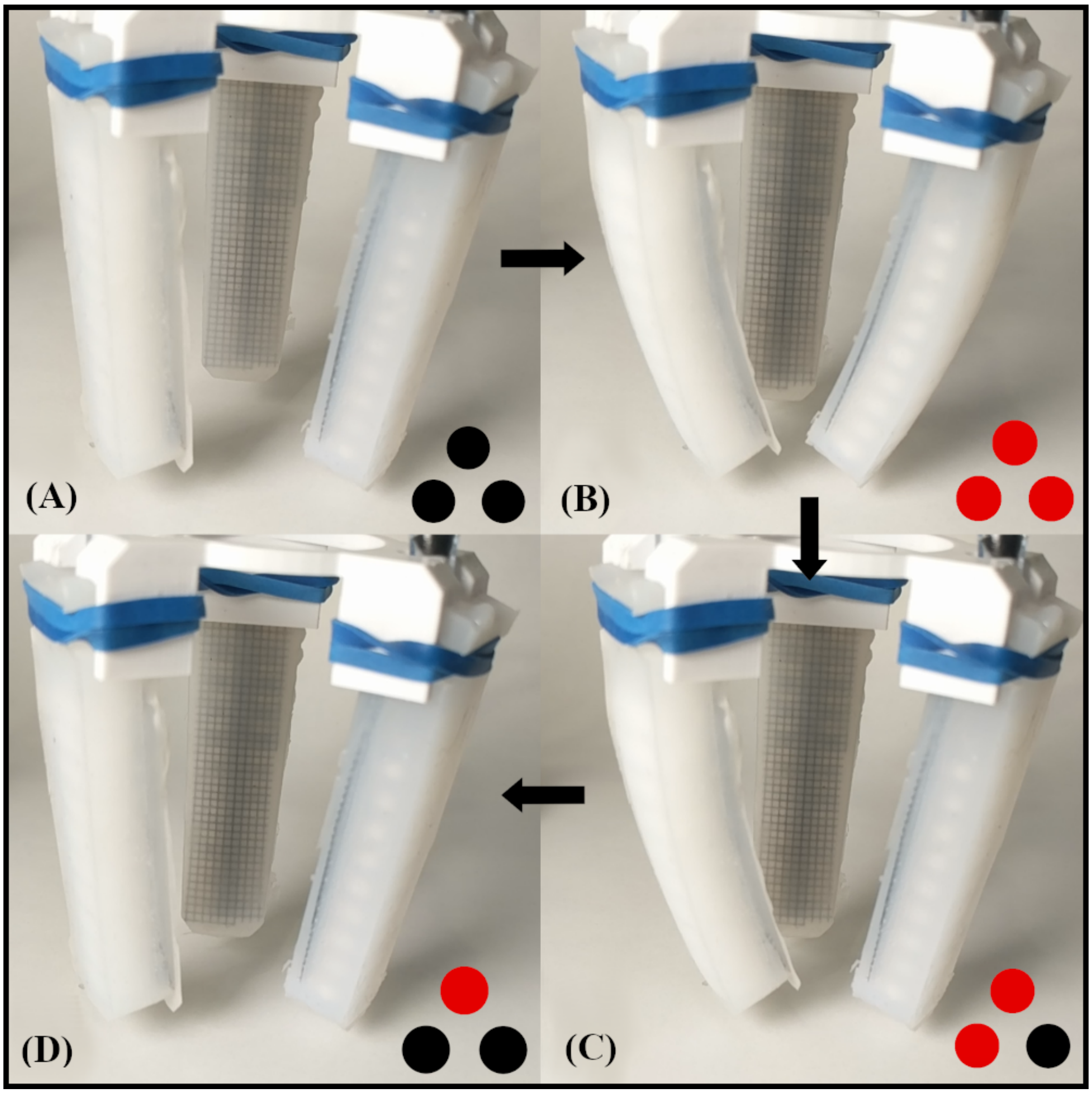

Figure 3.13: A demonstration of individual actuation using multiple ER valves by addressing every actuator all at once, and then deactivating each separately.

Acknowledgements

The authors would like to thank the members of mLab at Oregon State University for their assistance with using lab equipment and support throughout this project, in particular, Gina Olson, Callie Branyan, and Osman Dogan Yirmibesoglu.

Tuning the Grasping Strength of Soft Actuators with Magnetic Elastomer Fingertips

Notes on Chapter 4:

This following chapter contains a study which develops a magnetic elastomer and embeds it into a soft robotic gripper to enhance grip strength when coupled with permanent magnets in the palm. It contains a novel gripper design and demonstration of grip strength improvement when compared to similar scale soft grippers. The gripper design and the concepts surrounding its development can be integrated into other soft robotic systems to enable new grasp behaviors without the need for additional pressure chambers.

Authors: Nicholas Bira [1*], Pallavi Dhagat [2], Joseph R. Davidson [1]

1. Collaborative Robotics and Intelligent Systems Institute, Oregon State University, Corvallis, OR 97331, USA

2. School of Electrical Engineering and Computer Science, Oregon State University, Corvallis, OR 97331, USA

Published in Smart Materials and Structures (Volume 31, Number 4) on March 7, 2022

Chapter 4: ME-Tipped Soft Actuators

4.1 Abstract

In this work, we present an approach that uses multifunctional materials to increase the grip strength of soft grippers, while still maintaining the benefits of gripper compliance. Here, magnetic particles embedded in an elastomeric fingertip, or magnetic elastomers (MEs) are shown to increase grasping strength and influence actuation trajectories in soft robotic actuators when coupled with external magnets. Two PneuNet-style actuators with ME fingertips generated up to 45 N of holding force, compared to only 10 N without a magnet. The actuator demonstrated enhanced grip strength while the ME tip was within approximately 13 mm of the magnet. This paper characterizes numerous ME compositions and demonstrates specific applications where MEs expand upon soft robotic actuation methods. Both the opportunities as well as limitations presented by ME composition are discussed at length.

4.2 Introduction

Soft robotics presents unique advantages for applications such as grasping where the materials and geometry of soft structures enable adaptable grasps that conform to an object without prior knowledge of its precise shape. Another advantage is preventing damage, such as in agriculture, where a gentle but firm grasp is necessary to avoid bruising the produce being picked. A third advantage of soft robotic grasping is its inherent safety for use near humans, where accidental collisions or malfunctions are unlikely to result in the cuts or bruises that can occur upon collision with rigid components.

Soft robotics is a developing field seeing rapid advances in materials, mechanism and device design, and modeling and control techniques. Within the broader

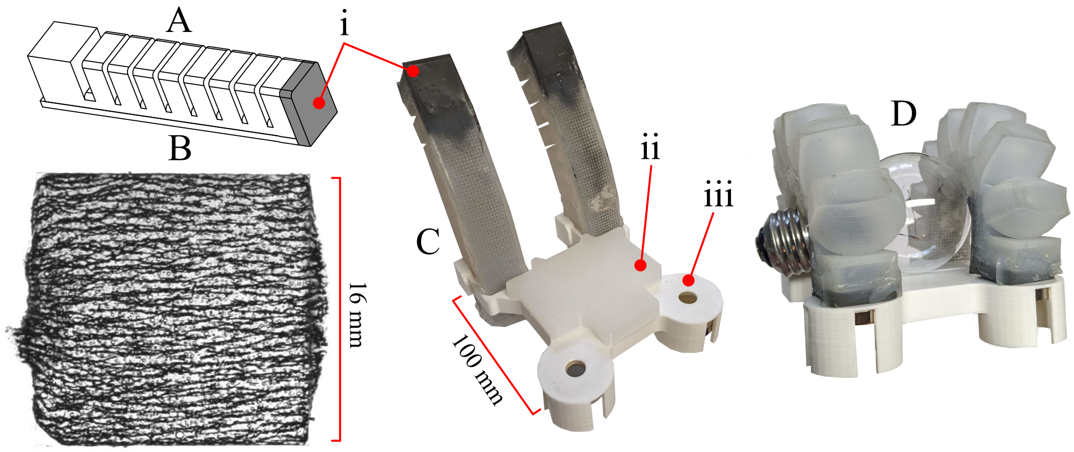

Figure 4.1: A) A 3D Model of the soft robotic PneuNet-style actuator with embedded ME in the distal tip (i). B) An optical microscope image of ME held between two glass slides, with dimensions of 16 mm on each side. The constituent iron particles can be seen to be aligned as a result of a magnetic field applied during curing of the elastomer. C) A soft robotic gripper designed with two PneuNet actuators with ME tips (i), a silicone palm for soft grasping (ii), and embedded magnets within the base (iii). A demonstration of the gripper grasping a glass light bulb without crushing.

field of robotics, soft robotics presents unique advantages for applications such as grasping where the materials and geometry of soft structures enable adaptable grasps that conform to an object without prior knowledge of its precise geometry. Another advantage is preventing damage, such as in agriculture, where a gentle but firm grasp is necessary to avoid bruising the produce being picked. A third advantage of soft robotic grasping is its inherent safety for use near humans, where accidental collisions or malfunctions are unlikely to result in the cuts or bruises that can occur upon collision with rigid components.

While soft, continuum structures have the advantages mentioned above, one major shortcoming is their relatively weak grasping strengths compared to traditional robotic grasps with rigid components and stiff actuation transmissions. Here, we define grasping strength as the disturbance force required to remove an object from a stable grasp. Actuators made from highly elastic materials such as silicone tend to demonstrate lower forces and slower deformations than actuators made from stiffer materials, relying on larger and faster changes in pressure to achieve rapid actuation or larger forces [111]. Additionally, controlling the grasping trajectories of soft actuators typically relies on adding additional pressure chambers to enable more degrees of freedom in the grasping motion. When choosing a material for a soft robotic gripper, this trade-off limits the design options for roboticists. Utilizing additional multi-functional materials presents opportunities to overcome some of these issues, by allowing designers to choose highly elastic materials while maintaining larger grasping strengths.

Many previous grasping methodologies utilizing soft actuators employ different actuator geometries or materials to control grasping strength and behavior. One approach utilized applied magnetism and soft grasping to create a suction-based gripper which can vary its stiffness by activating a magnetic field to alter the internally contained magnetorheological fluid (MRF) [92]. By varying the shear modulus of the liquid MRF, they could achieve up to 90% greater grip strengths compared to without an applied magnetic field (3.8 to 7.1 N). The suction-based design allows the gripper to unfold around the object to be grasped without having prior knowledge of its shape, and the stiffness of the MRF can be variably controlled with the applied field. Other researchers developed a rigid robotic gripper that contained adjustable permanent magnets embedded within a rigid grasping actuator to modify the initial joint flexibility [48]. On a small scale, researchers were able to fabricate a thermally-activated microgripper (3 mm in diameter) containing particles of Fe_2O_3 and move it within an aqueous medium with an external magnetic probe [22]. Recent work involving PneuNet-style actuators created a glove for human grip rehabilitation [158]. Five actuators were fabricated and placed on an inextensible layer on each of the fingers of a glove, seeking to increase grasping strength and precision by increasing the number of soft actuators used in parallel. Modeling and experiments demonstrated that the actuators were capable of a maximum grasping force of 6.4 N at a pressure of 150 kPa. These values for grip strength are similar to that of the MRF-suction gripper, and are adequate for light lifting tasks, such as the strength required to grip an apple weighing 220 grams [158]. A gripper consisting of three dual-chambered soft actuators and a textured palm was able to achieve grip strengths of up to 40 N at less than 100 kPa [193]. This relatively high grip strength was made possible by the higher pressures, fiber reinforcement, and six inflation chambers for stability. However, applications with higher pressures generally necessitate bulky compressors and tanks to generate and maintain these pressures. Some prior work makes use of reinforced soft actuators with fibers or meshes to constrain elongation and improve actuation strength [141, 143], while others increased the length of the actuator to allow it to wrap around an object and increase the contacting surface area, similar to a boa constrictor [45]. Eschewing elastomers entirely, shape-memory alloy wires have been used to enable variable stiffness and grasping strength of a flexible gripper [58]. Other recent research developed a folding-plate design with particle jamming to enable variable grasping stiffness [161].

Many robotic systems involving soft robotic actuators necessitate multiple actuators in a single device to achieve multiple degrees of freedom, such as in soft crawling or slithering robots [139, 20]. Others incorporate multiple inflating chambers within a single actuator for twisting, bending and contraction [116, 29]. These octopus-inspired actuators with many actuator sub-units achieve multiple degrees of freedom. Some approaches combine multiple soft actuators to control the trajectory of the end effector, while others incorporate left and right-handed shearing auxetics to achieve similar trajectory control or grasping [30]. Other researchers have created a soft actuator with multiple pressure chambers which deform in a specific direction based on origami-inspired folding [118]. All of these examples share in common their reliance on multiple actuators or pressure chambers to achieve a system capable of varied tip-trajectories. Increasing the complexity of a gripper with more chambers increases the complexity of the control strategies required to actuate them.

Few publications investigate the magneto-mechanical response of MEs, with most focusing on the rheological behavior of the material for use in damping systems [12]. A recent publication aimed to characterize the field-dependent Young's modulus of MEs, and developed a testing apparatus for this behavior and future studies [133]. Another publication discussed the effect of pre-strain on the resulting stress-strain relationship and magneto-mechanical properties of MEs using spherical carbonyl iron particles [155]. A separate study achieved up to 20% elongation of small ME cylinders under applied magnetic fields from an electromagnet at values of up to 400 kA/m [134]. These works touch upon several important attributes of MEs under applied magnetic fields, and begin to draw attention to the ways in which particle concentration, magnetic alignment, and magnetic particle choice each contribute to the behavior of the ME.

One specific application of a ME in soft robotics involves an inchworm-inspired locomotion strategy utilizing a soft body and ME-anchor points, manipulated with nearby magnets to create movement [78]. This approach demonstrates the viability of combining permanent magnets and MEs for controlling the movement of a soft robot. Another recent publication made a similar inchworm robot, but the authors embedded small magnetic elements with different alignments such that an externally applied field caused them all to deform and align with the field, producing an inchworm-like motion [123]. Additive manufacturing of magnetically aligned MEs containing neodymium iron boron alloy (NdFeB) allows for embedded magnetic domains which respond to an externally applied field, causing deformation and movement for various soft robotic applications [89]. These methods all demonstrate external magnetic fields modulating soft robotic behavior and performance, but none were deployed alongside more traditional soft robotic tools such as PneuNet [111] style actuators, or shown to work for grasping tasks at a larger scale.

In this paper, we describe the process by which we chose the magnetic particles for a ME, the fabrication process, and the design of a soft robotic gripper containing ME. We address the core concern of improving soft actuator grasping strength - while still retaining the benefits of the soft structure - by integrating a magnetic elastomer (ME) skin with a soft PneuNet style actuator. The PneuNet design consists of a single pressurized volume shared between multiple offset chambers, which deform elastically under increasing pressure to generate curvature in the actuator. As described in a previous review article, MEs address many of the constraints of soft robotics [12]. More specifically, our approach, shown in Fig. 4.1, is to embed an ME composite into the tip of a soft robotic actuator made from silicone (Fig. 4.1A), and then couple two actuators to a rigid base containing a permanent magnet (Fig. 4.1Ciii). This relatively small addition of the ME to the distal tip of the soft actuator results in magnetic coupling with the base during full inflation. This coupling increases the force required to overcome the grip without altering any other features of a traditional PneuNet design. We also show that by adjusting the location of the permanent magnets, the configuration of the actuated PneuNets can be tuned to create more stable grasps. While the base is rigid for positioning the magnets in the palm, we added a silicone layer to the palm (Fig. 4.1Cii) to ensure any contacts between the soft actuator and the base are fully soft. Fig. 4.1D demonstrates the capacity of the gripper to grasp delicate objects without damaging them.

During development of the ME for this application, the magnetic properties of candidate MEs are characterized by vibrating sample magnetometry (VSM), contributing to the understanding of the material and magnetic properties of MEs for future work in soft robotics. We then perform several characterization experiments with the ME-enhanced gripper prototype and demonstrate its various advantages and disadvantages. The primary contribution of this work is an approach that maintains the high elasticity and compliance of a soft gripper at low pressures, while greatly enhancing grasp strength. We then demonstrate how the trajectory of the soft actuator grasping motion can be modified by the location of magnets in the base. Furthermore, we show that grasp stability across variable object geometries can be potentially increased by controlling the location of the permanent magnets.

4.3 Background

Many previous grasping methodologies utilizing soft actuators employ different actuator geometries or materials to control grasping strength and behavior. One approach utilized applied magnetism and soft grasping to create a suction-based gripper which can vary its stiffness by activating a magnetic field to alter the internally contained magnetorheological fluid (MRF) [92]. By varying the shear modulus of the liquid MRF, they could achieve up to 90% greater grip strengths compared to without an applied magnetic field (3.8 to 7.1 N). The suction-based design allows the gripper to unfold around the object to be grasped without having prior knowledge of its shape, and the stiffness of the MRF can be variably controlled with the applied field. Recent work involving PneuNet-style actuators created a glove for human grip rehabilitation [158]. Five actuators were fabricated and placed on an inextensible layer on each of the fingers of a glove. Modeling and experiments demonstrated that the actuators were capable of a maximum grasping force of 6.4 N at a pressure of 150 kPa. These values for grip strength are similar to that of the MRF-suction gripper, and are adequate for light lifting tasks, such as the strength required to grip a apple weighing 220 grams [158]. A gripper consisting of three dual-chambered soft actuators and a textured palm was able to achieve grip strengths of up to 40 N at less than 100 kPa [193]. This relatively high grip strength was made possible by the higher pressures, fiber reinforcement, and six inflation chambers for stability.

Many robotic systems involving soft robotic actuators necessitate multiple actuators in a single device to achieve multiple degrees of freedom, such as in soft crawling or slithering robots [139, 20]. Others incorporate multiple inflating chambers within a single actuator for twisting, bending and contraction [116, 29]. These octopus-inspired actuators with many actuator sub-units achieve multiple degrees of freedom. Some approaches combine multiple soft actuators to control the trajectory of the end effector, while others incorporate left and right-handed shearing auxetics to achieve similar trajectory control or grasping [30]. Other researchers have created a soft actuator with multiple pressure chambers which deform in a specific direction based on origami-inspired folding [118]. All of these examples share in common their reliance on multiple actuators or pressure chambers to achieve a system capable of varied tip-trajectories. On a small scale, researchers were able to fabricate a thermally-activated microgripper (3 mm in diameter) containing particles of Fe_2O_3 and move it within an aqueous medium with an external magnetic probe [22]. A recent publication demonstrates different gaits for an origami-based soft robot with embedded magnets and linear magnetic fields to perform crawling and rolling [178].

Few publications investigate the magneto-mechanical response of MEs, with most focusing on the rheological behavior of the material for use in damping systems. One recent publication discussed the effect of pre-strain on the resulting stress-strain relationship and magneto-mechanical properties of MEs using spherical carbonyl iron particles [155]. Another recent article achieved up to 20% elongation of small ME cylinders under applied magnetic fields from an electromagnet at values of up to 400 kA/m [134]. These works touch upon several important attributes of MEs under applied magnetic fields, and begin to draw attention to the ways in which particle concentration, magnetic alignment, and magnetic particle choice each contribute to the behavior of the ME.

One specific application of a ME in soft robotics involves an inchworm-inspired locomotion strategy utilizing a soft body and ME-anchor points, manipulated with nearby magnets to create movement [78]. This approach demonstrates the viability of combining permanent magnets and MEs for controlling the movement of a soft robot. Another recent publication made a similar inchworm robot, but the authors embedded small magnetic elements with different alignments such that an externally applied field caused them all to deform and align with the field, producing an inchworm-like motion [123]. Additive manufacturing of magnetically aligned MEs containing neodymium iron boron alloy (NdFeB) allows for embedded magnetic domains which respond to an externally applied field, causing deformation and movement for various soft robotic applications [88]. These methods all demonstrate external magnetic fields modulating soft robotic behavior and performance.

Powder	**Maximum Particle Diameter** (μm)
Iron Filings	300
AlNiCo	44
Fe_3O_4	5
Carbonyl Iron	10
Carbonyl Iron	44
Permalloy	10

Table 4.1: Various magnetic powders investigated for the ME composite. The powders were embedded in a fixed ratio by volume in silicone and characterized by VSM. The VSM results are shown in Figure 4.5.

4.4 Methods

Before prototyping and characterizing the soft actuators, we first explored which ME composite would be most suitable for grasping. There is extensive ME characterization in the literature regarding the properties of MEs and methods to tune their characteristics. However, there is a noticeable lack of comparative analysis on MEs regarding the relative contributions of different soft magnetic particles in a given ME [12]. To investigate the effects of particle type on ME performance, we analyzed several different soft magnetic powders, at varying concentrations, with a vibrating sample magnetometer to establish their magnetic properties (Section 4.4.1). In Subsection 4.4.2, we describe experiments using stationary magnets and a material testing machine to characterize the attractive force versus strain relationship of a bulk ME sample. Section 4.4.3 describes the manufacturing process to fabricate soft actuators with ME fingertips; Sections 4.4.4 and 4.5 follow with characterization of the soft actuator performance in both grip strength and grasping slip resistance, respectively.

4.4.1 VSM Analysis and Particle Choice

For all of the powders listed in Table 1, each was mixed by hand for 1 minute into Dragonskin 10 Medium two-part platinum-cure silicone (Smooth-On, Macungie, PA) in volume concentrations ranging from 20 to 40 percent. The volume of each particle type was calculated by measuring the mass, then dividing by the density provided by the manufacturer. Each mixture was degassed for 5 minutes before being poured into 3D printed squat cylinder-shaped molds with the dimensions required for VSM analysis (height = 1 mm, diameter = 6.5 mm). After mixing and adding to the molds, the samples were placed into a curing oven at 60 °C for 20 minutes to prevent particle settling by quickly setting the silicone. The samples were then allowed to rest at room temperature overnight for full curing. For performing VSM analysis, each sample was adhered to a glass slide with Kapton Tape (10 mm width). The samples were loaded into the VSM and the magnetic field swept from 558 kA/m to -558 kA/m and back. We chose a fixed powder to silicone ratio of 0.3 (by volume) in all samples to enable a comparison of the magnetic properties and thereby, identification of the best-suited ME composition for the soft gripper. This would be analogous to comparing magnets of identical size and shape but made from different materials. For several of the powders, their apparent densities differed from their reported absolute densities. The reported absolute densities were used for calculations of volume percentage in the tested ME samples, but the effects of apparent density are discussed in Section 4.6.

4.4.2 ME Separation Force

For characterizing the attraction forces between a sample of ME and various magnetic fields, we 3D modeled and printed a testing apparatus from PET-G filament. The bottom half contained magnets of various thicknesses (between 1.5875 and 4.7625 mm) and grades (N42 and N52) and a constant diameter of 25.4 mm (1 inch, see Fig. 4.2). The sample of ME (carbonyl iron 10 μm particles, 20% volume) was placed in the top half of the jig and moved upwards, away from the interface with the fixed magnet, at a set rate of 100 mm/min. The force values were recorded with a Mark-10 Series 7 Model M7i force gauge (Mark-10, Copiague, NY) connected to the upper half of the separation testing apparatus.

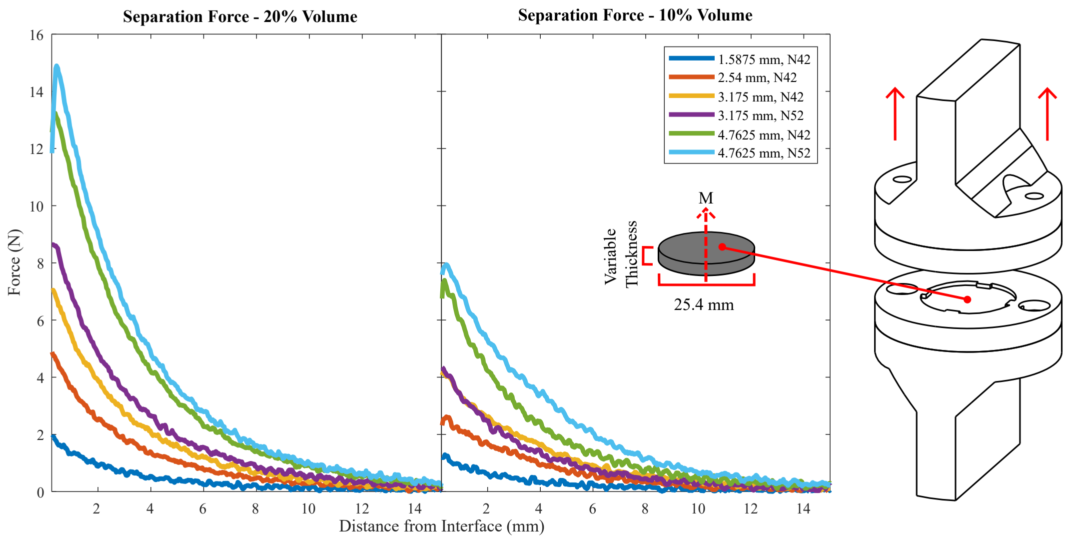

Figure 4.2: Left) The resulting force values as a function of distance from the interface of the ME (20% and 10% respectively, both 10 μm carbonyl iron particles) for various base magnets. Right) The ME (top) and magnet (bottom) separation assembly, where the top moves away from the magnet in the base.

4.4.3 Actuator Fabrication

We designed molds for a PneuNet style actuator in SolidWorks to enable embedding ME in the tip during the casting phase (Figure 4.3). Each actuator was molded with 3D printed forms made with a Prusa MK3S desktop 3D printer. The top and bottom halves of the actuator were cast from Dragonskin 10 Medium silicone. The ME tip on the bottom half of the mold was mixed from 10 μm carbonyl iron powder (Millipore Sigma, St. Louis, MO) at a concentration of 25% by volume with Dragonskin 10. This particle choice and concentration was found to be best suited for the gripper application (see discussion on magnetic particle properties

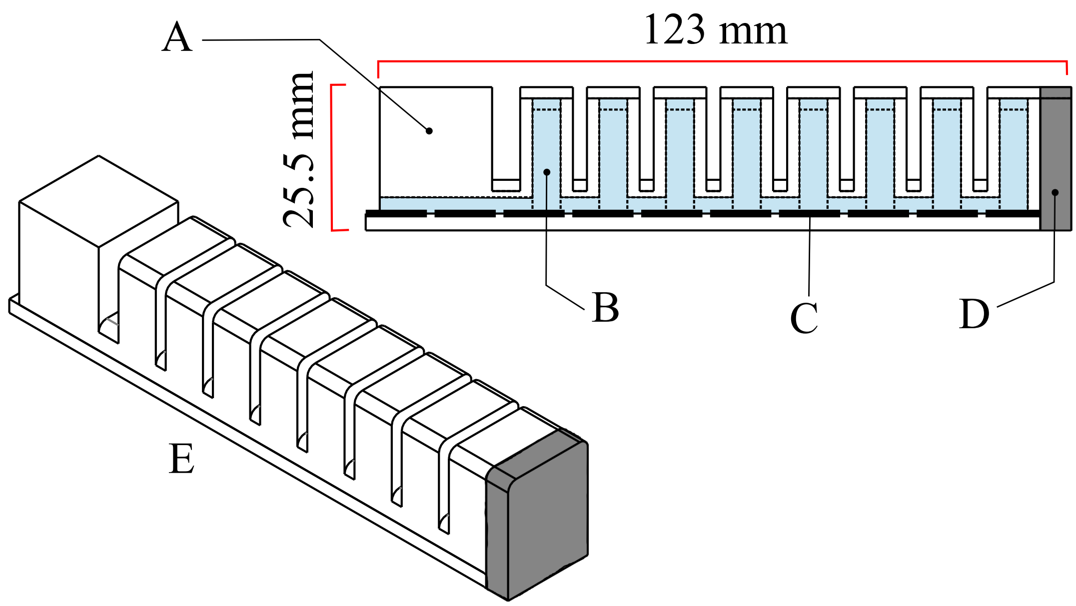

Figure 4.3: Fabrication of the PneuNet-style actuator with ME tip A) Dragonskin-10 body B) Pressurizable air chamber for generating actuation, with eight sub-chambers to generate curvature C) Inextensible, flexible mesh layer D) Iron particle and silicone ME tip E) Isometric view of completed actuator

in Section 4.6.1 and Figure 4.5). The ME was poured into the distal tip at the same time as the bottom half was poured, and an inextensible mesh layer was added to the bottom layer to reinforce it during actuation. After curing for 24 hours, the two halves were aligned with a third 3D printed mold, and a thin layer of additional Dragonskin was used to bond both pieces at the interface. After another 24 hours, 3.175 mm diameter tubing was inserted into the base and glued in place with Sil-Poxy (Smooth-On, Macungie, PA).

4.4.4 ME-Assisted Grasping Strength

To characterize the grasping strength of an ME-tipped PneuNet soft actuator, we manufactured two actuators in the same style as previously discussed. Each was placed in a rigid base, and connected to the same pressure source. During testing, the actuators were pressurized to 27.6 kPa (4 psi), and various 3D printed rigid geometries, which were initially enclosed by the pressurized actuators, were lifted upwards with the Mark-10 testing machine at a rate of 100 mm/min. For the data shown in Figure 4.6, rigid objects with four different cross-sectional profiles were used: a half-circle of 30 mm diameter, a half circle of 40 mm diameter (Fig. 4.4B), a three-quarters circle of 40 mm diameter, and a whole circle of 40 mm diameter (Fig. 4.4A). These various shapes provided a smooth contour for the actuators to wrap around and hold while the objects were pulled vertically. For each object, three magnets (N52 grade) of different thicknesses in the base generated different magnetic attraction force values.The compliant silicone palm shown in Figure 4.1C was excluded from this characterization, since the palm did not interact with the force measurement apparatus lifting upwards.

4.5 ME-Assisted Slip-Resistance

For the measurement of slip resistance, a similar test arrangement was used, but the 3D-printed object (with a circular profile) was oriented vertically instead of horizontally to the grasp. In this way, the cylinder slid out of the fingers, instead of pulling against them (Fig. 4.4C). Two cylinders were used, with 35 and 40 mm diameters. A single magnet, the strongest used in previous tests, (4.7625 mm thickness of grade N52) highlighted the extent of magnetic enhancement on the slip resistance and its relationship with the cylinder diameter. For these tests, the silicone palm was also excluded to place emphasis on the interaction between the actuators and the moving object. The results of these tests are shown in Table 4.2.

4.6 Results and Discussion

The actuators tipped with an ME skin showed increased grasp strength, demonstrating the efficacy of such an approach. Our initial tests of actuator grip strength (without magnets) demonstrated peak forces of $\sim$10 N at 27.6 kPa (4 psi) for a

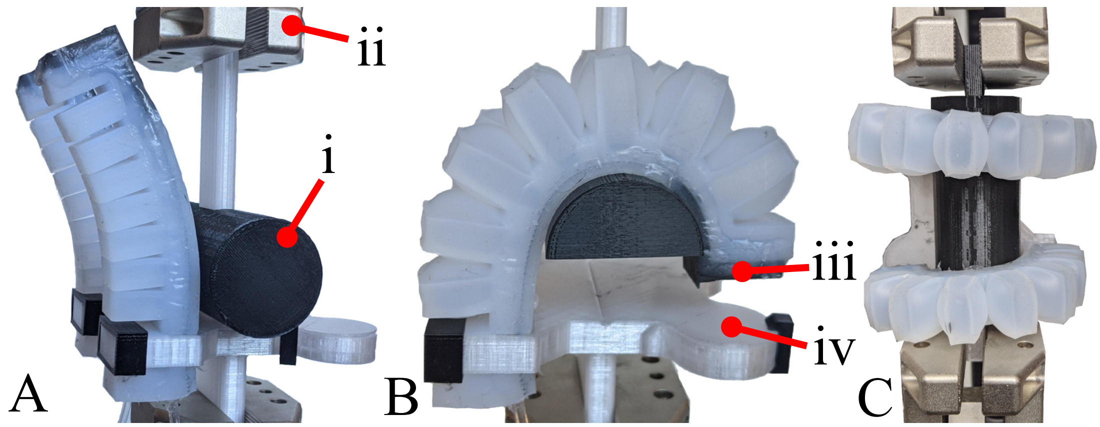

Figure 4.4: A) The actuator pullout strength testing apparatus with a horizontally oriented, vertically moving object (i) (circular profile, black). The force gauge (not shown) is attached to the clamp (ii) holding the connecting piece (white) to the object (i) on the top side of the apparatus. Two parallel actuators are at rest, anchored to the rigid base with a 3D printed fastener. B) Actuation of the soft actuators in the middle of data collection (pressurized to 27.6 kPa), where (iii) is the ME tip and (iv) is the magnet inside the rigid base. This object has a half-circular profile. C) The slip-resistance test, with a vertically oriented, vertically moving object with the actuators wrapped around the object body.

gripper with two parallel actuators. Throughout the grasp, this peak force stayed consistent around 10 N, until the grasped object raised far enough to decrease surface contact between the extended actuators and the object, resulting in the exerted forces dropping off with increasing distances greater than ∼60 mm (Figure 4.6B). Observing up to 4.5x greater grip forces demonstrates the effectiveness of the addition of magnetic grip enhancement. The increase in force from the interaction of the ME and base magnet increases grip strength, and as a result, grip stability. Sliding an object vertically from within the grasp of the soft gripper required greater forces to remove it as well (up to 3.5x greater force in select circumstances (Table 2)). In the following subsections, we break down the data and choices leading to the final design.

4.6.1 Magnetic Particle Properties and Shape

We performed VSM analysis of various MEs to attempt to address the lack of published literature on ME magnetic properties within the research space of soft robotics, and to investigate the reasons for using certain MEs, such as silicone with carbonyl iron particles, as frequently reported [12, 31]. Magnetic susceptibility is an important consideration in choosing a soft magnetic material; here, it is the slope of the VSM curve about the zero applied field position. This property contributes to the potential of a material to generate a pulling force when exposed to a magnet, which is the property of interest when designing a ME-tipped soft actuator. The pull force of a given magnet on a ME is greater for MEs with higher susceptibilities.

Figure 4.5A shows the magnetization response measured by the VSM for MEs made from various soft magnetic powders at 30% volume concentrations. The observed susceptibility for a given ME depends on the susceptibility of the powder material, and the effective shape factor, concentration, distribution and orientation of the powder particles [94, 124]. As seen from the data, MEs with Fe_3O_4 ($<$5 μm particle diameter) and AlNiCo (44 μm average particle diameter) exhibit hysteresis as well as lower saturation (or maximum) magnetization than the other MEs. An unexpected outcome came from the inclusion of 10 μm permalloy powder (ESPI Metals, Ashland, OR); the magnetic susceptibility of bulk permalloy is rated at 75,000 at $\sim$8 kA/m, or up to 300,000 at maximum, far greater than the susceptibility of bulk iron (approximately 5000). As such, we expected higher susceptibility in the ME containing permalloy. However, permalloy demonstrated comparable but slightly inferior magnetic susceptibility compared to carbonyl iron particles at the same concentrations.

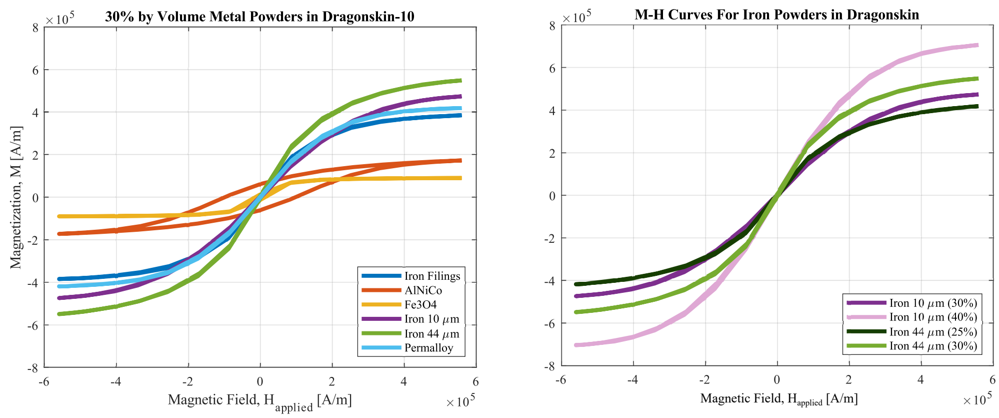

Figure 4.5: VSM results for Left) various metal powder-based MEs, and Right) carbonyl iron powders of different particle sizes (10 or 44 μm) in different ME concentrations.

This behavior is likely explained by two possibilities. First, the shape of the magnetic particles in all of the highest performing particles is roughly spherical, due to their small particle size (between 10 to 44 μm, depending on the powder). The susceptibility of the ME may be limited by the shape factor of the particles. If powders containing rod or ellipsoid particles were obtained, the susceptibility of the resulting ME would likely improve [156], especially with magnetic alignment prior to the curing step. Additionally, the concentration of the homogeneously dispersed powders prevents the magnetic particles from physically contacting each other and creating stronger magnetic domains. This even distribution was visually verified with a microscope. Pure powder samples of iron and permalloy were compared, and they demonstrated comparable values for susceptibility and saturation magnetization as with the samples at 30% volume in an ME (a value of ∼3.8 was measured for the susceptibility of pure permalloy powder, far lower than the anticipated values for bulk permalloy mentioned previously). As a result, carbonyl iron was picked, since there were no functional advantages within our application of the less commonly utilized powder. Initial tests with large iron particles (particle sizes greater than 300 μm diameter) visibly demonstrate particle chaining and alignment from magnetization during curing (see Figure 4.1B) but were unable to be mixed into silicone at higher volume percentages due to their particle size variability and apparent density preventing the resulting ME from curing and maintaining elastomeric properties (e.g. flexibility, elastic deformation). The large particles also settled in the silicone quickly, so maintaining a uniform dispersion in a cured ME would require constant rotation of the mold during curing or applied magnetic fields to evenly fix the particles.

One additional explanation for the discrepancies between magnetic powders relates to their reported densities. All iron powders, despite having different particle sizes (10, 44, and 300 μm), reported the same density of iron. This differs from the apparent density of the powder, since the volumetric packing of the powder depends on the particle geometry and size. This is examined in Figure 4.5B, where it is demonstrated that while at the same volume percentage, the 44 μm iron particles have slightly greater susceptibility. However, 10 μm particles can be introduced at greater volume percentages to obtain greater susceptibilities than larger particles at a lesser volume percentage without ME cure inhibition. The explanation is that while the calculations were performed for powders having the same density, the actual amount of magnetic material is more dictated by the apparent density of the powder. For this reason, 10 μm iron powder was chosen for the actuator design, due to its ability be mixed at higher concentrations than the larger particles. Iron particles at 44 μm were unable to be mixed and cured at percentages greater than 30%, which puts an upper limit on potential magnetic applications requiring greater susceptibility.

4.6.2 Magnetically Assisted Grasping

Choosing the 10 μm carbonyl iron particles for the ME for all remaining tests, we completed characterization of magnetic attraction between a short cylinder (6 mm height, 24.5 mm diameter) of ME and a base magnet during separation, and compared this data with magnetically-assisted and -guided grasping. For the magnet separation tests, increasing magnet strength through higher grades

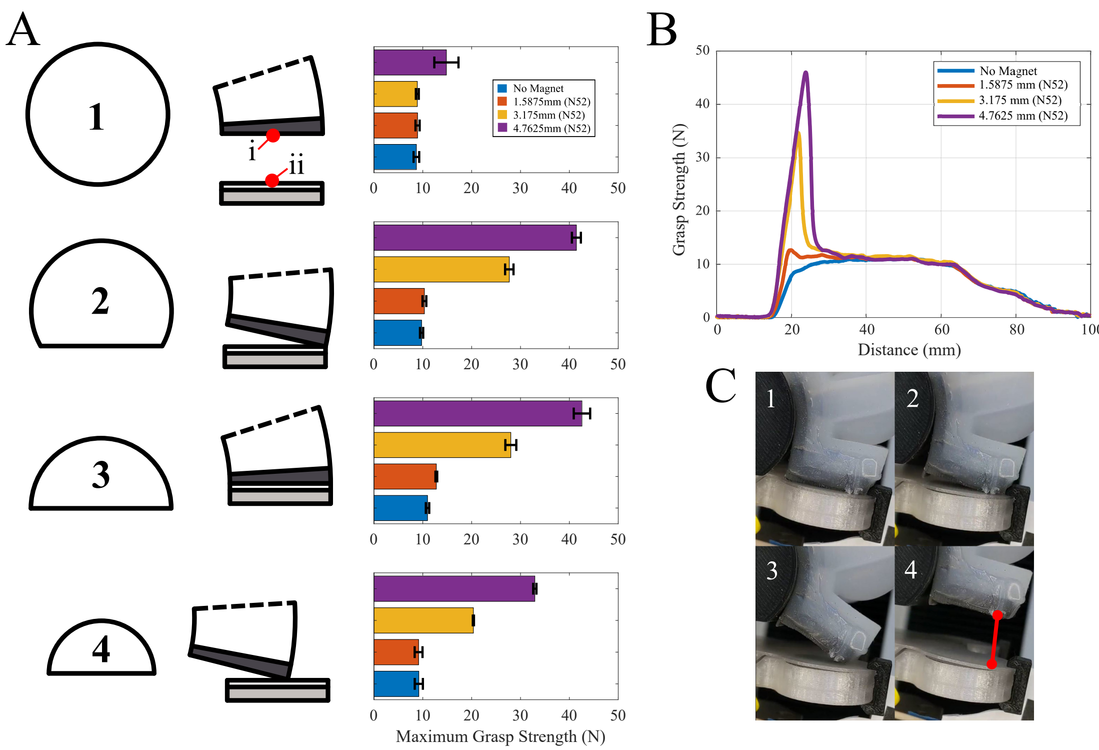

Figure 4.6: A) Four object geometries ((1) 40 mm circular, (2) 40 mm 3/4 circular, (3) 40 mm half-circular, and (4) 30 mm half-circular) demonstrate different tip separation behavior, which in turn contributes to their maximum force generation for different magnet strengths. i) ME tip, and ii) magnet base. B) The full set of force data for Object 3, showing the rapid rise in force generation dependent on the magnet in the base followed by the convergence of all trials to the same behavior when the ME tip escapes the region of significance near the magnet. Increasing magnetic flux density correlates to increasing grip force, up to ∼4.5x for the strongest magnet (N52, 4.7625 mm thickness). C) Side-view photos of progressive lifting of the ME tip from the base during a test, showing the attraction between the ME tip and base, before separating past the region of significance (∼13 mm).

or thicknesses was directly correlated to increasing forces required to separate and displace the ME. For the tests with the strongest magnets, some friction sticking occurred in the near region (<0.5 mm), displaying the slight dip in force before reaching maximum force at low displacement values. In an idealized set up of an infinitely wide soft magnetic plate, force from separation between a soft magnetic plate and a permanent magnet can be expected to follow a power-law decay function [8]. Given that in our setup the size of the permanent magnet and ME tip are comparable, the decrease in force with separation cannot be determined analytically and will require a finite element analysis approach. Such simulations, while not the goal of this work, will be undertaken in future efforts to optimize the gripper geometry.

For the gripper consisting of two ME-tipped actuators as shown in Figure 4.4A and B, experimental results demonstrated that the strength of the grasp increased in direct proportion to the magnetic flux density of the magnets used (increasing values as a result of magnet grade and thickness) with the grip (Figure 4.6A). Results also showed that the configuration at the interface between the actuator tip and magnet had a large effect on performance; grasp strength was greatest for the geometries that allowed the tip to linger near the magnet during the grasp, maintaining a parallel orientation, and as the object lifted (see objects 2 and 3 from Figure 4.6A). Object 1 was the largest (40 mm circular profile) and prevented the tip of the ME from getting close to the base due to the length of the actuator. This significantly reduced the influence of the magnets on the maximum force, with only the strongest magnet (4.7625 mm N52) raising the max force. Object 4 was narrower (30 mm half-circular profile), and it caused the actuator tip to curl inwards before lifting, creating an upwards force with less overlap between the tip and magnet than objects 2 and 3. This peeled the tip away at an angle faster than the other scenarios. The progression of this separation is visible in Figure 4.6C.

The grip where the object is vertically oriented, such that the slip resistance is evaluated (Fig. 4.4C), provides further insight into the role of tip spacing and alignment to the magnetic base. As shown in Table 2, the 45 mm diameter object performed similarly both with and without a magnet for maximum grip strength, whereas going down in diameter slightly (40 mm) greatly improved maximum grip strength. This highlights the importance of a fully closed grip for the ME, as the

Column Diameter	Magnet	Max Force
40 mm	No Magnet	3.70 +/- 2.00 N
45 mm	No Magnet	4.01 +/- 1.48 N
40 mm	4.7625 mm (N52)	15.25 +/- 0.85 N
45 mm	4.7625 mm (N52)	5.17 +/- 1.30 N

Table 4.2: Gripper slip-resistance for various cylinder shapes and magnetic strengths

maximum grip strength is only enhanced within the region near the base where the ME tip can be attracted to the magnet.

For the results shown in Figure 4.7A, the vertical position of the magnet beneath the palm was changed at the start of pull testing using a motion control system (shown in Figure 4.7B). This system raises and lowers the magnets, as well as moves them forward and back, using stepper motors for precise positioning. The grasp strengths shown in Figure 4.7 are highly dependent on both the strength of the magnet and its proximity to the fingertip. This agrees with the initial characterization from Figure 4.2, as well as the previous discussion about the influence of magnet strength from Figure 4.6A. In this case, by utilizing the same 40 mm half-circular profile (Object 3) for all the tests, we examine the impact of the initial distance between the fingertip and the magnet on grip strength.

This distance between the tip and the base, when compared with the data of the separation characterization in Figure 4.2, follows similar trends, where the effect of the magnet on force generation decays until distances above 13 mm, at which point the data resemble the data without magnets. These results demonstrate that the initial distance between the ME tip and the magnet in the base has a significant influence on grasp strength in this near region, but no functional impact on grasp strength at distances beyond 13 mm. Beyond these distances, the forces measured converge towards the same force for a grip with no magnet in the base.

One subject worth further study would be long-term cycle testing with larger manufacturing runs of identical actuators. The strain created in an actuator with

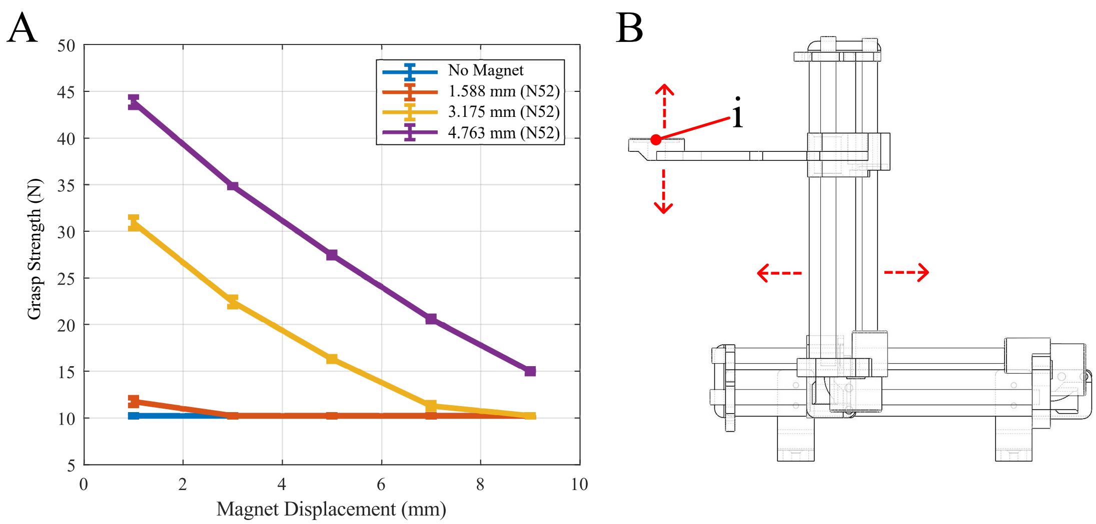

Figure 4.7: A) As the magnet moves away from the base vertically, the separation between the actuator tip and magnet surface increases (between 1 and 9 mm). B) Side view of the motion system allowing for the precise positioning of two magnets (i) beneath the rigid palm of the gripper (not shown, but located above the system to the top left).

a ME tip with a magnet in the base is greater, due to the larger forces generated when compared to without the magnet. While silicone is a highly elastic and robust material and the inextensible layer likely contains strain in the near region (less than 12 mm tip displacement), greater strains may accumulate with time, resulting in greater wear and tear on a gripper than one without magnetic enhancement.

4.6.3 Trajectory Guidance from the Magnet

An additional advantage of the presented actuator design is the ability to tune, or program, trajectories/configurations using varying magnet positions. As shown in Figure 4.8A, a magnet in five different locations (15 and 30 mm shifted left or right from the centerline) was able to produce a different grasping trajectory towards the base. Each trajectory only differed in the last 15-20 mm of the curling motion, where the influence of the magnet became strong enough to alter the actuator's

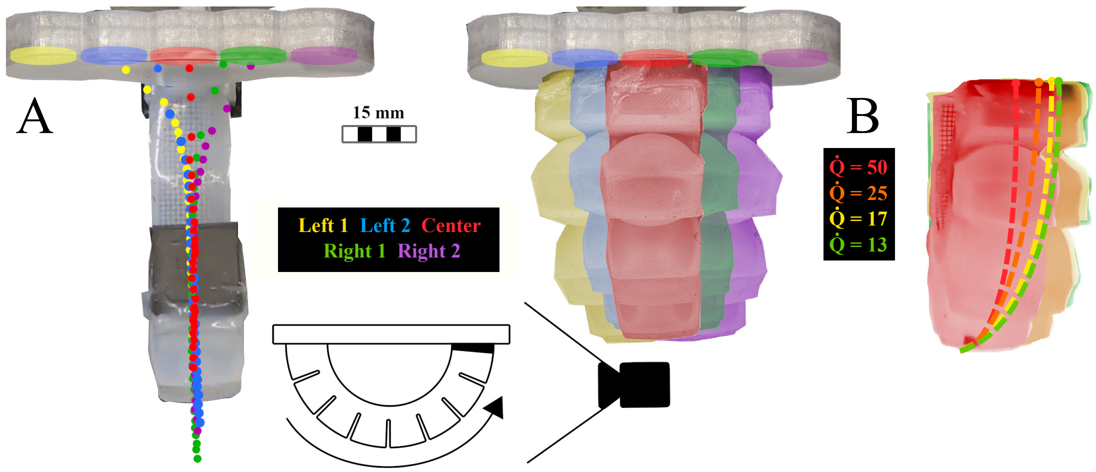

Figure 4.8: A) Five grasping trajectories of a single ME-tipped actuator, generated by moving a single magnet to five locations. Left) Tracked dots on the tip of an actuator as it moves to the final grasp during actuation Right) Each grasp is overlaid in a single image to demonstrate deviations from a central grasp Bottom) A diagram presenting the perspective from which video data were collected, for perspective clarity. B) The actuator was inflated at various flow rates (units of ml/sec) to demonstrate the inertial effects of the actuator on the trajectory guidance of the magnet, located in the Right 2 position. Higher flow rates and faster inflation resulted in less horizontal displacement.

movement and draw the tip towards the magnet, away from the centerline. This is in agreement with the previous discussion of the range in which the magnet can create an effect on the actuator. While not measured, the grasp strength of the central grasp trajectory would likely be the same as previous trials. In Figure 4.8B, we increased the flow rate of air into the actuator while keeping the magnet in the same location, and observed with pixel measurements that increasing flow rates produced less horizontal displacement from the mid-line (9.44 mm for 13 ml/sec, 8.80 mm for 17 ml/sec, 8.15 mm for 25 ml/sec, and 5.79 mm for 50 ml/sec). A 4x increase in the flow rate caused a 39% reduction in displacement. This is likely due to inertial effects as increasing flow rates start to dominate the attractive force of the magnet, resulting in a complete grasp before the magnet is able fully exert the deflecting force and draw the ME tip towards itself.

In Figure 4.9, the positioning of the magnet was shifted from the center position used for all testing towards the base of the actuator anchor point, drawing the actuators towards their base and narrowing the grip. This enables improved grasp quality tailored to the geometry of the object being grasped. Moving the magnets back to the neutral position attracted the actuator tips away from the small object, resulting in a failed grasp when picking the object up and rotating it (i.e. the object slipped from the gripper). The positioning of the magnet (front to back, left to right) impacts the positioning of the inflated actuator, and therefore the quality of the grasp for any given object. Moving the magnet up or down, closer or farther from the actuator tip, directly impacts the maximum grip strength (as shown in Figure 4.7).

Future applications utilizing this approach, either for grip strength enhancement or trajectory guidance, would benefit from the ability to control the applied magnetic field to vary the impact of the magnetic field on behavior. This could be accomplished by replacing the discrete permanent magnets with electromagnets. Tuning the magnetic field in real time to alter the maximum grip strength in response to the demands of a given task would significantly improve the design's usefulness. This would also improve the ability to control the grip behavior in the near region of grasping, as the need for enhanced grip force may only be necessary to activate when the actuator tip begins to separate from the base in the near region (<13 mm). The ability to turn off the magnetic field is necessary to release the grip at the end of a grasp, since the loss of pressure in the actuator does not decouple the ME tip and the magnet in the base.

4.7 Conclusions

In this paper, we created a multi-material, soft robotic grasping system by incorporating MEs into typical soft actuators of the PneuNet design [111] and utilizing magnets to influence their actuation behavior. By doing so, we demonstrated higher grip strengths (up to ~4.5x greater (see Figure 4.6)) and greater slip re-

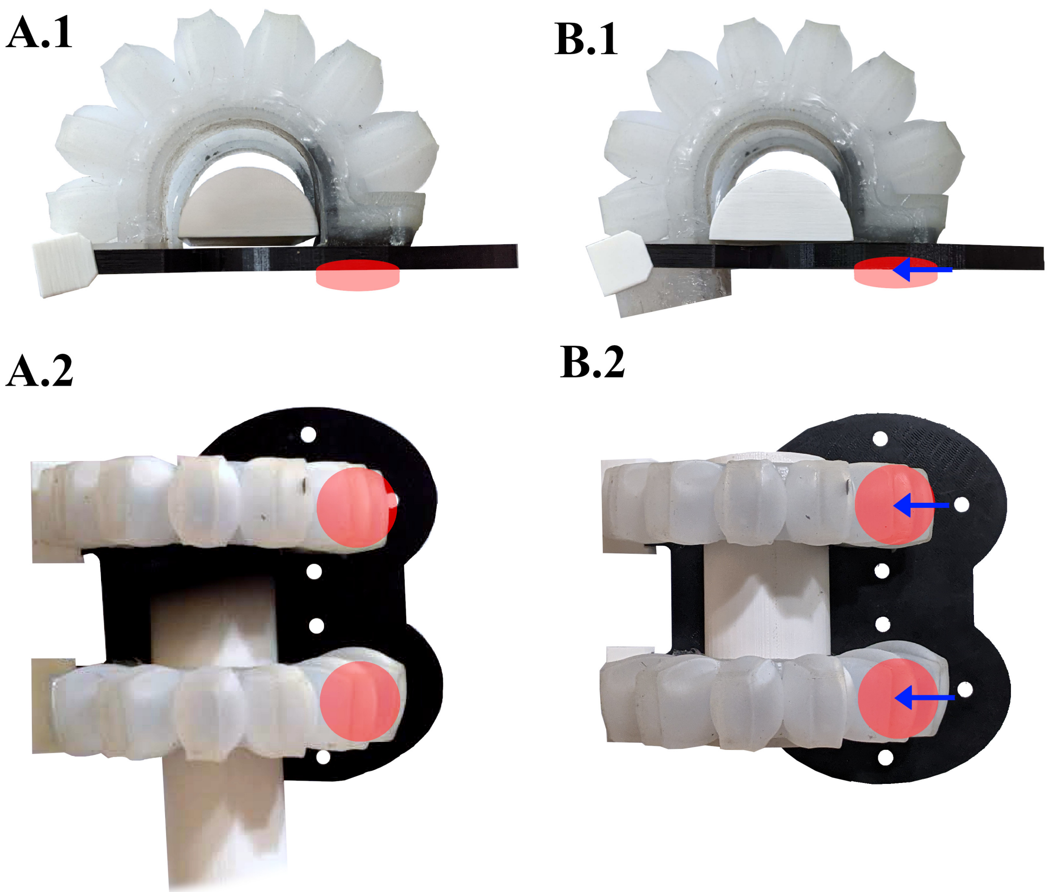

Figure 4.9: Positioning the magnets (shown in red) in the neutral (A.1) position is unable to grasp objects with a smaller diameter than the inner curvature of the soft actuators (A.2). Shifting the magnet placement closer towards the actuator base (10 mm) narrows the grip (B.1), allowing for grasping of smaller objects (B.2). These improved grasps would otherwise be impossible without adjusting the magnet location, as all other factors (actuator pressure (pressurized to 27.6 kPa), object size, magnet strength) remain constant.

sistance/grip strength in various orientations (see Table 2). This approach can be applied to other existing actuator designs in different configurations, such that relatively simplistic actuators, as well as more complex, multi-chambered designs, can gain additional functionality with a modification of the base and the addition of MEs into the fabrication. Also, this study did not address how to release the grip of the object in the presence of magnetic fields (i.e. open the hand). In future work, it may be possible to introduce electromagnets that introduce electronic control of the enhanced magnetic grip, or enable real-time trajectory control of an actuator.

Regarding MEs, the choice of magnetic particles for a given application is limited by the maximum concentrations within a given elastic medium. This is informed by the apparent density of the material, its inherent magnetic properties, the shape and regularity of its particles, and more. Due to these constraints, carbonyl iron particles (which are already commonly utilized in MEs) continue to be both an economical and feasible choice for magnetic applications in soft robotics. A future application of MEs could be elastic electromagnets, with MEs as the soft magnetic core. However, such an application would be practical only if greater susceptibilities via particle shape, alignment control, and higher volume percentages could be achieved. The MEs in this study exhibit a susceptibility that would at best allow for a four-fold increase in the magnetic field over an electromagnet with an air core. The scope of this study was limited to soft magnetic powders, but further work characterizing hard magnetic powders would further inform the choice and applications for MEs in soft robotics.

Acknowledgments

The authors would like to thank the members of the OSU robotics and electrical engineering departments for their input and assistance with collecting measurements, particularly Khalid Masood for his contributions to performing VSM. This material is based upon work supported by the National Science Foundation Graduate Research Fellowship under Grant No. 1840998.

A Low-Power Magnetorheological Fluid Clutch Utilizing Electropermanent Magnet Arrays

Notes on Chapter 4:

This following chapter contains a study which develops a low-power torque transmission device which utilizes electropermanent magnet arrays to control the yield stress of MRF within it. It demonstrates a novel method for low-power magnetic field generation within a MRF clutch, and models and characterizes the torque output of the device. The MRF clutch and EPM array have potential for deployment in robotic linkages and automotive braking systems, where low-power consumption and compact size are needed.

Authors: Nicholas Bira [1*], Pallavi Dhagat [2], Joseph R. Davidson [1]

1. Collaborative Robotics and Intelligent Systems Institute, Oregon State University, Corvallis, OR 97331, USA

2. School of Electrical Engineering and Computer Science, Oregon State University, Corvallis, OR 97331, USA

Submitted to Frontiers in Materials (Recent Development of Magnetorheological Fluids (MRFs) and Its Engineering Applications). Under Review.

Chapter 5: Low-Power MRF Clutch with EPMs

5.1 Abstract

In this work, we develop a compact, low-power and partially 3D-printed magnetorheological fluid (MRF) clutch that operates by variably and reversibly altering the shear stress of the fluid through the local activation of an array of electropermanent magnets (EPMs). By toggling the magnetization of each EPM independently on the order of a few milliseconds, we allow for rapid response times and variable torque transmission without further power input. Selectively polarizing the EPMs for different lengths of time results in repeatable and variable magnetic flux, in turn enabling further control precision. We present the design, modeling, and measured performance of this clutch with various control strategies, and demonstrate its utility as a low-power alternative to more traditional clutch designs.

5.2 Introduction

In robotics, there is widespread interest in expanding physical cooperation between people and robots, a field commonly referred to as physical human robot interaction (pHRI). This interest extends to diverse domains where people may physically wear the robot (e.g. exoskeletons, rehabilitative devices) or work with/around the robot in collaborative spaces (e.g. warehouses, shipping facilities, health care settings). For applications including pHRI, it is critical that the robot's design requirements consider safety of the human user. One popular approach for enabling safe and effective pHRI is to add compliance to the robot's actuators. Soft robotics, series elastic actuators, and variable stiffness actuators ([168]) are some of the methods that can be used to provide compliant actuation for pHRI.

Common implementations of soft robotics and compliant mechanisms utilize deformable materials, such as silicone or other elastomers, in their designs. Flexibility and elasticity improve overall compliance, but constructing robots from these materials often limits the overall strength and speed of a robot. Another method to implement pHRI is with smart materials that respond to specific stimuli to variably change their physical properties. This controllable property enables many control strategies, such as variable stiffness joints in actuated linkages, variable grip strength ([13]), and conformal grasping.

In this paper, we focus on the use of magnetorheological fluid (MRF), a smart material that variably alters its shear behaviour in the presence of an externally applied magnetic field (see Figure 5.1A). A MRF contains small ferromagnetic particles, usually iron, that create the magnetic response. Without an external field, the MRF is a liquid and flows with little resistance; with an applied field, the MRF behaves like a Bingham plastic ([11]), flowing with greater resistance after an initial yield stress defined by the magnetic field intensity. Since MRF requires magnetic fields of magnitudes considered safe for human exposure and demonstrates rapid response times, it is an appealing candidate for pHRI applications ([137]).

MRF reacts to an applied magnetic field rapidly and reversibly, and since the intensity of magnetic fields can be selectively controlled by electromagnets, this fluid has been deployed in the development of MRF-based actuators, brakes, clutches, dampers, and valves ([121]). A suction-based flexible gripper was developed using MRF and a controllable magnetic field, achieving improved grip strength while the magnetic field is active ([92]). Another study designed a laparoscopic actuator with MRF and electromagnets to control the joint stiffness between each link and alter its curvature ([90]). Another recent article developed a hybrid MRF and shape-memory alloy (SMA) linkage ([173]). The SMAs are deployed along the length of the linkage, while each joint of the linkage consisted of a MRF-filled bearing which responds to an electromagnet coil adjacent to it to increase local joint stiffness.

There is also substantial prior work on the use of MRF-based clutch mechanisms for transmitting torque between robotic linkages. One paper characterized an MRF clutch and modeled how the input magnetic field maps to an output torque, highlighting how MRF clutches can control the amount of transmitted torque through the intensity of the applied field ([172]). Other researchers developed a small-scale MRF clutch and compared it to that of a traditional DC motor for potential use in haptic feedback systems ([113]). Another publication developed and characterized a five degree-of-freedom robotic arm with MRF clutches in each joint; electromagnets in conjunction with a permanent magnet were used to control a specific range of magnetic field to variably control the joint stiffness at each joint ([122]). A recent article developed an upper leg prosthesis, combining a MRF clutch with an MRF brake to provide improved energy efficiency compared to a motor-reducer for walking ([40]). Later work by the same authors focused on the backdrivability of the MRF clutch in a leg exoskeleton, demonstrating its useful properties compared to traditional designs ([4]). Some desirable properties for all clutches are: small physical size, reduced complexity where possible, low power consumption, and high accuracy in the desired torque being transmitted to allow for reliable and predictable behavior. While an industrial manufacturing robot is less constrained by size and power concerns than a small, mobile robot, these design considerations apply in most circumstances.

One significant drawback of MRF devices utilizing conventional electromagnets is substantial power consumption – continuous use of relatively large currents is required to maintain the magnetic fields needed to keep the fluid in an active state. This constraint limits the potential for untethered, remote operation, and suggests that innovations in how the magnetic field is created and controlled can improve the utility of MRF devices. Electropermanent magnets (EPMs) are an alternative mechanism for magnetic field generation. EPMs are assemblies of both an electromagnet with a magnetic core (usually AlNiCo) and a hard permanent magnet nearby (usually NdFeB). These two elements are connected with soft magnetic material such as ferromagnetic iron or steel, and this connection enables the shaping of magnetic flux in the magnetic circuit. The electromagnet can be supplied with current in a positive or negative direction to magnetize the AlNiCo in either direction. The resulting assembly of magnets and iron components has two states, on or off, which represent the net magnetic flux present in the desired region when the magnetic circuit is at rest after polarization of the AlNiCo (see Figure 5.1B). This control method is possible due to the coercivity of AlNiCo being much smaller than that of NdFeB ($H_{c\_AlNiCo} << H_{c\_NdFeB}$). Toggling the magnetization of the AlNiCo still requires power, but it can be done on the order of milliseconds and then holding in a latched state, as opposed to needing continuous current delivery like a traditional iron-core electromagnet. This lends itself towards untethered operation, as the overall power consumption is reduced compared to always-on devices.

Prior work has demonstrated that EPMs are viable control tools for MRF-related actuation strategies, such as the work presented by Leps et al ([97]). This work developed a MRF valve for low-power, distributed control of flowing MRF in soft robotic systems. Similarly, recent research with MRF valves demonstrated control over the flow of MRF through a series of soft robotic actuators using EPMs, generating bending in the actuators by building pressure behind an EPM-based valve ([105]). These works highlight the importance of EPMs as latching, low-power devices, and their capacity to be used with MRF for controlling actuators. Another research group developed a soft robotic gripper which uses electropermanent magnets as the control input, combined with magnetic elastomers which deform in the presence of a magnetic field to create actuation ([187]). Other researchers developed a MRF clutch that uses a single permanent magnet in conjunction with an electromagnet, to modulate the overall field within the clutch and the resulting transmitted torque ([109]). This is not an EPM, since it does not represent latching on or off-states, but instead requires active input to raise or lower the effective output of the permanent magnet. This strategy is utilized in the robotic arm described in the previous paragraph ([122]).

With these recent developments in mind, in this paper we propose and demonstrate an MRF-filled clutch surrounded by an EPM array (abbreviated here as MEC). Our primary contribution is the use of this EPM array as a *low-power density* method for variably adjusting output torque in a repeatable and programmable manner with a compact form factor. We start by fabricating the EPM array from

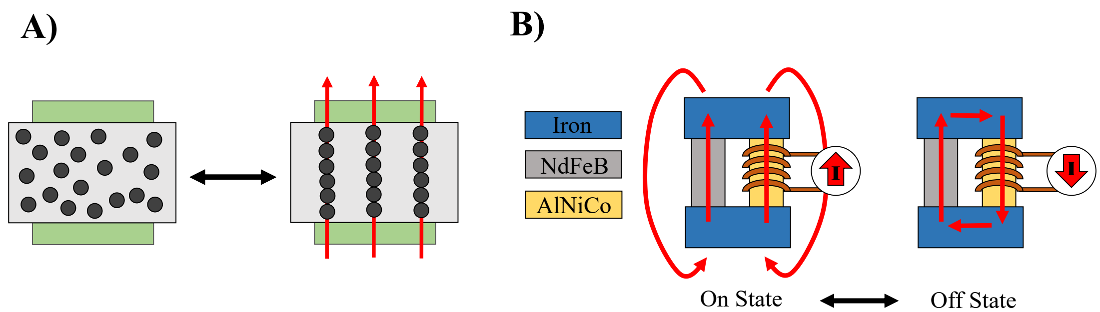

Figure 5.1: A) The principle of MRF, where an applied magnetic field causes the ferromagnetic particles in suspension to align and form polymer-like chains, affecting the fluid's shear behavior. B) The principle of an EPM, where two states can be toggled by the direction of the magnetization of the AlNiCo magnet.

available materials and size constraints, then characterize the typical magnetic field generation at the manufactured scale. Next, we simulate the performance of the EPMs in Ansys Maxwell and compare it to the observed behavior. We then develop an analytical model of torque transmission to examine the contribution of physical parameters on MEC performance, and we use this model alongside further simulation to inform our physical design and construction of the MEC. Lastly, we assemble and characterize the MEC prototype in a bench-top study, finishing with a discussion of its performance, control methods for torque transmission, and low-power requirements. Our prototype MEC and EPM designs are visible in Figure 5.2.

5.3 Methodology

Here we describe the process for developing and fabricating the MEC. We begin by creating several EPMs, testing their performance, and comparing this to simulations performed in Ansys Maxwell. Next we developed an analytical model for the potential MEC device to describe the transmitted torque. We also examined the field intensity within a 3D model in Ansys Maxwell using these same param-

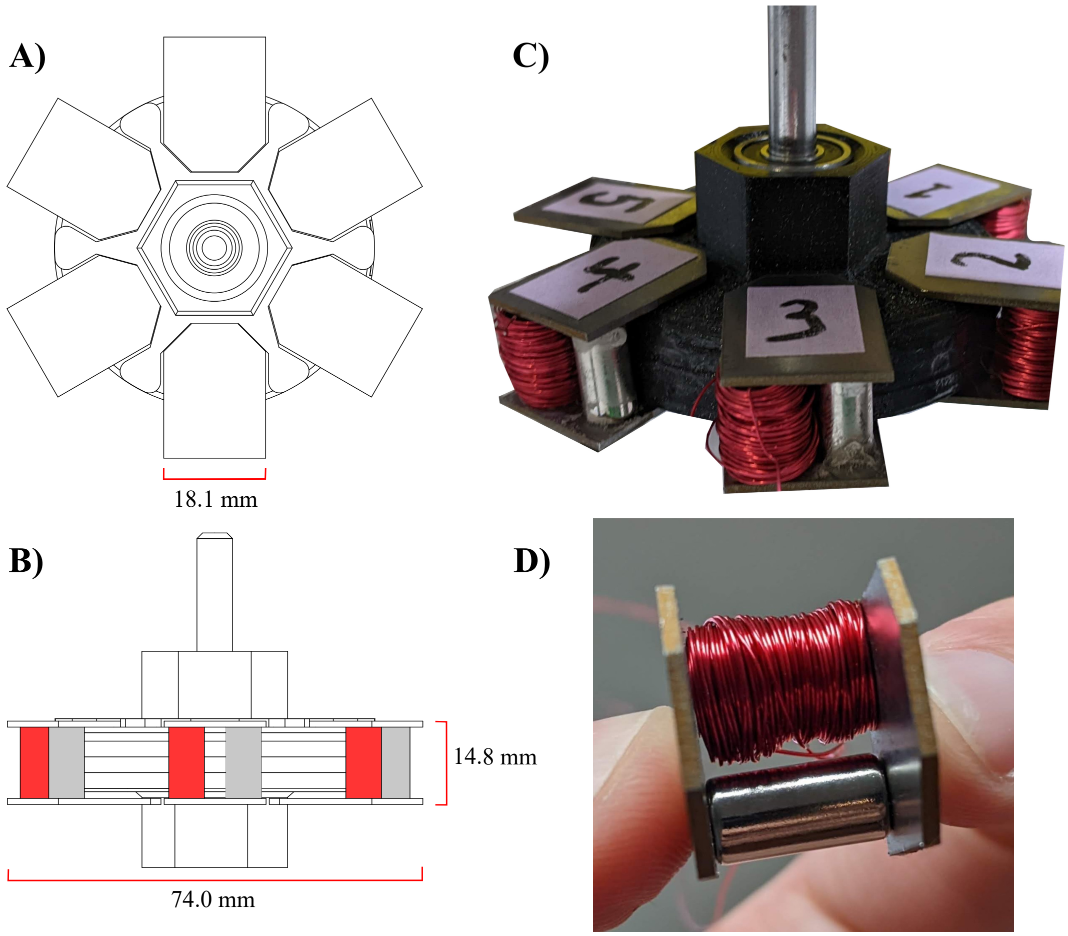

Figure 5.2: An assembled MRF Clutch with six EPMs. A) Top-view and B) Side-view. The coils are not depicted in the 3D rendering, but their locations are highlighted in red, while the NdFeB magnet is shown in gray. C) A photo of the final MEC, shown from the isometric view D) A single EPM, viewed head-on to see the two magnets and coil.

eters. From these models, we chose physical design parameters for the MEC, and then created a prototype. We placed the prototype into a experimental setup to measure its performance, allowing us to compare our model with the real-world behavior.

5.3.1 EPM Fabrication

First, we wanted to validate that the scale and design of an EPM array would perform within the boundaries of what is required to generate the MR effect in a fluid-based clutch. Physical parameters for a modular EPM were selected based on available materials, size, and power considerations. Each EPM consists of a NdFeB grade 42 hard permanent magnet (12.7 mm length and 6.35 mm diameter), an AlNiCo grade 5 magnet of the same dimensions, two thin steel rectangular plates (1008 cold rolled steel, 1.07 mm thickness) cut into a rectangular shape with the corners removed to accommodate closer positioning (see Figure 5.2A), and a copper magnet wire (AWG 28, 0.32 mm diameter) coil around the AlNiCo 5 magnet (120 windings each, evenly spaced along the length of the coil, approximately 3.3 m in length). Each magnet was positioned and glued in place with cyanoacrylate glue to the plates (see Figure 5.2D). After fabricating all six EPMs, each was tested for its polarizing and depolarizing ability, using a teslameter with resolution up to 10 μT ((TES11A model, Qingdao Tlead International Co, Qingdao China) to validate the amount of flux with more precision. The initially observed values for each EPM were between 45 to 55 mT in magnetic flux density in the centerline between the plates when on and approximately 0 to 5 mT when off. Each EPM was polarized by applying a current first in the positive direction to polarize the EPM, and later in the opposite direction to depolarize it. The EPMs were then wired into three motor controllers with high current ratings and H-bridge functionality (15A Dual Motor Drive Module, NYBG Electronics, Wuhan, China), each with the capacity to supply current in either direction with the control signal provided by an Arduino Mega running a custom program. Each EPM was polarized with increasing lengths of polarization time (on the order of 0 to 3000 μs). While this more precise characterization revealed differences between each EPM regarding the maximum amount of flux produced at the center point between each of the plates, the general variation was within standard deviation and therefore acceptable for the prototype design. The MRF will be flowing between the plates, so this first pass was sufficient for estimating the general capabilities of the EPMs. These variations are directly attributable to the irregularities introduced from hand-assembling each EPM, cutting the steel sheets and magnets to size, and hand-winding the coils. Furthermore, misalignments of the teslameter probe used when measuring the generated B field could account for discrepancies. The results of this characterization can be seen in Section 5.4, Figure 5.9.

5.3.2 Ansys EPM Simulation

We also modeled the EPM array in Ansys Maxwell Magnetostatic Simulation software to predict the magnetic field formation characteristics. The cylinder representing the AlNiCo 5 magnet was given properties corresponding to a magnetization in the positive or negative z-direction for a given simulation and at values appropriate for that grade of magnet (magnitude of magnetization provided by the existing material libraries in Ansys). The N42 magnet was given a constant magnetization of a set value using the built-in magnetic properties library for Maxwell. The results of this simulation are shown in Figure 5.3, and demonstrate that each EPM can be expected to generate up to $\approx$ 55 mT in ideal conditions when in the *on* state. It also demonstrated that the EPMs produce $\approx$ 0 mT between the plates when they are in the *off* state. These validation steps show good agreement between the observed behavior for a single EPM (maximum polarization of 49.264 +/- 2.01 mT) and the theoretical ideal behavior (55 mT). These simulation results provide a baseline for further modeling and construction of the MRF clutch, as described in the next section.

5.3.3 Analytical Modeling

To predict the torque transmission behavior of the clutch design, the MR effect was modeled in MATLAB (Mathworks, Natick, MA, USA) for various physical parameters of the MEC. Unlike with electric fields, magnetic fields are generally non-linear unless shaped by magnetic circuits. Since our EPMs, along with the steel fins of the MEC, present a region of high permeability for the magnetic

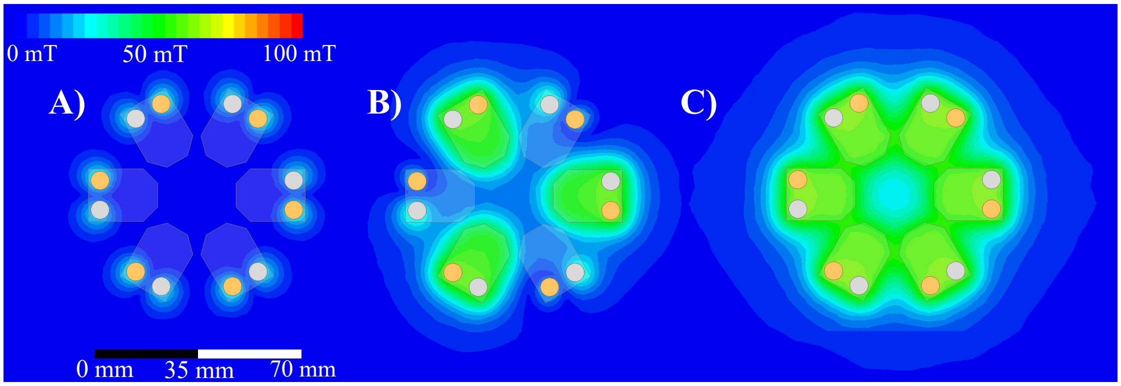

Figure 5.3: Depicted are three simulations completed in Ansys Maxwell of the EPM array from the top-down perspective. The AlNiCo magnet is orange, while the NdFeB magnet is white. A) All EPMs are in the OFF configuration. B) Three of the EPMs are ON, while the other three remain OFF. C) All six EPMs are active, demonstrating fields of approximately 55 mT in the regions of interest, at the midpoint between the plates of the EPM and where the MRF will reside.

flux, we approximated the magnetic field within the MEC as a constant scalar value for modeling simplicity. The majority of the volume of the MRF will be between the parallel plates of the EPM and the internal fins of the MEC, where the magnetic field is primarily linear (directed between the plates of the EPM). We utilized the Bingham model ([11]) for a viscoplastic fluid with a finite yield stress to represent the MRF's yield behavior as well as the characterization data from the manufacturer of the MRF fluid (LORD Corp, Cary, NC, USA). The first step towards modeling the torque is to approximate the magnetic field intensity within the active region of the MRF clutch design, denoted by a single value for H (units of kA/m). While the field does vary within the total active region, it does so only a few mT between the plates as shown in Figure 5.3C). This initial approximation is accomplished from the Ansys Maxwell simulations of our EPM characterization to estimate a typical magnetic flux density value provided by the EPMs, in this case, $\approx$ 50 mT. From the relationship between magnetic flux density (B) and magnetic field strength (H) in the B-H magnetization curves from the MRF materials datasheet, we estimated a H-value of $\approx$ 5 kA/m. This

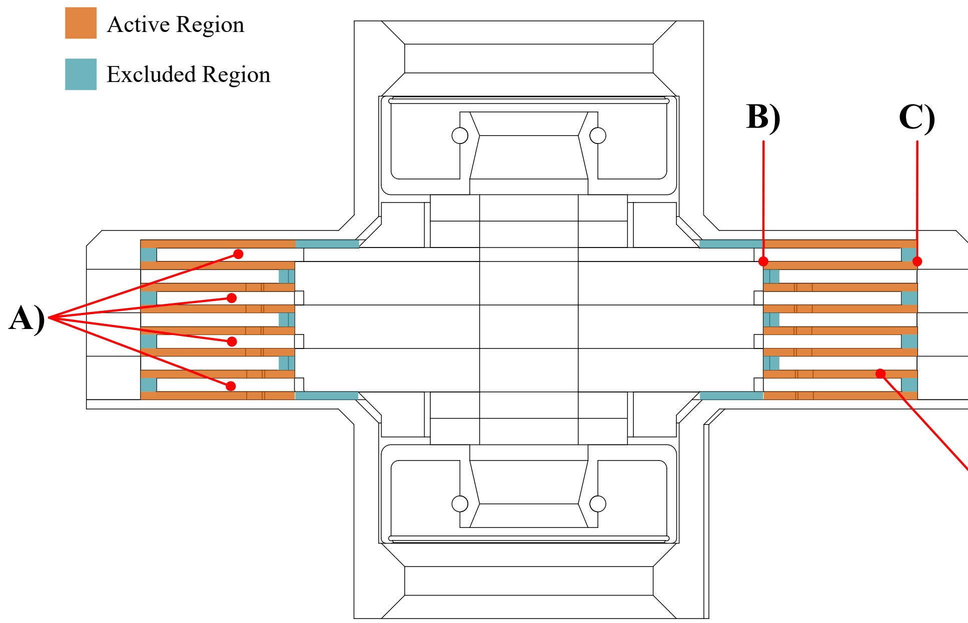

Figure 5.4: The cross-section of the active region of the MRF clutch design. The horizontal regions highlighted in orange are described with the total torque from Eq. 5.8, while the regions in blue are excluded from the model. A) The number of fins (here, there are four), B) The inner radius C) The outer radius, and D) the gap size.

approximation is for the magnetic field strength inside an EPM filled with MRF.

Having established a given static H value, we now approximate the effect of the magnetized MRF on the rotating steel fins of the MEC. The torque transferred from the input shaft of the motor is the summation of shear stresses developed between multiple stacked discs (See Figure 5.4). The active region (shown in orange) is where the analysis will be focusing on, since the other regions are much smaller and at the edges of the active region, experiencing less magnetic flux density. The Bingham model for a viscoplastic fluid with a finite yield stress is shown in Equation 5.1, where $\dot{\gamma}$ is the shear rate (sec^{-1}), τ_y is the yield stress (Pa), and μ_p (Pa·s) is the plastic viscosity. From the datasheet for the MRF, μ_p is estimated to be 0.28.

$$\begin{aligned} \dot{\gamma} &= 0 \text{ if } \tau < \tau_y \\ \tau &= \tau_y + \mu_p \dot{\gamma} \text{ if } \tau > \tau_y \end{aligned} \tag{5.1}$$

The calculation for τ_y is fit to the characterization data for the MRF from LORD Corp as a third order polynomial:

$$\tau_y\{H\} = -0.0000011503H^3 - 0.00098714H^2 + 0.52701H + 1.43 \tag{5.2}$$

From our earlier choice of 5 kA/m for H, this approximates the τ_y to be 20.9 kPa. The gap between the parallel steel fins is small (0.5 mm), so the flow can be approximated as a Couette flow during operation at a given rotational velocity $\dot{\theta}$. The significance of the Couette flow solution is that the viscous stress tensor is constant everywhere in the flow field ([38, 11]). The shear rate along the surface of one of the fins of the MEC is a function of the radius along the width of the fin, its rotational velocity, and the gap (g, shown in Figure 5.4D) between fins:

$$\dot{\gamma} = \frac{r\dot{\theta}}{g} \tag{5.3}$$

The differential torque dT generated by an element dA is:

$$dT = r(\tau\{H\}dA) = r(\tau\{H\}2\pi r dr) \tag{5.4}$$

Inserting the Bingham model from Equations 5.1 and 5.3 (which assumes we operate in the post-yield region) for shear stress yields the following equation for the differential torque:

$$dT = 2\pi \left(\tau_y\{H\} + \mu_p \left(\frac{r\dot{\theta}}{g} \right) \right) r^2 dr \tag{5.5}$$

The total torque from the surface of one fin is found by integrating the differential torque over the boundaries of the fin (between the inner and outer radius of the fin, shown in Figure 5.4B and C):

$$T_{fin} = 2\pi\tau_y\{H\}\int_{r_i}^{r_o} r^2 dr + \frac{2\pi\mu_p\dot{\theta}}{g}\int_{r_i}^{r_o} r^3 dr \tag{5.6}$$

Performing integration yields the following equation for the torque transferred to the surface of a single fin:

$$T_{fin} = \frac{2\pi}{3}\tau_y\{H\}(r_o^3 - r_i^3) + \frac{\pi\mu_p\dot{\theta}}{2g}(r_o^4 - r_i^4) \tag{5.7}$$

Since each fin attached to the central shaft has two surfaces, and there are a total of four fins used in the final design, we calculate the net torque transferred to the MEC to be equal to the sum of each of the individual fin surfaces' torques.

$$T_{total} = 2 * (4 * (T_{fin})) \tag{5.8}$$

By varying the applied field H to approximate the τ_y using Equation 5.2, we can plot the anticipated total torque from equation 5.8 as the result of various modifications to the geometric constraints of the MEC. The resultant effects on torque transmission are depicted in Figure 5.5. In that plot, we see that making the fins wider, as well as increasing the number of stacked discs, has a strong impact on the resultant torque transmitted. Increasing the gap size between fins decreases the transmitted torque, but the effect of gap size is much smaller than the effects from disc radius or number of discs (0.12% decrease at 48 kA/m from 0.5 mm to 1.0 mm gap size). In reality, altering the gap spacing would likely impact the assumed homogeneity of the applied magnetic field, and would contribute larger changes for different gap sizes. As expected, the conclusions from this modeling demonstrated generally that for larger surface areas, greater torque will be transmitted.

Taking these considerations in mind, and basing design choices on the physical constraints of the EPMs and the thickness of the steel stock material (0.9 mm thickness), we chose the parameters of 4 discs (see Figure 5.4A), 0.5 mm gap thickness, and a disc with an inner radius of 15.5 mm and an outer radius of 25

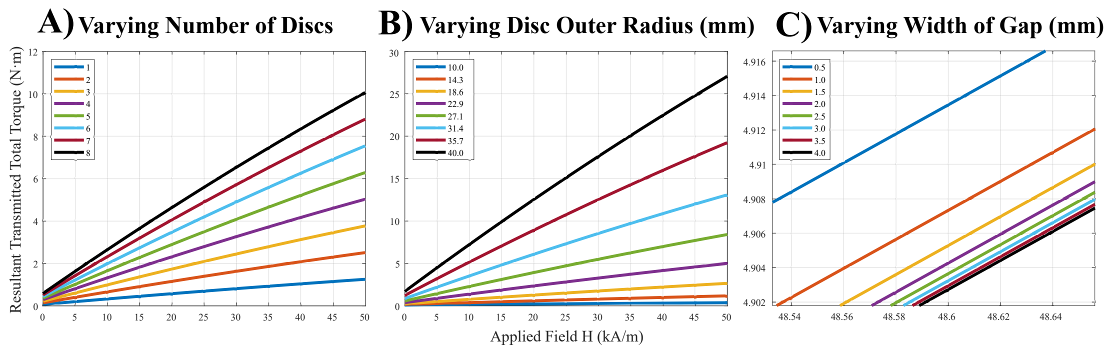

Figure 5.5: Three simulations of the effect of varying physical parameters of the MEC on transmitted torques. Transmitted torque increases with A) adding additional fins, and B) larger radii of the fins. Transmitted torque decreases with C) larger gap sizes, but by a relatively small amount (0.12% decrease at 48 kA/m from 0.5 mm to 1.0 mm gap size)

mm. The rest of the physical dimensions are described in Table 5.1 below.

5.3.4 Ansys MEC Simulation

Returning to magnetostatic simulations, we created a 3D model that best represents a balance between the takeaways from the previous section concerning gap and fin size. While more surface area is important for increasing transmitted torque, it also creates regions that are farther from the central active zone between the two plates of an EPM. Considering the physical constraints of the array of EPMs along with the design goal of increasing surface area, we chose dimensions for the steel fins that would ideally attract the flux and present a balance between more surface area and higher magnetic field intensity between the fins. We then simulated the magnetic fields for the design in Ansys Maxwell, retaining the settings from the previous simulations for only an array of EPMs (Figure 5.3). We also created B-H curve characterization data for the MRF from the provided manufacturer materials datasheet using curve fitting and input that into the simulation to model the effect of MRF in the spaces between the fins. The results of this simulation can be see in Figure 5.6A. In conclusion, the resulting MEC design will produce sufficiently high magnetic fields in the active regions, necessary for the operation of a MRF clutch (around 150 mT within the MRF between the fins, or a value of about 8 kA/m). With this value of H field, we anticipate the design to be capable of transmitting over 1.1 N·m of torque in ideal conditions (see Figure 5.6B), with a minimum value of 0.3 N·m without any applied field (this nominal value comes from the baseline yield stress of the MRF in the absence of an applied magnetic field).

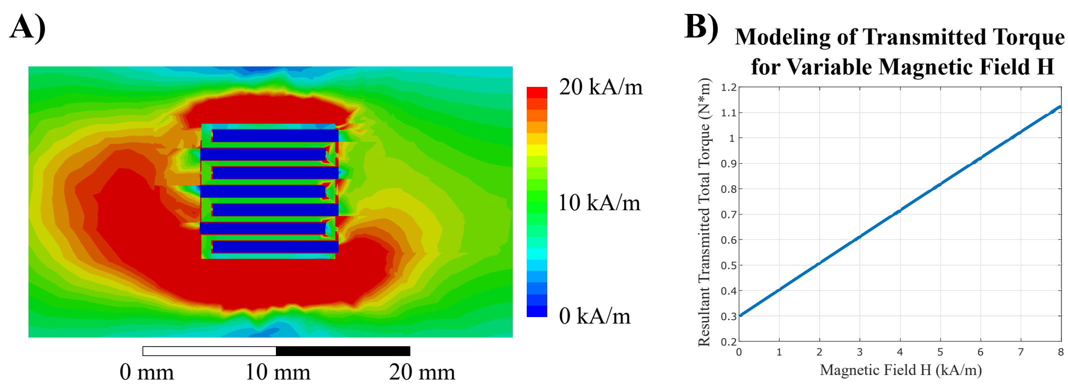

Figure 5.6: A) A cross-section (left half, right half not shown) of the MEC fins with MRF between them, simulated in Ansys Maxwell with EPMs actively generating their maximum magnetic field. This image indicates the magnetic field intensity (H-field) present within the MRF in the regions of interest is between 8 to 10 kA/m. B) A simulation using the previously derived equations of ideal-case torque transmission, for H-field values between 0 and 8 kA/m, showing a maximum transmitted torque of over 1.1 N·m. The blue regions of low H-field are the steel fins of the MEC. The center of the MEC shaft is not shown, and to the right of the active region.

5.3.5 MRF EPM Clutch Assembly

To fabricate the MEC, multiple fabrication and assembly steps are required. For the final design, multiple sub components were 3D-printed (Prusa MK3S, Prusa Research, Prague, Czech Republic) at 0.1 mm vertical resolution and 20% in-fill with standard PLA filament. For the metal fins, each was cut into discs from sheet metal (1008 grade cold-rolled steel, 0.3 mm thickness) using a water-jet (ProtoMAX Water Jet, OMAX Corp, Kent, Washington, USA). A 6.35 mm diameter aluminum rod was cut to a length of 150 mm for the central shaft. After all the individual pieces were fabricated, the layered fins consisting of metal rings and plastic hoops or discs were aligned and glued together using CA glue. All of the sub-elements of the MEC assembly are shown in Figure 5.7 and described in Table 5.1. The final design parameters for the miscellaneous elements of the clutch are as follows:

Table 5.1: A Bill of Materials for the Interior MEC Assembly.

Label	**Component**	**Dimensions**
A)	Aluminum Shaft	6.325 mm D, 150 mm L
B)	Steel Fin Outer Rings (3x)	31 mm D_i, 50 mm D_o
C)	Steel Fin Inner Rings (4x)	29 mm D_i, 48 mm D_o
D)	Plastic Cap for sealing	10.25 x 6.67 mm
E)	Shaft Seals (2x)	6.35 mm D_i, 19.05 mm D_o
F)	PLA Volume Filler Rings (2x)	13.46 mm D_i, 22.0 mm D_o
G)	Bearings 2(x)	6.35 mm D_i, 12.7 mm D_o
H)	MEC Top	57 mm D
I)	MEC Bottom	57 mm D
J)	PTFE Washers	6.35 mm D_i, 12.7 mm D_o

After all sub-components were fabricated, the MEC was assembled layer by layer, from bottom to top. The shaft seals (Table 5.1E) were press-fit into position on either side of the top (Table 5.1H) and bottom (Table 5.1I) 3D printed components, followed by a ball bearing (Table 5.1G) for shaft alignment and rotation. The aluminum rod (Table 5.1A) was placed and aligned in the bottom component,

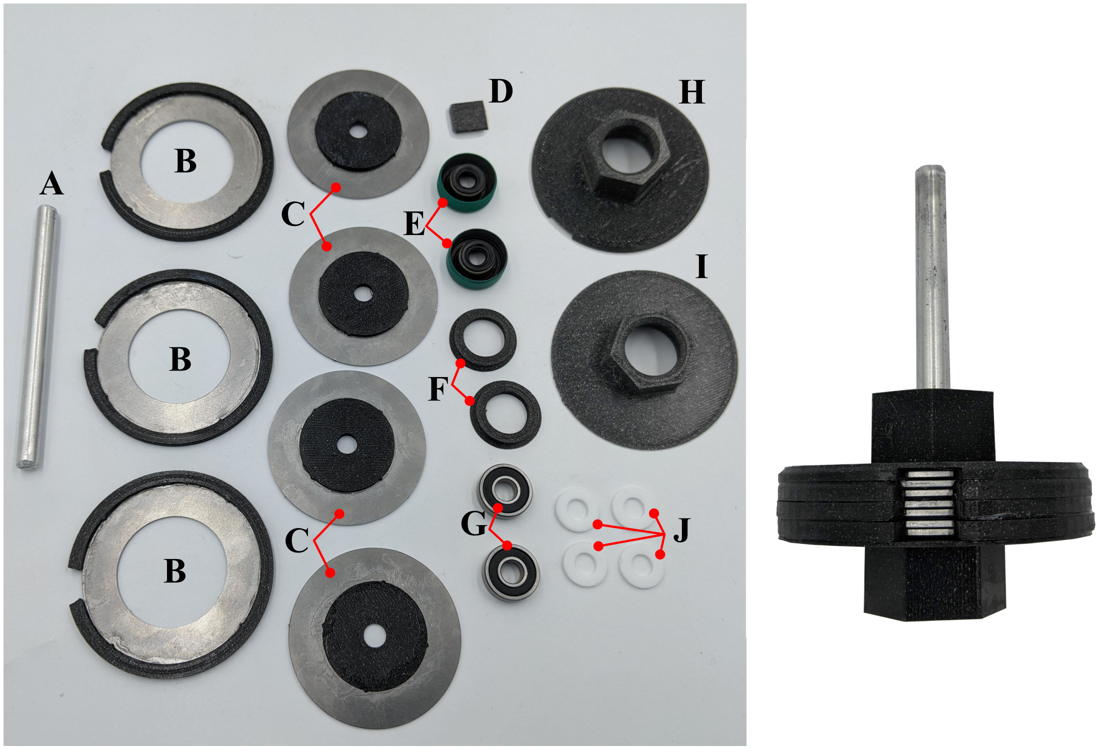

Figure 5.7: Left) All of the sub-elements included within the final MEC interior assembly, described in Table 5.1. Right) The completed assembly without EPMs or the cap (D), from the side view.

and PTFE washers (Table 5.1J) and 3D-printed spacers (Table 5.1F) were placed on top of the shaft seal to ensure proper spacing of the fins. Then, successive layers of inner (Table 5.1C) and outer (Table 5.1B) fins were positioned and glued to either the central rod or the outer housing. The top component was assembled the same way as the bottom, but in reverse order (PTFE washers, 3D-printed spacers, top sub-assembly with shaft seal and bearing). After all layers were positioned and glued, with time to allow the glue to dry, the assembled MEC was visually inspected and tested for free, low friction rotation.

The MEC needs MRF to be filled into all of its void spaces, and the authors decided upon filling the MEC using a non-magnetic metal syringe through an opening in the outer housing that allows access to all of the internal spaces (see the right of Figure 5.7). After all internal voids were filled with the MRF (MRF-144CG, Lord Corp), the shaft was rotated to ensure no bubbles remained. Then, the opening was capped and glued shut with a 3D-printed cap (Table 5.1D) and CA glue.

Having assembled all the internal elements of the MEC, six EPMs were then positioned radially around the perimeter of the completed sub-assembly of the MEC, such that each EPM has its active region targeting about 1/6th of the overall volume. The 3D-printed top and bottom elements provide alignment features for even spacing. The complete MEC was ready for testing and performance analysis, and was placed into a custom-designed testing apparatus to evaluate its performance (see Figure 5.8). This apparatus utilizes a stepper motor spinning at a constant RPM controlled by a power supply, an Arduino Uno, and a stepper driver. The output shaft of the stepper motor was coupled to the input shaft of the MEC with a shaft collar and set screw, and the outer housing of the MEC was fixed at the bottom to a 6-axis force/torque sensor (Figure 5.8D) (Mini40 Six-Axis Force/Torque Sensor, ATI, Apex, NC, USA) rigidly attached between the base of the test-bed and the clutch. This sensor collected force and torque data at 10000 Hz, to observe changes on the same timescale of our EPM pulse lengths (100s of μs).

5.4 Results

In this section, we describe the characterizations performed for both the EPM array (shown below in Figure 5.9) as well as the completed prototype MEC. We report on the torque transmission capabilities of the MEC, and we utilize a control strategy developed from curve-fitting functions to observed data at different EPM pulse lengths. The resulting set-point control method is demonstrated in Figure 5.12, and this is followed by an examination of the MEC response to variable pulse lengths applied rapidly, as well as different rotational velocities.

For the characterization of the final MEC, the stepper motor was driven at 50

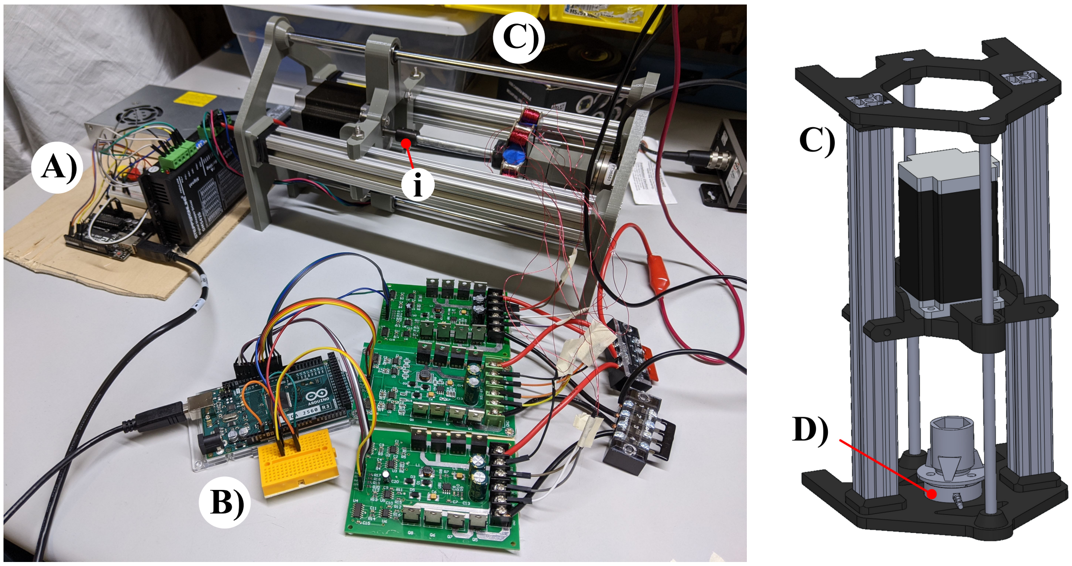

Figure 5.8: The full test-bed for measuring the torque transmission of the MEC, consisting of A) an Arduino Uno with power supply and stepper driver to control a stepper motor for the input torque to the MEC, B) an Arduino Mega to control three H-bridge Motor Driver connected to a bench-top power supply for current supply to the MEC (not shown), and C) the mounting frame allowing the stepper motor to slide linearly into place and be coupled to the MEC input shaft (see Figure 5.7A) with a set screw collar (i), and D) the force-torque sensor on the bottom, with a collar for holding the bottom component of the MEC.

RPM, a medium speed for the stepper motor. A number of tests were performed to highlight the overall performance of the MEC, as well as possibilities from different low-power control strategies. First, we completed two tests that examined the immediate response of the MEC to an input sequence where multiple EPMs are activated in sequence. This sequence of turning on sequential EPMs one by one, or two at a time, resulted in rapid changes in transmitted torque from the input shaft and was repeatable in both the rising and falling directions. These control patterns are shown in Figure 5.10, where each plot represents the average of three separate data series following the same control input. All torque values were normalized to the baseline torque of the MEC with all EPMs off (0.10 N·m without MRF added,

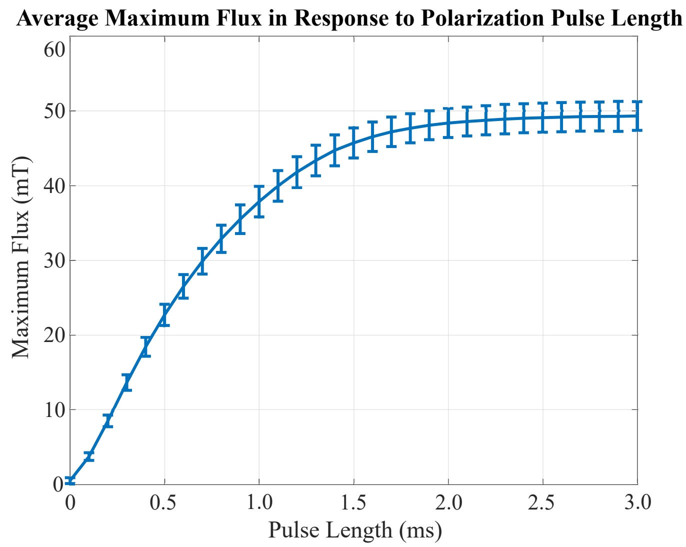

Figure 5.9: The characterization of all six EPMs, showing the magnetic flux density generated between the steel plates at the midpoint between each plate as a result of the current pulse length applied to each EPM. Data was collected with a teslameter, as described in Section 5.3.1.

from friction, and 0.16 N·m with MRF). A typical rise time from EPM activation until the MEC has reached its next target transmitted torque is 3.97 ms for the single-step modality (see Figure 5.10A), where each EPM activates individually. (this value was averaged from nine separate activation trials, with a standard deviation of 1.98 ms), while the rise time for the two-step modality (see Figure 5.10B) was 23.14 ms on average (with a standard deviation of 0.98 ms). These values coincide with the length of polarization for each individual EPM, which was set to 5.0 ms for these tests to ensure complete polarization and activation of each EPM. The two-step mode would take 11.0 ms to polarize two EPMs fully, with programmed delays in the arduino script. The two-step mode took longer than the single-step mode for its rise time, but it was also rising a greater amount. These results demonstrate the rapid, repeatable, and reversible nature of the MEC design.

Next, we studied how the length of polarization affected the overall transmitted

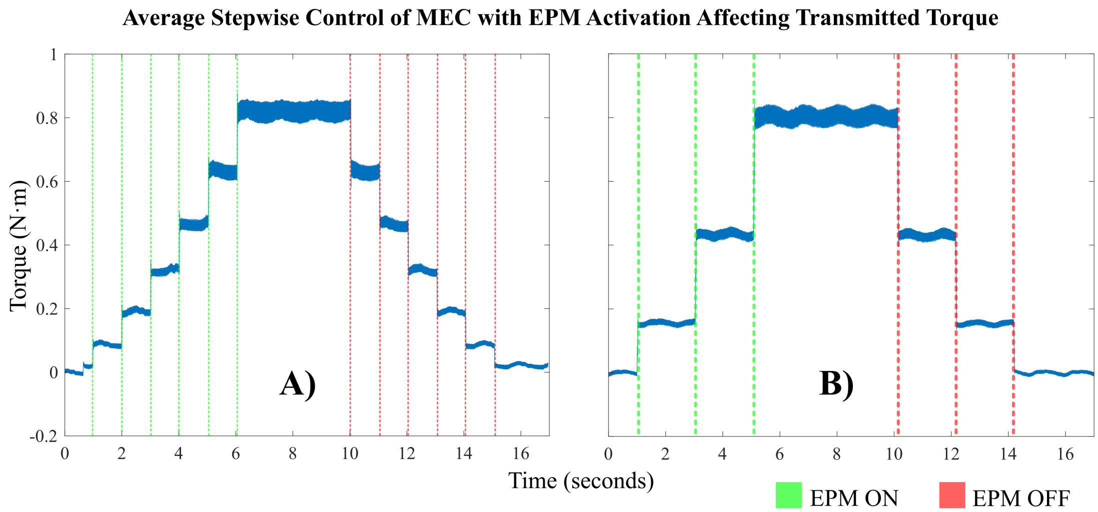

Figure 5.10: Demonstrating step-wise control of the MEC. A) Each EPM is activated sequentially, resulting in six steps up until being held at the maximum value, before stepping back down to zero. B) Two EPMs (on opposite sides of the MEC) are activated at once, resulting in larger jumps between each step, but behaving similarly to when single steps are made.

torque in the MEC. Data was recorded for both polarization and depolarization of the MEC at different pulse lengths. For polarization, the pulse length was applied after all EPMs were depolarized completely with a pulse of 5 ms. For depolarization, all EPMs were fully polarized at 5 ms before applying the depolarizing pulse. The transmitted torque was measured 9 times, and the average changes in transmitted torque as a function of pulse length are shown in Figure 5.11. This plot demonstrates significant hysteresis between polarization and depolarization for the length of pulse required to affect a change in the total torque transmission. This aligns with the general principles of the magnetization behavior of a permanent magnet such as AlNiCo; these outcomes are discussed in Section 5.5.

After collecting this data, we fit two functions to the polarizing and depolarizing data, utilizing the MATLAB curve-fitting toolbox. The resulting two inverse-

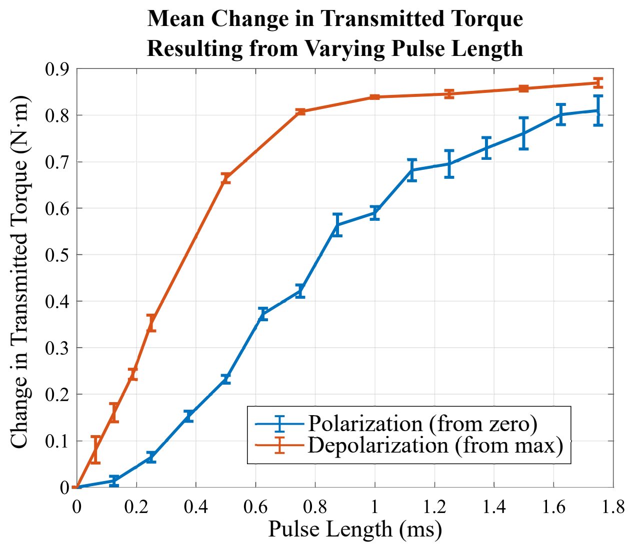

Figure 5.11: The change in average transmitted torque as a function of pulse length for the MEC. Polarization requires greater pulse lengths to achieve the largest possible transmitted torque, while depolarization can have larger changes with shorter pulse lengths.

tangent equations can then be used to choose an arbitrary set point within the range of possible torque values for the MEC. The inverse-tangent was chosen as it provided the greatest fit for polarization while keeping calculations simple (adjusted R^2-value was 0.97). These equations calculate the length of a pulse required to then magnetize or demagnetize all six EPMs from zero or saturation by the desired amount to reach the set point. Solving for the pulse length (x, in seconds) and calculating the change in target torque from the current torque (δ), the two equations take the form of:

$$\begin{aligned} x_{polarize} &= (tan(\delta/0.9)/759.0) \\ x_{depolarize} &= (tan(-\delta/0.9)/1713.0) \end{aligned} \tag{5.9}$$

Utilizing this control strategy, we defined a series of arbitrary set points in sequence, and applied Equation 5.9 to adjust the transmitted torque by activating the EPMs for a set pulse length determined by the new set point. The results of this experiment are shown in Figure 5.12. It can be seen that the initial increase in torque overshoots the control signal by ≈ 0.03 N·m, and this initial offset propagates throughout the rest of the test. While the direction and magnitude of the corrections are close to the control signal, these errors compound over time, leading to overshooting or undershooting the targeted torque. These results are discussed further in Section 5.5.

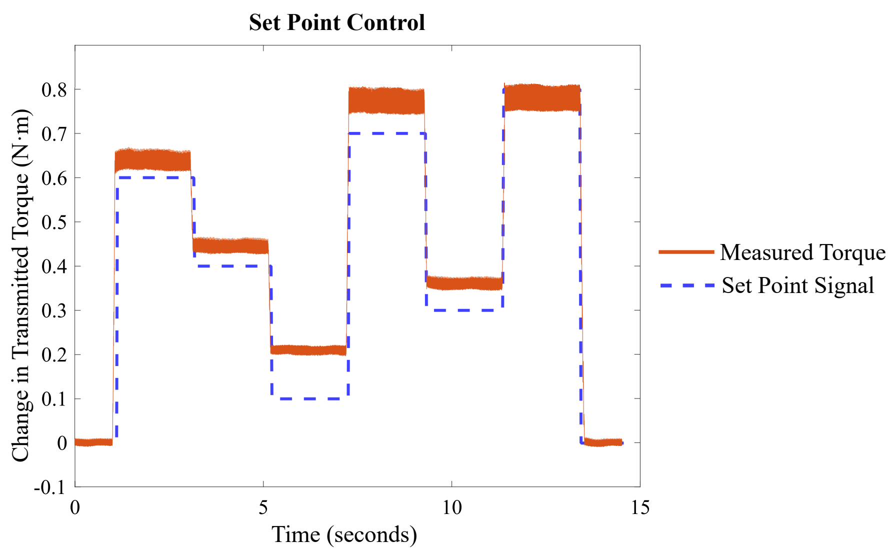

Figure 5.12: Demonstrating the set-point control strategy using the equations derived from the data in Figure 5.11.

After observing the differences between the targeted torque and the actual behavior of the MEC while following the control signal, we sought to observe more closely how the pulse length affects the torque transmission, focusing on small pulse lengths applied in rapid succession (30 times total) to slowly increase the overall magnetization of the EPMs. This was measured for two pulse lengths, each being applied to all six EPMs sequentially (taking about 30 ms total) with a short pause (300 ms) in between. The result is shown in Figure 5.13A, and demonstrates that a pulse length of only 100 μs raised the transmitted torque to about 0.2 N·m before stopping, while doubling the pulse length to 200 μs was sufficient to raise the transmitted torque a maximum value of about 0.65 N·m. The significance of this behavior is discussed in Section 5.5 alongside the previous figures. Lastly, the input motor RPM was considered for its effect on the results of the tests. Shown in Figure 5.13B, there was a slight increase in total transmitted torque as the RPM increased, but the effect was within standard deviation for each speed, and therefore negligible.

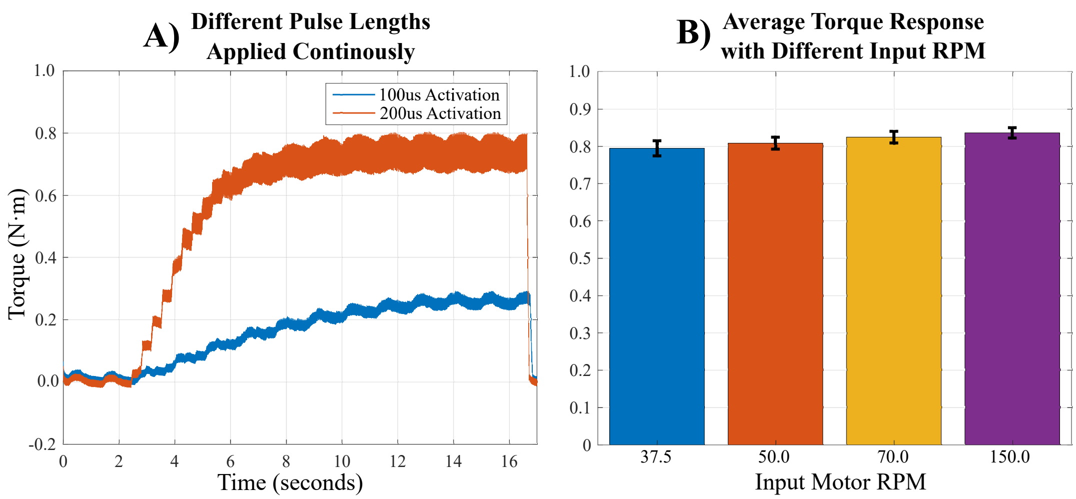

Figure 5.13: A) This plot demonstrates how cumulative pulses (5 ms to each EPM until all have been activated, with 300 ms in between each step) can gradually bring the torque up to a set maximum, which is determined by the pulse length. B) This bar plot compares how RPM affects maximum transmitted torque, with all EPMs being full saturated/active.

5.5 Discussion

In this section, we discuss the results of our experiments and consider shortcomings and advantages of the chosen design. We consider possible reasons for the discrepancies between our tested control strategy and the actual performance of the MEC. We also highlight the potential power-consumption advantages of the MEC and its place within the broader research topic of MRF-based transmission devices.

We completed various experiments to demonstrate the torque-transmitting capabilities of the MEC and to characterize its behavior. While the MEC was highly repeatable for the individually addressed EPM tests shown in Figure 5.10, there was greater variability introduced when attempting to utilize the magnetization properties of the AlNiCo (not full saturation) in the EPM array to control a specific torque. Controlling pulse length did demonstrate that each EPM could be controlled in the amount of magnetic flux density it would generate (Figure 5.9, but the developed equations fit to observational data in Figure 5.11 were less accurate at producing an arbitrarily targeted torque. This is likely the cause of the hysteresis present during the magnetization of the AlNiCo core magnet. This phenomenon can be seen in the data in Figure 5.11; when starting from zero (demagnetized) magnetization, greater pulse lengths are required to create a change in torque; or, more accurately, to create a change in the magnetization of the AlNiCo magnet that then results in the net magnetic field generated by the EPM. When the AlNiCo magnet is fully magnetized and saturated, much shorter pulse lengths rapidly cause a decrease in transmitted torque (more directly, a decrease in the magnetization of the AlNiCo magnet). This phenomenon is seen in other MRF-based clutch designs, and adaptive control strategies were deployed to compensate ([171]).

The magnetic hysteresis of AlNiCo is visible in characterization $B - H$ curves ([177]), but differs from our design due to the shape-dependent demagnetization field. Our control strategy (shown in Figure 5.12), which considered only the magnitude of difference between the current torque value and the projected torque value, fails to incorporate this hysteresis into its calculation, assuming the magnitude of change is relative to either fully magnetized or fully demagnetized. This is an important consideration for future control implementations, and existing characterization curves for AlNiCo can be utilized to realise more sophisticated strategy that tracks the current magnetization of the EPM. Additionally, some sensing feedback of the current transmitted torque could be incorporated, allowing for control strategies such as PID to fine tune transmitted torque with small pulse lengths to adjust the current torque to the target torque on short time scales (tens of milliseconds).

Other control strategies can combine both the individual EPM control shown in Figure 5.10 with the pulse-length control in Figure 5.11 to realize unique patterns of EPM activation to realize more complex torque transmission modalities, such as linearly or exponentially ramping the torque as opposed to jumping from one set point to another. Combinations of both pulse length and individually addressing each EPM allow for granular control of transmitted torque across the entire spectrum of possible torques. Additionally, the significant manufacturing differences between each EPM and the overall construction of the MEC are the source of much of the variability present in the characterization data. Improvements to manufacturing methodology, better precision machining, and better tolerances will contribute greatly to minimize variability between each EPM and the overall MEC behavior. This reduction in variability, while unlikely to account for all the discrepancies previously described, would give greater confidence to all control strategies developed for accurate torque transmission.

In the modeling performed in Section 5.3, we predicted a possible maximum transmitted torque of about 1.1 N·m. As shown by the maximum holding torque in Figure 5.10 of $\approx$ 0.8 N·m, the difference between the two is a delta of about 0.3 N·m. In Figure 5.14, the simulation from Figure 5.6 is plotted along with a theoretical ideal-case behavior, where each EPM contributes 1/6th of the total torque as it is added in sequence. By the time all six have been added, it reaches the maximum torque. Plotted in yellow is the average behavior of the MEC with all six EPMs activating in sequence, drawn from Figure 5.10A. The measured data looks quite similar to the theoretical data, and, if it were shifted up 0.2 N·m, would be in excellent agreement. This demonstrates that our modeling approach captures the overall scale and slope of the MEC's behavior, but overestimates the initial holding torque of the MEC without any applied field. The yield stress contribution from friction and the MRF was observed to translate into only 0.1 N·m of torque. This error likely comes from estimations and approximations made from the provided manufacturer data, since estimates of the yield stress at low fields may be inaccurate. Other sources of error could arise from differences between the MRF's physical properties once shaken and poured into the MEC, and the ideal conditions assumed by the manufacturer.

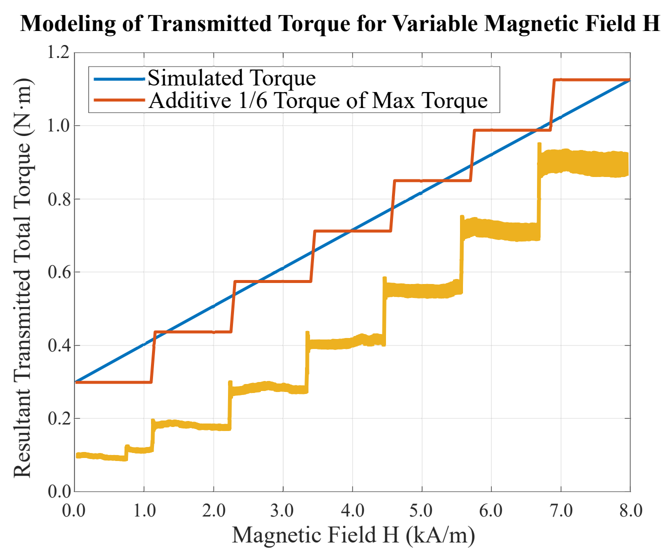

Figure 5.14: A simulation plotted with averaged data for torque transmission, where each EPM is activated in sequence, adding 1/6th of the total possible torque until the average H field applied from the EPMs reaches 8 kA/m around the perimeter of the entire MEC when all are active. The observed maximum is about 0.3 N·m less (27%) than the model predicted.

The MEC consumes several orders of magnitude less power than a traditional MRF-based clutch utilizing electromagnets for its control. For consideration, some simple calculations begin to demonstrate the significance of being able to set any torque within the operational range without any additional power input, once set.

One EPM has a wattage of about 75 W (15 Volts at 3 Ohms, drawing about 5 Amps), and can achieve maximum torque output with a pulse of 5 ms. This translates to a power consumption of 0.104 mWh, or 0.626 mWh for all 6 EPMs in the array. Turning the MEC into the on state and then back to the off state requires pulsing both directions, so to transmit maximum torque with the MEC for one hour and then turn it back off, the total power consumption would be about 1.25 mWh. Other relevant MRF-based clutch designs that utilize active electromagnets to transmit torque require being on for the entirety of maximum (or minimum) torque transmission for one hour. One sample design using this modality requires about about 3.5 W ([122]), which translates to 3500 mWh of power consumption for maximum torque transmission. The MEC consumes several orders of magnitude less energy than comparable devices for the same function (in this calculation, only 0.036% of the electromagnet-based design). While the MEC and the compared devices are not equivalent, and this calculation does not represent a real-world power-consumption scenario, it still serves to highlight how low-power the MEC can be. Additional optimizations in manufacturing tolerances, parameter optimization and EPM design will reduce the power and power consumption further.

In essence, the MEC only needs to be supplied current for the time it takes to fully magnetize the EPMs (tens of milliseconds), whereas an electromagnet must be supplied power for the entire length of operation. These differences are inconsequential on the timescale of tens of milliseconds, but the power draw becomes significant the longer active operation is required. This decrease in power consumption opens the door for many desirable applications, since this could significantly extend the time of remote operation and reduce energy costs. Electric vehicles or robots that currently utilize MRF clutches could significantly reduce their power consumption by adopting a similar design, improving battery life and range.

5.6 Conclusions

In this work, the authors designed and fabricated a prototype MRF-based device utilizing an array of EPMs for low-power, variable control of torque transmission. The authors designed and simulated the performance of EPMs for the purpose of controlling the behavior of MRF in a clutch design, and then fabricated and characterized the EPMs, seeing good agreement between real-world performance and simulation. The MEC was then designed and analytically modeled, demonstrating that potential torque transmission would be significant enough to be possible. After picking design parameters for the application that considered the physical constraints of the system and modeling insights, the authors fabricated the full MEC and a testing apparatus.

In conclusion, the various experiments to characterize the real-world performance of the MEC demonstrate that can transmit between 0.16 and 0.96 N·m of torque, with rapid response times (≈5 to 20 ms) and low-power consumption (1.25 mWh). Future work to optimize the MEC will explore different form factors, increase the torque transmission capabilities, and further lower power consumption. The EPM arrangement approach is scalable, and can be modified to a wide range of possible clutch form factors. The MEC represents a new control strategy for MRF-based torque transmission devices, and has many applications in varied robotic and automotive research areas.

Acknowledgments

The authors would like to thank the members of the OSU robotics and electrical engineering departments for their assistance in investigating current research in this field and relating to this topic. Additionally, the authors thank Maren Gingerich for their contributions during their REU in the summer of 2021, as well as the insight from Prof. Rafhael M. Andrade into the magnetic properties of plastic. This material is based upon work supported by the National Science Foundation Graduate Research Fellowship under Grant No. 1840998.

Chapter 6: General Conclusions

The purpose of all the work described in this document is to demonstrate the utility of a selection field-activated smart materials and their applications for robotic systems. This was achieved through three projects, including soft robotic fluidic control through the use of 3D printed ERF valves, developing magnetic elastomers coupled with permanent magnets to enhance soft actuator grip strength, and leveraging the low-power properties of EPMs to enable variable torque transmission with a MRF clutch.

Chapter 3 expands upon the basic principles of ERF introduced in Chapter 2 to develop an ERF-based high voltage valve for soft robotic actuators. The design of the valve was created with the intention of being low-cost and easily reproducible, to lower the barrier to entry for making use of ERF in soft robotic projects. The resulting valve design was 3D printed on a standard desktop 3D printer, and capable of maintaining large pressures sufficient for inflating and actuating multiple soft actuators. This chapter emphasises the importance of improving control strategies for soft robotic systems, and provides an alternative to the more common pneumatic control systems found in soft robots. It also embeds the means of control into a compact and portable PCB and valve, both of which are far more suitable for implementation in soft robots than the more cumbersome alternatives provided by traditional control boards and equipment. The resulting system considers the importance of controlling soft robot with untethered operation and repeatability of design, presenting much more accessible designs to other researchers who lack the expensive equipment often required to perform soft robotics research.

Chapter 4 introduces the importance of alternative grasping strategies in soft robotic systems, and describes the broad implications of grasping techniques in different fields. Building on the analysis from Chapter 2 regarding MEs, we developed a specific formulation of soft ME and thoroughly characterize its magnetic properties, comparing it with similar materials found in other applications. Taking this characterization, we deploy the ME in a soft actuator gripper, and demonstrate the range of grip strength possible as a result of adding magnets into the base of the palm. The resulting gripper is able to modulate its grip strength by modifying the position of the permanent magnet, as well as alter its path trajectory. These two improvements over a standard pneumatic soft actuator are just two of the possible additional modalities introduced into soft robotic systems made possible by incorporating field-activated smart materials, and the chapter describes possible improvements and methods for introducing MEs into more soft robotic applications.

Chapter 5 describes how designing a MRF clutch with intelligently planned electropermanent arrays allows for reduced power consumption and enables novel control strategies for torque transmission in robotic devices. With a growing need for battery operation and untethered, remote robotics, creating more compact and energy-efficient devices is of great interest to the broader field of study. These design goals are realized through the use of the field-activated smart fluid MRF and a method for generating controllable magnetic fields in the absence of power-hungry devices. The resulting design is modeled and tested to demonstrate the concept, and a prototype MRF clutch demonstrates its rapid response times and repeatability. The first attempts at controlling the transmitted torque for arbitrary set points demonstrates reasonable agreement, and highlights the potential for future improvement, as well as the large improvements in energy consumption over comparable designs utilizing standard electromagnets (or electromagnet and permanent magnet arrays).

This dissertation addresses a major challenge in robotics: how to extend the possibilities for control and actuation beyond the optimized tools we already have? Many technologies such as motors and pneumatic control boards are mature technologies, and as a result are commonly used in robotic systems. Introducing smart materials, as well as controllable electromagnetic fields, is demonstrated to create new control strategies and improve on existing actuation limits in. This dissertation also demonstrates that by bridging the gap between the concepts of soft or hard robotics, we can begin to draw from the spaces of both, enhancing each in turn. Physically hard magnets and small valves can be embedded in soft robotic systems, improving their utility across a broader range of applications, without compromising the innate softness required of them. Smart fluids and variable materials can be incorporated into hard systems, imparting variable stiffness and torque transmission to systems composed entirely of hard components. New arrangements of electromagnetic elements allow for embodied, localised control in robotic systems, and stand to improve power consumption and increase untetherability. These insights can be disseminated through many different robotic systems and expand and improve on the existing toolset available to roboticists in the design and fabrication of energy-efficient, responsive, and safe robots.

6.1 Contributions of this Work

3D-Printed Electroactive Hydraulic Valves for Use in Soft Robotic Applications

- Low-cost, repeatable design for a ERF valve using 3D printing
- Embeddable, compact valve form factor useful in untethered operation
- High pressure holding capability sufficient to actuate a group of soft actuators
- An alternative control strategy for soft robotic systems
- Miniaturized and low cost electronics to improve untetherability and accessibility
- Demonstration of all components capable of grasping various objects and opening and closing independent actuators from a single pressure source

Tuning the grasping strength of soft actuators with magnetic elastomer fingertips

- Focus on grasping and the importance of soft grasping strength
- Emphasis on the strengths and weaknesses of hard and soft grasping strategies
- Analysis of the applications of MEs in grasping
- Development and characterization of a ME to improve soft grasping strength
- Demonstration of variable grasp strength resulting from ME fingertips and permanent magnets
- Varied grip positions benefit from increased and variable grasp strength
- Positioning of the magnets in the base can control soft actuator trajectories out-of-plane
- MEs in soft robotic systems add additional control strategies for novel movements and strengths impossible without additional pressure chambers in traditional designs

A low-power magnetorheological fluid clutch utilizing electropermanent magnet arrays

- Emphasis on compliance and variable stiffness in a rigid mechanism
- Discussion on the potential of EPMs for low-power operation
- Modeling and simulation of EPM arrays with good agreement with the measured performance of prototypes
- Detailed guide on the fabrication of an MRF Clutch with EPM array and how the magnetic flux density creates the variable torque transmission response
- Analytical model of transmitted torque for different physical parameters of the clutch

- A prototype MEC capable of transmitting up to 0.8 N·m of torque without any additional power input beyond the polarization step
- Low-power consumption device with orders of magnitude less power consumption on large timescales, improving remote operation potential and incorporation into robotic systems
- Proof of concept for EPM arrays as control mechanisms in robotic systems, enabling future designs across soft and hard robotics

6.2 Practical Implications

The papers in this dissertation all have physical prototypes and demonstrations of their intended purpose. Each of these demonstrations have applications beyond the narrow focus of each paper, and encompass multiple fields (robotics, mechanical engineering, electrical engineering, materials science) in their potential uses. Practical implications of these works include:

3D-Printed Electroactive Hydraulic Valves for Use in Soft Robotic Applications

- Compact electronics for embodied high voltage control
- Methods for 3D printing and fabricating fluid valves
- Reducing hydraulic loop complexity with localized control
- Multipurpose hydraulic fluids, combining pressure transport with flow control

Tuning the grasping strength of soft actuators with magnetic elastomer fingertips

- Multi-material soft robotic actuators, containing smart materials fulfil multiple functions simultaneously
- Improving soft actuator range of motion, degrees of freedom, actuation strength, and actuation speed

- Designing and tuning bulk material properties for specific applications and precise behavior of soft systems
- Approaching soft robotic design constraints with physically hard elements to enhance the performance without losing the soft properties of the robotic system

A low-power magnetorheological fluid clutch utilizing electropermanent magnet arrays

- Deploying EPM arrays for distributed, localized, low-power magnetic field control in robotic systems
- Zero-power torque transmission for longer operation at any given set point in a known range, beyond the initial input power
- Underactuated rigid linkages with compliant and variably stiff joints consisting of a MEC, enabling variable and controllable linkage trajectories
- Embedding EPM arrays into soft robotic systems containing MRF for large maximum holding pressure, multiples greater than current research allows

6.3 Limitations

All of the incorporated works leverage smart materials and controllable electromagnetic fields to expand robotic control strategies. Current limitations present in all of the papers involve the use of commercial-grade materials. Utilizing simpler and more accessible generic alternatives for ERF and MRF would enable more research into their use. With the ME fingertips, the studied magnetic powders were relatively difficult to source, and all varied significantly in their particle dimensions and purity. Sourcing the materials necessary to perform this research, and reducing variables between samples of different materials, would greatly benefit future work in these spaces. Each work demonstrates a prototype involving the concepts involved, but none of the papers took the concepts farther to develop a complete or fully operational, independent robot, instead creating sub-elements that could be used in a larger robot.

In Chapter 3, a major limitation of ERF is the aforementioned lack of access to materials. The fluid used was several years old at the time of testing, and the manufacturer stopped producing it during the testing period. Alternatives based on corn-starch and silicone coil present promising replacements, but lack the shelf-stability of the premium-grade fluid. ERF also settles out quickly, which can be a significant barrier to robotic applications that sit inactive for extended periods of time. The pressure source for the ERF during operation still required a standard bench-top syringe pump, limiting the portability and untetherability of the concept. Combining the miniaturized electronics with further miniaturized pressure sources that could be incorporated into the body of a potential soft robot would reduce this shortcoming.

In Chapter 4, a limitation of the prototype was the use of permanent magnets. While these are widely accessible, solid discs of those dimensions which require manual repositioning, or bulky lead-screws for precise positioning, stand in the way of practically implementing the design in a functional robotic gripper. While this approach was demonstrated to work, being able to have more compact magnetic field generation of similar magnitude would greatly improve the utility of this approach. The EPM arrays in Chapter 5 could fill this need, as they utilize compact arrangements of permanent magnets to selectively control magnetic flux density. This would assist with the magnitude of magnetic field; however, for the modality where the soft actuator deflects away from its standard motion to follow the direction of the magnetic field lines would still require physical positioning of the magnet, or at least, several parallel magnets with controllable fields.

In Chapter 5, a major limitation of the control strategy developed is the assumption that the EPM would polarize as intended from any set point, since it was characterized either from magnetic saturation or from zero field. This assumption failed to hold true, demonstrating magnetic hysteresis of AlNiCo. More sophisticated control strategies are needed to account for this, and the ability to sense the current magnetization would greatly assist with this objective. The MEC has no internal state-sensing, assuming that any control strategy knows its prior state before taking action. The MEC in its current form would need to be modified to be implemented into a functional robotic linkage or other functional device; the prototype demonstrates the torque transmission properties, but it would require significant remodeling of the outer shell before it could be input into a functional design. Additionally, the physical parameters of the EPM were limited by the ability to source the right dimensions of AlNiCo magnet, which is relatively uncommon compared to other magnetic materials. Improving sourcing of materials would allow for greater physical diversity and further exploration of optimal parameters for a given application.

6.4 Open Research Questions

In each of these works, the development of the device was completed and left in its current form; each of these papers could be further optimized, with improved control strategies deployed to capitalize on the lessons learned from these prototypes. Each would benefit from using more sophisticated control methods with feedback to fine-tune the behavior of each. In Chapter 5, the MEC was briefly shown to have the capacity to raise the transmitted torque gradually by successive current pulses to the whole EPM array. This was only touched on, and it deserves a thorough analysis of possible set-point following methods, as opposed to an on-off strategy. Beyond that, there needs to be further investigation into the relationship of the inductance of the coil in each EPM, the magnetic reluctance of the EPM, and their relationships to the overall response of the MEC.

6.5 Future Research Directions

Field-activated smart materials in robotic systems are currently limited by a lack of thorough characterization for various potential smart materials that could be used.

In Chapter 4, we characterized the material properties of a few MEs; if there were a well-established and current database of MEs and their magnetic and magnetorheological properties, selecting the correct material for a given application would be far simpler. As it stands, most demonstrations in the literature that use MEs are required to provide their own characterization for each kind, and often make arbitrary choices for magnetic material particle size, relative concentrations, elasticity and related physical properties, and isotropic or anisotropic magnetization. All of these elements are important considerations for any application utilizing a magnetic smart material, and having a better foundation for this class of materials would greatly expedite further research in this space. Additionally, studying the relationship between all of these parameters and the other parameters would be highly informative for future research. Most existing literature usually focuses on a subset of these properties, but does not consider how all are connected holistically.

Developing additional smart fluids with a similar range of potential function would also expand research opportunities. As it stands, most research requires off-the shelf products, and many convergent solutions are the result of limited fluid choices. Some recent research developed their own, custom-tailored MRF for their application ([105]), which allows them to modify it as needed and produce more whenever their supply gets low, instead of relying on limited and expensive supply. More research into generic alternatives, as well as variations on the fluid formula, would greatly improve the spectrum of possible designs in robotic systems using these fluids.

Much of the work in magnetic elastomers has been focused on homogeneous mixtures, with a given magnetic particle mixed evenly into the elastomer composite. I anticipate that even more complex behaviors can arise by programming not just magnetic domains, as some research has done, but also by varying the relative concentrations of magnetic particle, and type of magnetic particle. These hybrid structures, like EPMs, stand to produce novel mechanisms and uses. A few theoretical examples could be an fully flexible EPM, made from elastic magnetic composites with AlNiCo and NdFeB powders, or a flexible magnetic sheet of elastomer containing hundreds of steel spheres (1mm in diameter) that will likely behave very differently than a homogeneous composite with an equivalent volume of steel, but in the form of millions of small particles (as is typical at the moment).

The research regarding the MEC suggests that EPMs can be further integrated into robotic applications where electromagnets are currently used to improve power consumption and reduce heat generation. Many modern technologies rely on electromagnets for magnetic field generation. While common, EPMs have the potential to replace electromagnets in many applications where constant magnetic flux is needed, but doesn't need to change constantly. MRF brakes are a clear example, since an applied field is necessary for creating a braking force, but it doesn't necessarily benefit from constant change, and instead performs as intended with a constant applied field.

All of the prototypes and demonstrations in these chapters would benefit from being placed into a functional robot. Future work can and should be done to integrate these mechanisms fully into a robot, such as:

- An elastic octopus robot with all its pressure source, electronics, and high voltage valves self-contained

- A robotic arm with a soft grasper containing MEs on the end effector, optimized for high grasping strength to be able to pick fruit from a tree without any bruising

- A MEC at each joint in a robotic linkage, able to modulate the end effector trajectory by controlling joint stiffness, and running off of battery power for extended operation

Each of these projects introduce novel concepts regarding how to control robotic systems with smart materials and electromagnetic fields. These works address the challenge of improving robotic control and capability, and bridging the gap between soft and hard systems to achieve more than can be done in fully hard or fully soft spaces. This research exists in the spaces between several fields, and was made possible through interdisciplinary research topics. Research in robotics stands to benefit greatly from further interdisciplinary research, as robotics are applicable to nearly all research fields in some capacity. Field-activated materials will continue to demonstrate their value within the field of robotics, and overcoming challenges to their development creates novel opportunities for robots to sense and act on their environments. Smart materials and electromagnetic control strategies expand what is currently possible, and finding new ways to bring different research spaces together will result in more opportunities for better, faster, safer, and smarter robotic designs in the future.

Bibliography

[1] Prasad Akella, Roland Siegwart, and Mark Cutkosky. Manipulation with soft fingers: Contact force control. In *Proceedings - IEEE International Conference on Robotics and Automation*, volume 1, pages 652–657. IEEE, 1991.

[2] Ahmed Alfadhel and Jürgen Kosel. Magnetic Nanocomposite Cilia Tactile Sensor. *Advanced Materials*, 27(47):7888–7892, 2015.

[3] Abdullah S. Almansouri, Nouf A. Alsharif, Mohammed A. Khan, Liam Swanepoel, Altynay Kaidarova, Khaled N. Salama, and Jurgen Kosel. An Imperceptible Magnetic Skin. *Advanced Materials Technologies*, 4(10):1900493, 2019.

[4] Rafhael M. Andrade, Pedro H. F. Ulhoa, and Claysson B. S. Vimieiro. Designing a highly backdrivable and kinematic compatible magneto-rheological knee exoskeleton. In *2022 International Conference on Robotics and Automation (ICRA)*, pages 5724–5730, 2022.

[5] Muhammad Arslan Hafeez, Muhammad Usman, Malik Adeel Umer, and Asad Hanif. Recent progress in isotropic magnetorheological elastomers and their properties: A review. *Polymers*, 12(12):3023, 2020.

[6] A. K. Bastola, V. T. Hoang, and L. Li. A novel hybrid magnetorheological elastomer developed by 3D printing. *Materials and Design*, 114:391–397, jan 2017.

[7] Majid Behrooz, Xiaojie Wang, and Faramarz Gordaninejad. Modeling of a new semi-active/passive magnetorheological elastomer isolator. *Smart Materials and Structures*, 23(4):45013, 2014.

[8] Marco Beleggia, David Vokoun, and Marc De Graef. Forces between a permanent magnet and a soft magnetic plate. *IEEE Magnetics Letters*, 3, 2012.

[9] C. Bellan and G. Bossis. Field dependence of viscoelastic properties of MR elastomers. *International Journal of Modern Physics B*, 16(17-18):2447–2453, 2002.

[10] R. Adam Bilodeau, Asian Miriyev, Hod Lipson, and Rebecca Kramer-Bottiglio. All-soft material system for strong soft actuators. In *2018 IEEE International Conference on Soft Robotics, RoboSoft 2018*, pages 288–294. IEEE, 2018.

[11] Eugene Cook Bingham. *Fluidity and plasticity*, volume 2. McGraw-Hill, 1922.

[12] Nicholas Bira, Pallavi Dhagat, and Joseph R Davidson. A review of magnetic elastomers and their role in soft robotics. *Frontiers in Robotics and AI*, 7:146, 2020.

[13] Nicholas Bira, Pallavi Dhagat, and Joseph R Davidson. Tuning the grasping strength of soft actuators with magnetic elastomer fingertips. *Smart Materials and Structures*, 31(4):045013, mar 2022.

[14] Nicholas Bira and Yigit Menguc. Measurement of tissue stiffness using soft eGa-in sensors and pressure application. In *2018 IEEE International Conference on Soft Robotics, RoboSoft 2018*, pages 228–232. IEEE, 2018.

[15] BiraN2019. 3d printed erf valve files, Sep 2019.

[16] H. Böse. Viscoelastic properties of silicone-based magnetorheological elastomers. *Proceedings of the 10th International Conference on Electrorheological Fluids and Magnetorheological Suspensions*, 21(28n29):51–57, 2007.

[17] H Böse and R Röder. Magnetorheological elastomers with high variability of their mechanical properties. In *Journal of Physics: Conference Series*, volume 149, page 012090. IOP Publishing, 2009.

[18] Holger Böse, Raman Rabindranath, and Johannes Ehrlich. Soft magnetorheological elastomers as new actuators for valves. *Journal of Intelligent Material Systems and Structures*, 23(9):989–994, 2012.

[19] Landen Bowen, Mary Frecker, Timothy W. Simpson, and Paris Von Lockette. A Dynamic Model of magneto-active elastomer actuation of the waterbomb base. *Proceedings of the ASME Design Engineering Technical Conference*, 5B(1), 2014.

[20] C Branyan, R L Hatton, and Y Mengüç. Snake-Inspired Kirigami Skin for Lateral Undulation of a Soft Snake Robot. *IEEE Robotics and Automation Letters*, 5(2):1728–1733, 2020.

[21] Callie Branyan, Chloe Fleming, Jacquelin Remaley, Ammar Kothari, Kagan Tumer, Ross L. Hatton, and Yigit Menguc. Soft snake robots: Mechanical design and geometric gait implementation. *2017 IEEE International Conference on Robotics and Biomimetics, ROBIO 2017*, 2018-Janua:282–289, 2018.

[22] Joyce C. Breger, Changkyu Yoon, Rui Xiao, Hye Rin Kwag, Martha O. Wang, John P. Fisher, Thao D. Nguyen, and David H. Gracias. Self-folding thermo-magnetically responsive soft microgrippers. *ACS Applied Materials and Interfaces*, 7(5):3398–3405, 2015.

[23] R. Bustamante, A. Dorfmann, and R. W. Ogden. On variational formulations in nonlinear magnetoelastostatics. *Mathematics and Mechanics of Solids*, 13(8):725–745, 2008.

[24] J. D. Carlson, D. M. Catanzarite, and K. A.St Clair. Commercial magneto-rheological fluid devices. *International Journal of Modern Physics B*, 10(23-24):2857–2865, 1996.

[25] J. David Carlson and Mark R. Jolly. MR fluid, foam and elastomer devices. *Mechatronics*, 10(4):555–569, 2000.

[26] James D Carrico and Kam K Leang. Fused filament 3d printing of ionic polymer-metal composites for soft robotics. In *Electroactive Polymer Actuators and Devices (EAPAD) 2017*, volume 10163, pages 70–82. SPIE, 2017.

[27] Mark Cartolano, Boxi Xia, Aslan Miriyev, and Hod Lipson. Conductive fabric heaters for heat-activated soft actuators. In *Actuators*, volume 8, page 9. Multidisciplinary Digital Publishing Institute, 2019.

[28] Lin Chen, X L Gong, and W H Li. Microstructures and viscoelastic properties of anisotropic magnetorheological elastomers. *Smart Materials and Structures*, 16(6):2645, 2007.

[29] Yinglong Chen, Junhao Zhang, and Yongjun Gong. Utilizing anisotropic fabrics composites for high-strength soft manipulator integrating soft gripper. *IEEE Access*, 7:127416–127426, 2019.

[30] L Chin, J Lipton, R MacCurdy, J Romanishin, C Sharma, and D Rus. Compliant electric actuators based on handed shearing auxetics. In *2018 IEEE International Conference on Soft Robotics (RoboSoft)*, pages 100–107, 2018.

[31] Dong-Soo Choi, Tae-Hoon Kim, Seok-Han Lee, Changhyun Pang, Jin Woo Bae, and Sang-Youn Kim. Beyond Human Hand: Shape-Adaptive and Reversible Magnetorheological Elastomer-Based Robot Gripper Skin. *ACS Applied Materials and Interfaces*, 12(39):44147–44155, 2020.

[32] Ching-Ping Chou and Blake Hannaford. Measurement and modeling of McKibben pneumatic artificial muscles. *IEEE Transactions on robotics and automation*, 12(1):90–102, 1996.

[33] Jacopo Ciambella, David C Stanier, and Sameer S Rahatekar. Magnetic alignment of short carbon fibres in curing composites. *Composites Part B: Engineering*, 109:129–137, 2017.

[34] E Coquelle and G Bossis. Mullins effect in elastomers filled with particles aligned by a magnetic field. *International Journal of Solids and Structures*, 43(25-26):7659–7672, 2006.

[35] Peet Cremer, Hartmut Löwen, and Andreas M Menzel. Tailoring superelasticity of soft magnetic materials. *Applied Physics Letters*, 107(17):171903, 2015.

[36] Robbie Damiani and L Z Sun. Microstructural characterization and effective viscoelastic behavior of magnetorheological elastomers with varying acetone contents. *International Journal of Damage Mechanics*, 26(1):104–118, 2017.

[37] Joseph R. Davidson and Hermano Igo Krebs. An Electrorheological Fluid Actuator for Rehabilitation Robotics. *IEEE/ASME Transactions on Mechatronics*, 23(5):2158–2167, 2018.

[38] Joseph R Davidson and Hermano Igo Krebs. An electrorheological fluid actuator for rehabilitation robotics. *IEEE/ASME Transactions on Mechatronics*, 23(5):2156–2167, 2018.

[39] L. C. Davis. Model of magnetorheological elastomers. *Journal of Applied Physics*, 85(6):3348–3351, 1999.

[40] Rafhael Milanezi de Andrade, Jordana Simões Ribeiro Martins, Marcos Pinotti, Antônio Bento Filho, and Claysson Bruno Santos Vimieiro. Novel active magnetorheological knee prosthesis presents low energy consumption during ground walking. *Journal of Intelligent Material Systems and Structures*, 32(14):1591–1603, 2021.

[41] Lei Deng, Shuaishuai Sun, Shida Jin, Zhixiong Li, Haiping Du, Shiwu Zhang, and Weihua Li. Development of a new magnetorheological impact damper with low velocity sensitivity. *Smart Materials and Structures*, 2022.

[42] A Dorfmann and R W Ogden. Magnetoelastic modelling of elastomers. *European Journal of Mechanics-A/Solids*, 22(4):497–507, 2003.

[43] Jean Numa Foulc. Electrorheological Fluids. *Dielectric Materials for Electrical Engineering*, 258(5083):379–402, 2013.

[44] Junji Furusho, Guoguang Zhang, and Masamichi Sakaguchi. Vibration suppression control of robot arms using a homogeneous-type electrorheological fluid. In *Robotics and Automation, 1997. Proceedings., 1997 IEEE International Conference on*, volume 4, pages 3441–3448. IEEE, 1997.

[45] Kevin C Galloway, Kaitlyn P Becker, Brennan Phillips, Jordan Kirby, Stephen Licht, Dan Tchernov, Robert J Wood, and David F Gruber. Soft robotic grippers for biological sampling on deep reefs. *Soft robotics*, 3(1):23–33, 2016.

[46] Kevin C Galloway, Panagiotis Polygerinos, Conor J Walsh, and Robert J Wood. Mechanically programmable bend radius for fiber-reinforced soft actuators. In *2013 16th International Conference on Advanced Robotics (ICAR)*, pages 1–6. IEEE, 2013.

[47] G. Georgiades and S. O. Oyadiji. Effects of electrode geometry on the performance of electrorheological fluid valves. *Journal of Intelligent Material Systems and Structures*, 14(2):105–111, feb 2003.

[48] Lucas Gerez, Geng Gao, and Minas Liarokapis. Employing magnets to improve the force exertion capabilities of adaptive robot hands in precision grasps. In *2019 IEEE/RSJ International Conference on Intelligent Robots and Systems (IROS)*, pages 7630–7635. IEEE, 2019.

[49] John M Ginder, Mark E Nichols, Larry D Elie, and Janice L Tardiff. Magnetorheological elastomers: properties and applications. In *Smart Structures and Materials 1999: Smart Materials Technologies*, volume 3675, pages 131–139. International Society for Optics and Photonics, 1999.

[50] X L Gong, X Z Zhang, and P Q Zhang. Fabrication and characterization of isotropic magnetorheological elastomers. *Polymer testing*, 24(5):669–676, 2005.

[51] Faramarz Gordaninejad and Darrell G Breese. Heating of magnetorheological fluid dampers. *Journal of intelligent material systems and structures*, 10(8):634–645, 1999.

[52] Benjamin Gorissen, Dominiek Reynaerts, Satoshi Konishi, Kazuhiro Yoshida, Joon-Wan Kim, and Michael De Volder. Elastic Inflatable Actuators for Soft Robotic Applications. *Advanced Materials*, 29(43):1604977, nov 2017.

[53] D. Vaughan Griffiths and I.M. Smith. *Numerical Integration*. Elsevier Science,, Saint Louis :, 2020.

[54] Ivar Gudmundsson. *A feasibility study of magnetorheological elastomers for a potential application in prosthetic devices*. PhD thesis, University of Iceland, 2011.

[55] M Gurka, L Johnston, and R Petricevic. New electrorheological fluids - Characteristics and implementation in industrial and mobile applications. *Journal of Intelligent Material Systems and Structures*, 21(15):1531–1535, 2010.

[56] Mohd Nor Hazwan Hadzir, Muhamad Husaini Abu Bakar, and Ishak Abdul Azid. Effect of the magnetic field on magnetic particles in magnetorheological elastomer layers. In *Advanced Engineering for Processes and Technologies*, pages 135–143. Springer, 2019.

[57] Mohd Nor Hazwan Hadzir, Muhamad Husaini Abu Bakar, and Ishak Abdul Azid. Effect of the magnetic field on magnetic particles in magnetorheological elastomer layers. In *Advanced Engineering for Processes and Technologies*, pages 135–143. Springer, 2019.

[58] Yin Haibin, Kong Cheng, Li Junfeng, and Yang Guilin. Modeling of grasping force for a soft robotic gripper with variable stiffness. *Mechanism and Machine Theory*, 128:254–274, 2018.

[59] Daehoon Han, Cindy Farino, Chen Yang, Tracy Scott, Daniel Browe, Wonjoon Choi, Joseph W Freeman, and Howon Lee. Soft robotic manipulation

and locomotion with a 3d printed electroactive hydrogel. *ACS Applied Materials and interfaces*, 10(21):17512–17518, 2018.

[60] Yi Han, Wei Hong, and LeAnn E Faidley. Field-stiffening effect of magneto-rheological elastomers. *International Journal of Solids and Structures*, 50(14-15):2281–2288, 2013.

[61] Nicholas S Hare Sr. Electro-rheological shock absorber, 1992.

[62] Ahmed H. Helal. *Designing devices using electro-active yield stress fluids.* PhD thesis, Massachusetts Institute of Technology, 2016.

[63] Tess Hellebrekers, Nadine Chang, Keene Chin, Michael Ford, Oliver Kroemer, and Carmel Majidi. Soft Magnetic Tactile Skin for Continuous Force and Location Estimation using Neural Networks. *IEEE Robotics and Automation Letters*, 2020.

[64] Wolfgang Hilber. Stimulus-active polymer actuators for next-generation microfluidic devices. *Applied Physics A*, 122(8):751, 2016.

[65] Lindsey Hines, Kirstin Petersen, Guo Zhan Lum, and Metin Sitti. Soft Actuators for Small-Scale Robotics. *Advanced Materials*, 29(13):1603483, apr 2017.

[66] Dónal P Holland, Evelyn J Park, Panagiotis Polygerinos, Gareth J Bennett, and Conor J Walsh. The soft robotics toolkit: Shared resources for research and design. *Soft Robotics*, 1(3):224–230, 2014.

[67] B Horváth and I Szalai. Structure of electrorheological fluids: A dielectric study of chain formation. *Physical Review E - Statistical, Nonlinear, and Soft Matter Physics*, 86(6):1–5, 2012.

[68] Wenqi Hu, Guo Zhan Lum, Massimo Mastrangeli, and Metin Sitti. Small-scale soft-bodied robot with multimodal locomotion. *Nature*, 554(7690):81–85, jan 2018.

[69] D Hua, X Liu, S Sun, M A Sotelo, Z Li, and W Li. A Magnetorheological Fluid Filled Soft Crawling Robot with Magnetic Actuation. *IEEE/ASME Transactions on Mechatronics*, page 1, 2020.

[70] Filip Ilievski, Aaron D Mazzeo, Robert F Shepherd, Xin Chen, and George M Whitesides. Soft robotics for chemists. *Angewandte Chemie*, 123:1930–1935, 2011.

[71] Booyong Im and Jungwon Yoon. Development of a soft haptic sensor capable of measuring contact forces based on magnetorheological elastomers. In *2022 19th International Conference on Ubiquitous Robots (UR)*, pages 225–230, 2022.

[72] Dmytro Ivaneyko, Vladimir P Toshchevikov, Marina Saphiannikova, and Gert Heinrich. Magneto-sensitive Elastomers in a Homogeneous Magnetic Field: A Regular Rectangular Lattice Model. *Macromolecular Theory and Simulations*, 20(6):411–424, 2011.

[73] K J Kim J. D. Carrico and K. K. Leang. 3D-Printed Ionic Polymer-Metal Composite Soft Crawling Robot. In *IEEE International Conference on Robotics and Automation (ICRA), Sands Expo and Convention Centre, Marina Bay Sands in Singapore, May 29 - June 3, 2017*, 2017.

[74] Sungwoong Jeon, Ali Kafash Hoshiar, Kangho Kim, Seungmin Lee, Eunhee Kim, Sunkey Lee, Jin-young Kim, Bradley J Nelson, Hyo-Jeong Cha, Byung-Ju Yi, and Others. A magnetically controlled soft microrobot steering a guidewire in a three-dimensional phantom vascular network. *Soft robotics*, 6(1):54–68, 2019.

[75] Mark R Jolly, Jonathan W Bender, and J David Carlson. Properties and applications of commercial magnetorheological fluids. *Journal of intelligent material systems and structures*, 10(1):5–13, 1999.

[76] Mark R Jolly, J David Carlson, and Beth C Munoz. A model of the behaviour of magnetorheological materials. *Smart Materials and Structures*, 5(5):607, 1996.

[77] Mark R Jolly, J David Carlson, Beth C Muñoz, and Todd A Bullions. The magnetoviscoelastic response of elastomer composites consisting of ferrous particles embedded in a polymer matrix. *Journal of Intelligent Material Systems and Structures*, 7(6):613–622, 1996.

[78] Erina B Joyee and Yayue Pan. A Fully Three-dimensional printed inchworm-inspired soft robot with magnetic actuation. *Soft robotics*, 6(3):333–345, 2019.

[79] B X Ju, M Yu, J Fu, Q Yang, X Q Liu, and X Zheng. A novel porous magnetorheological elastomer: preparation and evaluation. *Smart Materials and Structures*, 21(3):35001, 2012.

[80] Hyo Seung Jung, Seung Hyuk Kwon, Hyoung Jin Choi, Jae Heum Jung, and Young Gil Kim. Magnetic carbonyl iron/natural rubber composite elastomer and its magnetorheology. *Composite Structures*, 136:106–112, 2016.

[81] Marke Kallio. *The elastic and damping properties of magnetorheological elastomers*. VTT Espoo, Finland, 2005.

[82] Shunta Kashima, Fumikazu Miyasaka, and Katsuhiro Hirata. Novel soft actuator using magnetorheological elastomer. *IEEE Transactions on Magnetics*, 48(4):1649–1652, 2012.

[83] Barkan Kavlicoglu, Faramarz Gordaninejad, Cahit Evrensel, Alan Fuchs, and George Korol. A Semi-Active, High-Torque, Magnetorheological Fluid Limited Slip Differential Clutch. *Journal of Vibration and Acoustics*, 128(5):604–610, 2006.

[84] MarcF-Andre Keip and Matthias Rambausek. Computational and analytical investigations of shape effects in the experimental characterization of magnetorheological elastomers. *International Journal of Solids and Structures*, 121:1–20, 2017.

[85] Gary L Kenaley and Mark R Cutkosky. Electrorheological fluid-based robotic fingers with tactile sensing. In *Proceedings, 1989 International Conference on Robotics and Automation*, pages 132–136. IEEE, 1989.

[86] Jiyun Kim, Su Eun Chung, Sung-Eun Choi, Howon Lee, Junhoi Kim, and Sunghoon Kwon. Programming magnetic anisotropy in polymeric microactuators. *Nature Materials*, 10(10):747–752, oct 2011.

[87] Yoonho Kim, German A Parada, Shengduo Liu, and Xuanhe Zhao. Ferromagnetic soft continuum robots. *Science Robotics*, 4(33):eaax7329, 2019.

[88] Yoonho Kim, Hyunwoo Yuk, Ruike Zhao, Shawn A. Chester, and Xuanhe Zhao. Printing ferromagnetic domains for untethered fast-transforming soft materials. *Nature*, 558(7709):274–279, jun 2018.

[89] Yoonho Kim, Hyunwoo Yuk, Ruike Zhao, Shawn A Chester, and Xuanhe Zhao. Printing ferromagnetic domains for untethered fast-transforming soft materials. *Nature*, 558(7709):274, 2018.

[90] Sousaku Kitano, Toshihiko Komatsuzaki, Ikuto Suzuki, Masamichi Nogawa, Hisashi Naito, and Shinobu Tanaka. Development of a Rigidity Tunable Flexible Joint Using Magneto-Rheological Compounds—Toward a Multi-joint Manipulator for Laparoscopic Surgery. *Front. Robot. AI 7: 59. doi: 10.3389/frobt*, 7(April):1–6, 2020.

[91] Soo Jin Adrian Koh, Xuanhe Zhao, and Zhigang Suo. Maximal energy that can be converted by a dielectric elastomer generator. *Applied Physics Letters*, 94(26):262902, 2009.

[92] Anastasia Koivikko, Dirk-Michael Drotlef, Metin Sitti, and Veikko Sariola. Magnetically switchable soft suction grippers. *Extreme Mechanics Letters*, page 101263, 2021.

[93] A Kollias and A D Dimarogonas. Properties of zeolite-and cornstarch-based electrorheological fluids at high shear strain rates. *Journal of intelligent material systems and structures*, 4(4):519–526, 1993.

[94] Marcel Le Floc'H, Alexis Chevalier, and Jean-Luc Mattei. The magnetic susceptibility in soft magnetic composite materials. *Le Journal de Physique IV*, 8(PR2):Pr2–355, 1998.

[95] Dingxin Leng, Tongtong Wu, Guijie Liu, Xiaojie Wang, and Lingyu Sun. Tunable isolator based on magnetorheological elastomer in coupling shear–squeeze mixed mode. *Journal of Intelligent Material Systems and Structures*, 29(10):2236–2248, 2018.

[96] T Leps, P E Glick, D Ruffatto III, A Parness, M T Tolley, and C Hartzell. A low-power, jamming, magnetorheological valve using electropermanent magnets suitable for distributed control in soft robots. *Smart Materials and Structures*, 29(10):105025, 2020.

[97] T Leps, PE Glick, D Ruffatto III, A Parness, MT Tolley, and C Hartzell. A low-power, jamming, magnetorheological valve using electropermanent magnets suitable for distributed control in soft robots. *Smart Materials and Structures*, 29(10):105025, 2020.

[98] Wen Bo Li, Wen Ming Zhang, Hong Xiang Zou, Zhi Ke Peng, and Guang Meng. A Fast Rolling Soft Robot Driven by Dielectric Elastomer. *IEEE/ASME Transactions on Mechatronics*, 23(4):1630–1640, 2018.

[99] Yancheng Li, Jianchun Li, Weihua Li, and Haiping Du. A state-of-the-art review on magnetorheological elastomer devices. *Smart materials and structures*, 23(12):123001, 2014.

[100] Mattias Lokander and Bengt Stenberg. Performance of isotropic magnetorheological rubber materials. *Polymer Testing*, 22(3):245–251, 2003.

[101] Guo Zhan Lum, Zhou Ye, Xiaoguang Dong, Hamid Marvi, Onder Erin, Wenqi Hu, and Metin Sitti. Shape-programmable magnetic soft matter. *Proceedings of the National Academy of Sciences*, 113(41):E6007—-E6015, oct 2016.

[102] Guo Zhan Lum, Zhou Ye, Xiaoguang Dong, Hamid Marvi, Onder Erin, Wenqi Hu, and Metin Sitti. Shape-programmable magnetic soft matter. *Proceedings of the National Academy of Sciences*, 113(41):E6007–E6015, 2016.

[103] L Manamanchaiyaporn, T XU, and X. wu. Magnetic soft robot with the triangular head-tail morphology inspired by lateral undulation. *IEEE/ASME Transactions on Mechatronics*, page 1, 2020.

[104] Vadim A Markel. Introduction to the Maxwell Garnett approximation: tutorial. *JOSA A*, 33(7):1244–1256, 2016.

[105] Kevin J. McDonald, Lorenzo Kinnicutt, Anna Maria Moran, and Tommaso Ranzani. Modulation of magnetorheological fluid flow in soft robots using electropermanent magnets. *IEEE Robotics and Automation Letters*, 7(2):3914–3921, 2022.

[106] Philipp Metsch, Karl A Kalina, Christian Spieler, and Markus Kästner. A numerical study on magnetostrictive phenomena in magnetorheological elastomers. *Computational Materials Science*, 124:364–374, 2016.

[107] Carl G Meyer, Kim N Holland, and Yannis P Papastamatiou. Sharks can detect changes in the geomagnetic field. *Journal of the Royal Society Interface*, 2(2):129–130, 2005.

[108] Aslan Miriyev, Kenneth Stack, and Hod Lipson. Soft material for soft actuators. *Nature Communications*, 8(1):596, 2017.

[109] Masoud Moghani and Mehrdad R Kermani. A lightweight magnetorheological actuator using hybrid magnetization. *IEEE/ASME Transactions on Mechatronics*, 25(1):76–83, 2019.

[110] Daniel Morales, Etienne Palleau, Michael D Dickey, and Orlin D Velev. Electro-actuated hydrogel walkers with dual responsive legs. *Soft matter*, 10(9):1337–1348, 2014.

[111] Bobak Mosadegh, Panagiotis Polygerinos, Christoph Keplinger, Sophia Wennstedt, Robert F Shepherd, Unmukt Gupta, Jongmin Shim, Katia Bertoldi, Conor J Walsh, and George M Whitesides. Pneumatic networks for soft robotics that actuate rapidly. *Advanced functional materials*, 24(15):2163–2170, 2014.

[112] Michael P Murphy and Robert Playter. Electrorheological valve, 2015.

[113] Nima Najmaei, Mehrdad R Kermani, and Rajni V Patel. Suitability of small-scale magnetorheological fluid-based clutches in haptic interfaces for improved performance. *IEEE/ASME Transactions on Mechatronics*, 20(4):1863–1874, 2014.

[114] Biswajit Nayak, Santosha K Dwivedy, and Kondepudi S R K Murthy. Fabrication and characterization of magnetorheological elastomer with carbon black. *Journal of Intelligent Material Systems and Structures*, 26(7):830–839, 2015.

[115] Jason Nikitczuk, Brian Weinberg, and Constantinos Mavroidis. Control of electro-rheological fluid based resistive torque elements for use in active rehabilitation devices. *Smart Materials and Structures*, 16(2):418, 2007.

[116] Gina Olson, Scott Chow, Austin Nicolai, Callie Branyan, Geoffrey Hollinger, and Yigit Menguc. A generalizable equilibrium model for bending soft arms with longitudinal actuators. *The International Journal of Robotics Research*, page 0278364919880259, 2019.

[117] Claudio Pacchierotti, Federico Ongaro, Frank den Brink, ChangKyu Yoon, Domenico Prattichizzo, David H Gracias, and Sarthak Misra. Steering and

control of miniaturized untethered soft magnetic grippers with haptic assistance. *IEEE transactions on automation science and engineering*, 15(1):290–306, 2017.

[118] Laura Paez, Gunjan Agarwal, and Jamie Paik. Design and analysis of a soft pneumatic actuator with origami shell reinforcement. *Soft Robotics*, 3(3):109–119, 2016.

[119] Jefferson Pardomuan, Nobuhiro Takahashi, and Hideki Koike. Astre: Prototyping technique for modular soft robots with variable stiffness. *IEEE Access*, 2022.

[120] Giorgio Pessot, Peet Cremer, Dmitry Y Borin, Stefan Odenbach, Hartmut Löwen, and Andreas M Menzel. Structural control of elastic moduli in ferrogels and the importance of non-affine deformations. *The Journal of chemical physics*, 141(12):15005, 2014.

[121] Do Xuan Phu and Seung-Bok Choi. Magnetorheological fluid based devices reported in 2013–2018: mini-review and comment on structural configurations. *Frontiers in Materials*, 6:19, 2019.

[122] Sergey Pisetskiy and Mehrdad Kermani. High-performance magnetorheological clutches for direct-drive actuation: Design and development. *Journal of Intelligent Material Systems and Structures*, page 1045389X211006902, 2021.

[123] Song Qi, Hengyu Guo, Jie Fu, Yuanpeng Xie, Mi Zhu, and Miao Yu. 3D printed shape-programmable magneto-active soft matter for biomimetic applications. *Composites Science and Technology*, 188:107973, 2020.

[124] R Ramprasad, P Zurcher, M Petras, M Miller, and P Renaud. Magnetic properties of metallic ferromagnetic nanoparticle composites. *Journal of applied physics*, 96(1):519–529, 2004.

[125] Steven I. Rich, Robert J. Wood, and Carmel Majidi. Untethered soft robotics. *Nature Electronics*, 1(2):102–112, 2018.

[126] John A. Rogers. A clear advance in soft actuators. *Science*, 341(6149):968–969, 2013.

[127] Wilhelm Conrad Röntgen. Ueber die durch Electricität bewirkten Form- und Volumenänderungen von dielectrischen Körpern. *Annalen der Physik*, 247(13):771–786, 1880.

[128] Philipp Rothemund, Alar Ainla, Lee Belding, Daniel J Preston, Sarah Kurihara, Zhigang Suo, and George M Whitesides. A soft, bistable valve for autonomous control of soft actuators. *Science Robotics*, 3(16):eaar7986, 2018.

[129] Daniela Rus and Michael T Tolley. Design, fabrication and control of origami robots. *Nature Reviews Materials*, 3(6):101, 2018.

[130] Alì Sadeghi, Lucia Beccai, and Barbara Mazzolai. Innovative soft robots based on electro-rheological fluids. In *Intelligent Robots and Systems (IROS), 2012 IEEE/RSJ International Conference on*, pages 4237–4242. IEEE, 2012.

[131] Ali Sadeghi, Lucia Beccai, and Barbara Mazzolai. Innovative soft robots based on electro-rheological fluids. In *Proceedings of the ... IEEE/RSJ International Conference on Intelligent Robots and Systems. IEEE/RSJ International Conference on Intelligent Robots and Systems*, pages 4237–4242, 2012.

[132] Danial Sangian, Ali Jeiranikhameneh, Sina Naficy, Stephen Beirne, and Geoffrey M Spinks. Three-Dimensional Printed Braided Sleeves for Manufacturing McKibben Artificial Muscles. *3D Printing and Additive Manufacturing*, 2018.

[133] Maxime Savary, Svenja Hermann, Christophe Espanet, Valentin Préault, Gaël Chevallier, Pauline Butaud, and Jean-François Manceau. Development of a magneto-mechanical bench and experimental characterization of magneto-rheological elastomers. *IEEE Transactions on Magnetics*, 2021.

[134] Dmitry V Saveliev, Inna A Belyaeva, Dmitry V Chashin, Leonid Y Fetisov, Dirk Romeis, Wolfgang Kettl, Elena Yu Kramarenko, Marina Saphiannikova, Gennady V Stepanov, and Mikhail Shamonin. Giant extensional strain of magnetoactive elastomeric cylinders in uniform magnetic fields. *Materials*, 13(15):3297, 2020.

[135] Geoffrey W Schmitz. Hydraulically energized magnetorheological replicant muscle tissue and a system and a method for using and controlling same, 2001.

[136] M Seed, G S Hobson, R C Tozer, and A J Simmonds. Voltage-controlled electrorheological brake. In *Proceedings of the IASTED International Symposium on Measurements, Processes and Controls*, pages 280–284, 1986.

[137] Alex S Shafer and Mehrdad R Kermani. On the feasibility and suitability of mr and er based actuators in human friendly manipulators. In *2009 IEEE/RSJ International Conference on Intelligent Robots and Systems*, pages 2904–2909. IEEE, 2009.

[138] Mohsen Shahinpoor and Kwang J Kim. Ionic polymer-metal composites: I. Fundamentals. *Smart materials and structures*, 10(4):819, 2001.

[139] Robert F Shepherd, Filip Ilievski, Wonjae Choi, Stephen A Morin, Adam A Stokes, Aaron D Mazzeo, Xin Chen, Michael Wang, and George M Whitesides. Multigait soft robot. *Proceedings of the national academy of sciences*, 108(51):20400–20403, 2011.

[140] Robert Michael Sheridan. *Modeling magneto-active elastomers using the finite element method*. PhD thesis, Penn State, 2014.

[141] Jun Shintake, Vito Cacucciolo, Dario Floreano, and Herbert Shea. Soft robotic grippers. *Advanced Materials*, 30(29):1707035, 2018.

[142] A J Simmonds. Electro-rheological valves in a hydraulic circuit. *Power international*, 38(430):9–12, 1992.

[143] Nina R Sinatra, Clark B Teeple, Daniel M Vogt, Kevin Kit Parker, David F Gruber, and Robert J Wood. Ultragentle manipulation of delicate structures using a soft robotic gripper. *Science Robotics*, 4(33), 2019.

[144] J. E. Stangroom. Electrorheological fluids. *Physics in Technology*, 14(6):290–296, nov 1983.

[145] James E Stangroom. Electrorheological fluids. *Physics in Technology*, 14(6):290, 1983.

[146] R Stanway, J L Sproston, and A K El-Wahed. Applications of electro-rheological fluids in vibration control: a survey. *Smart Materials and Structures*, 5(4):464, 1996.

[147] Cynthia Sung, Rhea Lin, Shuhei Miyashita, Sehyuk Yim, Sangbae Kim, and Daniela Rus. Self-folded soft robotic structures with controllable joints. In *2017 IEEE International Conference on Robotics and Automation (ICRA)*, pages 580–587. IEEE, 2017.

[148] K Suzumori, S Iikura, and H Tanaka. Applying a flexible microactuator to robotic mechanisms. *IEEE Control Systems Magazine*, 12(1):21–27, feb 1992.

[149] Naoyuki Takesue, Guoguang Zhang, Junji Furusho, and Masamichi Sakaguchi. Precise position control of robot arms using a homogeneous ER fluid. *IEEE control systems*, 19(2):55–61, 1999.

[150] Wing Yim Tam, Guang Hua Yi, Weijia Wen, Hongru Ma, M. M.T. Loy, and Ping Sheng. New Electrorheological Fluid: Theory and Experiment. *Physical Review Letters*, 78(15):2987–2990, apr 1997.

[151] Jingda Tang, Zongfei Tong, Yukun Xia, Ming Liu, Zengyao Lv, Yang Gao, Tongqing Lu, Shejuan Xie, Yongmao Pei, Daining Fang, and Others. Super tough magnetic hydrogels for remotely triggered shape morphing. *Journal of Materials Chemistry B*, 6(18):2713–2722, 2018.

[152] Yichao Tang, Mingtong Li, Tianlu Wang, Xiaoguang Dong, Wenqi Hu, and Metin Sitti. Wireless miniature magnetic phase-change soft actuators. *Advanced Materials*, page 2204185, 2022.

[153] Alice Tonazzini, Ali Sadeghi, and Barbara Mazzolai. Electrorheological valves for flexible fluidic actuators. *Soft Robotics*, 3(1):34–41, 2016.

[154] Zsolt Varga, Genovéva Filipcsei, and Miklós Zrínyi. Magnetic field sensitive functional elastomers with tuneable elastic modulus. *Polymer*, 47(1):227–233, 2006.

[155] Hossein Vatandoost, Ramin Sedaghati, Subhash Rakheja, and Masoud Hemmatian. Effect of pre-strain on compression mode properties of magnetorheological elastomers. *Polymer Testing*, 93:106888, 2021.

[156] RK Walser, W Win, and PM Valanju. Shape-optimized ferromagnetic particles with maximum theoretical microwave susceptibility. *IEEE transactions on magnetics*, 34(4):1390–1392, 1998.

[157] Yanxiang Wan, Yeping Xiong, and Shengming Zhang. Temperature effect on viscoelastic properties of anisotropic magnetorheological elastomers under compression. *Smart Materials and Structures*, 28(1):15005, 2018.

[158] Jiangbei Wang, Yanqiong Fei, and Wu Pang. Design, modeling, and testing of a soft pneumatic glove with segmented pneunets bending actuators. *IEEE/ASME Transactions on Mechatronics*, 24(3):990–1001, 2019.

[159] Sihan Wang, Liang He, Alessandro Albini, Peizhi Zhang, and Perla Maiolino. A magnetorheological elastomer based proportional valve for soft pneumatic actuators. *Authorea Preprints*, 2022.

[160] Xiaojie Wang, Faramarz Gordaninejad, Mert Calgar, Yanming Liu, Joko Sutrisno, and Alan Fuchs. Sensing behavior of magnetorheological elastomers. *Journal of Mechanical Design*, 131(9), 2009.

[161] Hang Wei, Yu Shan, Yanzhi Zhao, Lizhe Qi, and Xilu Zhao. A soft robot with variable stiffness multidirectional grasping based on a folded plate mechanism and particle jamming. *IEEE Transactions on Robotics*, pages 1–11, 2022.

[162] Weijia Wen, Xianxiang Huang, Shihe Yang, Kunquan Lu, and Ping Sheng. The giant electrorheological effect in suspensions of nanoparticles. *Nature materials*, 2(11):727, 2003.

[163] Weijia Wen, Xianxiang Huang, Shihe Yang, Kunquan Lu, and Ping Sheng. The giant electrorheological effect in suspensions of nanoparticles. *Nature materials*, 2(11):727–30, nov 2003.

[164] George M. Whitesides. Soft Robotics. *Angewandte Chemie - International Edition*, 57(16):4258–4273, 2018.

[165] M. Whittle and W. A. Bullough. The structure of smart fluids. *Nature*, 358(6385):373, 1992.

[166] Roswitha Wiltschko and Wolfgang Wiltschko. Magnetoreception in birds. *Journal of the Royal Society Interface*, 16(158):20190295, 2019.

[167] WM Winslow. Method and means for translating electrical impulses into mechanical force, 1947.

[168] Sebastian Wolf, Giorgio Grioli, Oliver Eiberger, Werner Friedl, Markus Grebenstein, Hannes Höppner, Etienne Burdet, Darwin G. Caldwell, Raffaella Carloni, Manuel G. Catalano, Dirk Lefeber, Stefano Stramigioli, Nikos Tsagarakis, Michaël Van Damme, Ronald Van Ham, Bram Vanderborght, Ludo C. Visser, Antonio Bicchi, and Alin Albu-Schäffer. Variable stiffness actuators: Review on design and components. *IEEE/ASME Transactions on Mechatronics*, 21(5):2418–2430, 2016.

[169] Chenjun Wu, Xinpeng Fan, Qingxu Zhang, Wei Wang, Yihu Song, and Qiang Zheng. Magnetorheological elastomer peristaltic pump capable of flow and viscosity control. *Journal of Intelligent Material Systems and Structures*, page 1045389X20916803, 2020.

[170] Chenjun Wu, Qingxu Zhang, Xinpeng Fan, Yihu Song, and Qiang Zheng. Smart magnetorheological elastomer peristaltic pump. *Journal of Intelligent Material Systems and Structures*, 30(7):1084–1093, 2019.

[171] Peyman Yadmellat and Mehrdad R Kermani. Adaptive control of a hysteretic magnetorheological robot actuator. *IEEE/ASME Transactions on Mechatronics*, 21(3):1336–1344, 2016.

[172] Peyman Yadmellat and Mehrdad Radji Kermani. Adaptive modeling of a magnetorheological clutch. *IEEE/ASME Transactions on Mechatronics*, 19(5):1716–1723, 2013.

[173] Jian Yang, Shuaishuai Sun, Xiaoyan Yang, Yufan Ma, Guolin Yun, Ruizhe Chang, Shi-Yang Tang, Masami Nakano, Zhixiong Li, Haiping Du, Shiwu Zhang, and Weihua Li. Equipping new sma artificial muscles with controllable mrf exoskeletons for robotic manipulators and grippers. *IEEE/ASME Transactions on Mechatronics*, pages 1–12, 2022.

[174] Kazuhiro YOSHIDA, Souta HARA, Sang In EOM, and Shinichi YOKOTA. A novel soft microgripper using divided-electrode type flexible ER valves. *Mechanical Engineering Journal*, 2(6):15–340, 2015.

[175] Kazuhiro Yoshida, Noboru Tsukamoto, Joon-wan Kim, and Shinichi Yokota. A study on a soft microgripper using MEMS-based divided electrode type flexible electro-rheological valves. *Mechatronics*, 29:103–109, 2015.

[176] Kikuchi Yoshida, M Kikuchi, J-H Park, and S Yokota. Fabrication of micro electro-rheological valves (ER valves) by micromachining and experiments. *Sensors and Actuators A: Physical*, 95(2-3):227–233, 2002.

[177] Chuang Yu, Shuangxia Niu, Siu Lau Ho, Weinong Fu, and Longnv Li. Hysteresis modeling in transient analysis of electric motors with alnico magnets. *IEEE Transactions on Magnetics*, 51(3):1–4, 2014.

[178] Sishen Yuan, Sifan Cao, Junnan Xue, Shijian Su, Junyan Yan, Min Wang, Wenchao Yue, Shing Shin Cheng, Jun Liu, Jiaole Wang, Shuang Song, Max Q.-H Meng, and Hongliang Ren. Versatile motion generation of magnetic origami spring robots in the uniform magnetic field. *IEEE Robotics and Automation Letters*, 7(4):10486–10493, 2022.

[179] Guolin Yun, Shi-Yang Tang, Shuaishuai Sun, Dan Yuan, Qianbin Zhao, Lei Deng, Sheng Yan, Haiping Du, Michael D Dickey, and Weihua Li. Liquid metal-filled magnetorheological elastomer with positive piezoconductivity. *Nature communications*, 10(1):1–9, 2019.

[180] Guolin Yun, Shi-Yang Tang, Qianbin Zhao, Yuxin Zhang, Hongda Lu, Dan Yuan, Shuaishuai Sun, Lei Deng, Michael D Dickey, and Weihua Li. Liquid Metal Composites with Anisotropic and Unconventional Piezoconductivity. *Matter*, 2020.

[181] Piotr Zajac, Jerzy Kaleta, Daniel Lewandowski, and Aleksandra Gasperowicz. Isotropic magnetorheological elastomers with thermoplastic matrices: structure, damping properties and testing. *Smart Materials and Structures*, 19(4):45014, 2010.

[182] Alex Zatopa, Steph Walker, and Yigit Menguc. Fully Soft 3D-Printed Electroactive Fluidic Valve for Soft Hydraulic Robots. *Soft Robotics*, page soro.2017.0019, apr 2018.

[183] Jianbin Zeng, Youguang Guo, Yancheng Li, Jianguo Zhu, and Jianchun Li. Two-dimensional magnetic property measurement for magneto-rheological elastomer. *Journal of Applied Physics*, 113(17):17A919, 2013.

[184] Jiachen Zhang and Eric Diller. Untethered miniature soft robots: Modeling and design of a millimeter-scale swimming magnetic sheet. *Soft robotics*, 5(6):761–776, 2018.

[185] Jiangtao Zhang, Yanliang Qiao, Mei Zhang, and Pengcheng Zhai. Magnetorheological behavior of isotropic silicone rubber-based magnetorheological elastomers under coupled static–dynamic compressive loads. *Smart Materials and Structures*, 31(9):095010, 2022.

[186] Li Zhang, Jake J. Abbott, Lixin Dong, Bradley E. Kratochvil, Dominik Bell, and Bradley J. Nelson. Artificial bacterial flagella: Fabrication and magnetic control. *Applied Physics Letters*, 94(6):64107, 2009.

[187] Peizhi Zhang, Mitsuhiro Kamezaki, Zhuoyi He, Hiroyuki Sakamoto, and Shigeki Sugano. Epm–mre: Electropermanent magnet–magnetorheological elastomer for soft actuation system and its application to robotic grasping. *IEEE Robotics and Automation Letters*, 6(4):8181–8188, 2021.

[188] Wei Zhang, Xing-long Gong, Jian-feng Li, Hong Zhu, and Wan-quan Jiang. Radiation vulcanization of magnetorheological elastomers based on silicone rubber. *Chinese Journal of Chemical Physics*, 22(5):535–540, 2009.

[189] Dan Zhao, Bing Wang, Zhenghang Zhao, Shuaihu Wang, Song Yang, and Na Dong. The Simulation of Magneto-Mechanical Properties of Magnetorheological Elastomers. In *IOP Conference Series: Materials Science and Engineering*, volume 649, page 12003. IOP Publishing, 2019.

[190] Ruike Zhao, Yoonho Kim, Shawn A Chester, Pradeep Sharma, and Xuanhe Zhao. Mechanics of hard-magnetic soft materials. *Journal of the Mechanics and Physics of Solids*, 124:244–263, 2019.

[191] Jin Jiang Zhong, Jian Guo Zhu, You Guang Guo, and Zhi Wei Lin. Improved measurement with 2-D rotating fluxes considering the effect of internal field. *IEEE transactions on magnetics*, 41(10):3709–3711, 2005.

[192] G. Y. Zhou. Shear properties of a magnetorheological elastomer. *Smart Materials and Structures*, 12(1):139–146, 2003.

[193] J Zhou, S Chen, and Z Wang. A Soft-Robotic Gripper With Enhanced Object Adaptation and Grasping Reliability. *IEEE Robotics and Automation Letters*, 2(4):2287–2293, 2017.